MODELING AND VERIFICATION OF CRYOGENIC PERMEABILITY OF GRAPHITE EPOXY LAMINATES WITH DELAMINATIONS AND STITCH CRACKS

By

ABILASH RAJENDRAN NAIR

Bachelor of Technology

Indian Institute of Technology

Kharagpur, India

June, 2003

Submitted to the Faculty of the
Graduate College of the
Oklahoma State University
In partial fulfillment of
the requirements for
the Degree of
MASTER OF SCIENCE
July, 2006

MODELING AND VERIFICATION OF CRYOGENIC

PERMEABILITY OF GRAPHITE EPOXY

LAMINATES WITH DELAMINATIONS

AND STITCH CRACKS

Thesis Approved:

Samit Roy

Thesis Advisor

Hongbing Lu

Demir Coker

A. Gordon Emslie

Dean of the Graduate College

To my parents and my beloved brother Kapil

Ipsa scientia potestas est
"Knowledge itself is power"

ACKNOWLEDGEMENTS

I wish to express my gratitude to my family, friends and research colleagues for their confidence in me. I would like to thank them for their consistent encouragement and love.

I would like to express my sincere thanks to my adviser, Dr. Samit Roy for his supervision, constructive guidance and financial support throughout the study. I would like to thank him for providing me with sophisticated work environment. I would also like to extend my sincere appreciation to Dr. Demir Coker and Dr. Hongbing Lu for providing invaluable guidance and encouragement throughout this study.

I would like to thank Dr. Vernon Bechel for providing the experimental data required to verify the analytical model presented in this thesis.

Finally, I would like to thank the Department of Mechanical and Aerospace Engineering for providing me with the opportunity to pursue M.S. at Oklahoma State University. Special thanks are also in place for the University of Alabama, Tuscaloosa for providing me with the facilities to complete my thesis towards the end of my research.

This project has been funded by the grant (NAG-1-02016) from the National Aeronautics and Space Administration (NASA), Langley, VA. I would like to thank Dr. Thomas Gates for his interest and support of this work.

TABLE OF CONTENTS

Chapter **Page**

LIST OF TABLES

Table **Page**

LIST OF FIGURES

Figure **Page**

CHAPTER 1

INTRODUCTION

1.1. Introduction

Composite materials are one of the many advanced level structural materials available for next generation flight vehicles. Its unique and attractive properties make it the perfect solution for the design of next generation Space Shuttle. One such initiative is the Reusable Launch Vehicle (RLV) program, in which the impetus is towards using a mostly composite airframe in order to increase payload and decrease vehicle weight while not compromising on the other properties that the vehicle would have had if it was made of conventional material. However, with its application arise problems which have to be addressed before it is fully incorporated into production. One such problem is the permeation of liquid propellant through micro-cracks in the composite structure.

One of the major design features of a next generation space shuttle will be internal cryogenic fuel tanks (usually holding liquid hydrogen) made entirely of polymer composite. The cryogenic temperatures combined with the action of various flight loads (e.g. re-entry, repeated take-off, landing, i.e. fatigue type loads) can cause the tank to develop micro-crack as shown in Fig. 1.1. The micro-cracks usually appear through the

thickness of the composite structure in the form of transverse matrix cracks. It is easy to imagine the micro-cracks forming a micro-size network of connecting pathways (See Fig. 1.2) through the thickness of the structure leading to the leakage of cryogenic fuel (permeant). Needless to say, the situation is not desirable and warrants scientific investigation.

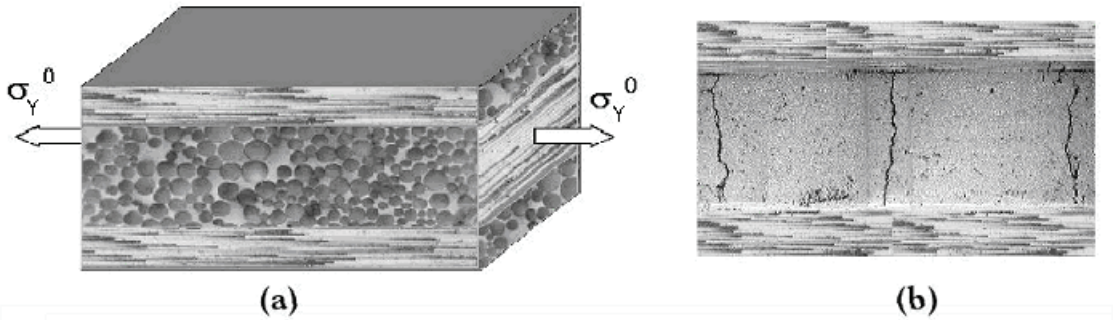

Fig. 1.1 Cross-ply laminate subjected to uniaxial loading and resulting damage.

Shown in Fig. 1.2 is an idealized version of connecting pathways in a composite laminate of arbitrary ply orientation. It has been observed that at the junctions of these intersecting micro-cracks, delaminations may occur which, coupled with the crack opening displacements, will enable the permeant to escape. It is hence of primary importance that an analytical solution be developed inorder to model, predict and understand the damage mechanism(s) behind the permeation process.

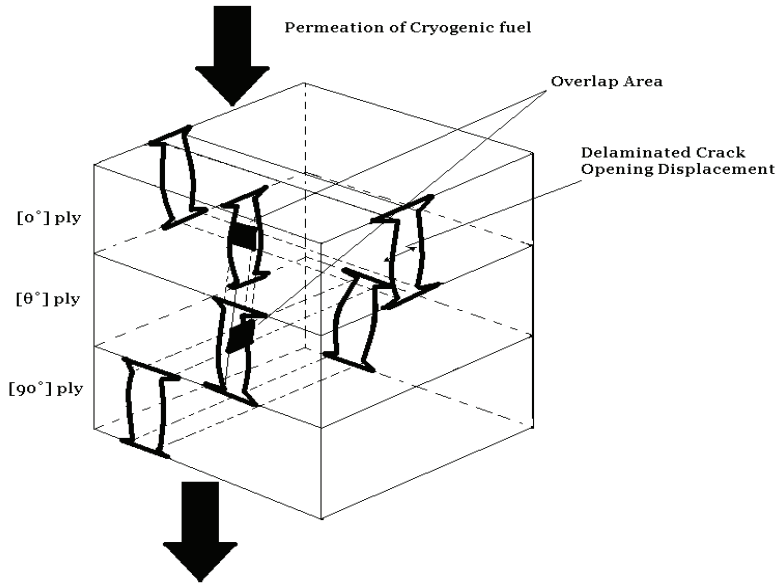

Fig.1.2 Permeation path at overlap of transverse cracks in arbitrarily orientated plies.

1.2. Thesis Overview

In this thesis, an analytical model is presented to analyze composite laminates with transverse matrix cracks and delaminations in them. The model will be used to determine the crack opening of damaged laminates subjected to mechanical and/or thermal loads. Since, in the past researchers have limited the study to orthotropic or balanced laminates, the model suggested in this thesis will be generalized to study a generic symmetric laminate. Further, the model will be used to determine the distribution of delaminated crack opening displacement (DCOD) through the thickness of the laminate. The results from the crack opening analysis will be used to determine the permeability of the damaged composite using the analytical model suggested by Roy and Benjamin [36]. Finally, the analytical model will be used to study the damage evolution of transverse matrix cracks and delaminations within the cracked ply of the laminate.

The proposed micro-mechanics model is based on the classical lamination theory (CLT) for composites. The substructure of the damaged laminate is defined using sublaminates or ply groups into which uncracked and cracked plies are grouped as per their position within the laminate. Further, since the load transfer from the cracked to the uncracked ply (ply or sublaminate) is primarily through shear transfer, the model uses a sublaminate wise first order shear deformation theory to simulate the load transfer between the plies.

Most previous models have used either a one- or two-dimensional shear lag model to analyze damage of composites. The use of first order shear deformation assumptions makes the current model superior in analysis, since the transverse shear effects are included in the model through its governing equations and it does not separately need the inclusion of interface shear terms to simulate the interactions between the cracked and uncracked plies. Further, of the models that have been proposed to solve for general configuration laminates previously, most have not addressed the issue of stitch cracks that has been observed in off-axis plies of a general anisotropic laminate. In this report, an analytical model is suggested to address these experimental observations. The stitch crack model will be a part of the extended model of the current analysis that will be used to analyze a laminate of general configuration. The extended model will be used to predict the delaminated crack opening displacement (DCOD) (with and with-out stitch cracks – as per cracked-ply configuration) for each layer in the IM7/5250-4 laminate of lay-up $[0/45/-45/90]_s$ and will be verified against 2-D FEA results for both mechanical and thermal load cases.

Subsequently, the results (delaminated crack opening displacements) from the analysis of a generic laminate system will be used as input to the permeability model, from which the permeability of the damaged laminate will be evaluated. In this thesis, the combined DCOD-permeability model [36] is verified using experimental results for a IM7/5250-4 composite of lay-up $[0/45/-45/90]_s$.

An equally important contribution of this model is to the study of damage evolution in general configuration laminates. The model developed in thesis is capable of handling cracks in different layers and predicting the damage evolution in the laminate using parameters calculated from the suggested analytical model. The damage evolution (in the form of both uniform matrix cracks and interlaminar delamination) for the IM7/5250-4 laminate of configuration $[0/45/-45/90]_s$ is predicted using this model and verified using two dimensional finite element analysis (FEA).

CHAPTER 2

LITERATURE REVIEW

Due to the challenge involved in the analytical modeling of composites, significant interest has been generated in the scientific community to propose models that will best solve a given problem easily and accurately. References [1-3] used a continuum damage mechanics approach to determine the degradation of mechanical properties of the laminate. The damage in the laminate (e.g., interfacial debond, matrix crack, delamination) is included in the definition of internal damage variables which is then used to extract the properties of the damaged laminate. While this method is widely used in the analysis of homogenous isotropic materials, the anisotropic nature of most composite fracture problems makes this method harder to use in the analysis of composite damage. Many researchers in this field tend to use the structural mechanics approach wherein, an approximate distribution of the stresses and displacements in the cracked region is determined, from which the damage state of the laminate is easily extracted. Two and three dimensional finite element analysis [4], [31], [34] and [35] has also been used to numerically simulate transverse crack multiplication in cross-ply laminates.

References [5-8] use variational approach to study the stress field in the cracked orthotropic laminates. The solutions from the analysis in [5]-[7] were verified with experiments. Nairn [6,7], used a two-dimensional variational approach to analyse the stress fields in cracked laminates with delaminations originating from the crack tip for $[S/90_n]_s$ laminates (where, S is the balanced set of sublaminates). He observed that for lower crack densities the damage grows in the damaged ply through pure matrix cracks until the crack density becomes too large (called the saturation crack density) after which point the damage mode switches to delamination growth. The variational solution methods have shown good agreement with experimental results for cross-ply laminates. However, the extension of this solution procedure to the analysis of general laminate configurations would be difficult.

McCartney [9,10], proposed and determined an approximate solution for the stresses in cross-ply laminates. Through its analysis the model simulates stress transfer between the plies of an orthotropic laminate with cracks in the 90 ply. The model was validated and shown to produce the same results as the variational solution by Schoeppner and Pagano [8] (refer [10]).

Since, it was evident that the damage mechanism in the cracked laminates could be studied in detail by using approximate stress transfer methods, researchers have frequently employed to shear-lag type analysis. Hong *et al* [12] and Han *et al* [13] used one-dimensional shear lag model to determine the drop in mechanical properties of the laminate with pure matrix cracks. Henaff-Gardin *et al* [14] derived a simple closed form solution for strain energy release in mixed mode conditions (in case of a general in-plane loading) for damage in cross-ply laminates using one-dimensional shear lag. Zhang *et al*

[15]-[18], improved the one-dimensional shear lag model inorder to satisfy the equilibrium equations for the inplane shear stress. In this method, the out of plane shear stresses was approximated to vary linearly along the laminate length. Zhang and Fan [15], proposed the use of an equivalent constrained model (ECM) to evaluate the damage parameters of the laminate system. The ECM considers the damaged laminate to be a perfectly bonded set of laminates with stiffness of the laminate equal to that of the damaged laminate. Using the 2-D shear lag along with ECM assumptions the degradation in material properties were evaluated for both non-uniform matrix cracking and delamination growth in laminates of $[\pm\theta_m/90_n]_s$ configuration. It was noted that the use of 2-D shear lag/ECM made an improvement in predictions in stiffness degradation over the 1-D shear lag ([16]-[18]). Kashtalayan and Soutis [19] used the modified ECM/2-D shear lag to predict the stiffness degradation of damaged cross-ply laminates with transverse matrix cracks in the 90˚ plies and fiber breakage in the 0˚ plies. Their model compared well with the variational solutions of Hashin [5], Schoeppner and Pagano [8], and the shear lag solutions of Henaff-Gardin *et al* [14].

The first order shear plate model avoids the use of "fictional" boundary shear to simulate the transfer of load between the cracked and uncracked plies. This model is based on the modified classical lamination theory to include first order deformation approximation. It was first used by Armanios *et al* [20] to solve for stiffness degradations in composite laminates with a cracked 90˚ middle ply. The model was further extended to the five layer ECM by Zhang *et al* [21]. As per the assumptions of the first order plate theory, load shearing in the cracked laminate is assumed to occur purely through the shear deformations of the ply groups (or sublaminates) of the model. Using this model,

Armanios *et al* [20] was able to simulate the reduction in delamination onset strain for $[\pm 25/90_n]_s$ laminates with increase in 'n' (or the number of cracked plies in the laminate), as observed in experiments. From the analysis of the five layer ECM, Zhang *et al* [21] showed that the strain energy release rate for local delamination is strongly influenced by the constraining layers immediately adjacent to the cracked 90 ply group. This effect of local laminate architecture cannot be simulated through regular shear lag models. The FLM proposed in [21] was extended to solve for multilayer cracking in laminates of any orientation in [22]. The solution was restricted to pure intra-lamina cracks (or matrix cracks) with no delaminations.

References [23]-[27] list some of the studies to characterize damage in off-axis plies. O'Brien and Hooper [23] and O'Brien [24] used tensile tests and quasi-three dimensional FEA to characterize and model damage in $[0/+\theta_2/-\theta_2]_s$ laminates, for θ=15˚, 20˚, 25˚ and 30˚. It was observed from FEA that the stresses normal to the fiber in off-axis plies were compressive at the interior of the laminate and tensile at the edge of the laminate, and that the matrix cracks in the off-axis plies initiates at the edge of the laminate. Further, they observed from experiments that the local delamination is only uniform at the edge of the ply, whereas in the interior of the laminate the local delamination is restricted to an area bounded by the angle ply matrix cracks. Two strain energy release rates solutions were derived: one for uniform through-width delamination growing from angle ply matrix crack while another for a delamination growth from the matrix crack confined to a localized area around the angle-ply crack. Salpekar, O'Brien and Shivkumar [25] used three dimensional FEA to model delaminations in graphite epoxy laminates of lay-up $[0/+\theta/-\theta]_s$ and $[-\theta/+\theta/0]_s$, for θ=15˚ and 30˚. They computed the

strain energy release rate (SERR) at the delamination front using three techniques: the virtual crack closure technique (VCCT), the equivalent domain integral (EDI) and global energy balance. Kashtalayan and Soutis [26] extended the ECM/two dimensional shear lag model [18] to derive closed form expressions for SERRs in mode I and mode II in terms of the in-situ damage functions for laminates with off-axis plies. They compared this model with the closed form expression for mode II SERR from O'Brien [24]. They observed that O'Brien's solution significantly overestimates the SERR for delamination growth. Using their model they saw that the damage induced stiffness changes for unbalanced laminates were significantly higher than balanced laminates. However, since the model was not verified more rigorously against experimental data the validity of the conclusions are questionable. Varna *et al* [27] used a synergistic damage mechanics approach to study the cracks in off-axis plies. They verified their theoretical model with experimental data for glass fiber/epoxy laminates of configuration $[0/\pm\theta_4/0_{1/2}]_s$, for θ=55˚, 70˚ and 90˚. Using this model they were able to capture the stiffness degradations of the cracked ply quite well.

References [28]-[31] document the experimental verification of the various analytical models suggested for matrix crack growth in laminates. Henaff-Gardin *et al* [28] developed a simple one-dimensional shear lag model to analyse cross-ply laminates and tested the solution with experimental data of cycling of T300/914 laminates in thermal load. They used the biaxial nature of thermal loads to create cracks in the 0 and 90 plies of the cross-ply laminate. Takeda *et al* [29] verified McCartney's stress transfer solution [9] for axial displacements, using a ply-refinement method for the case of cracks in the 90 ply of a cross-ply laminate. They observed that the model predictions for axial

displacements cross-ply laminates compared well with the experimental ply-refinement technique. McManus and Maddocks [30] used a modified shear-lag analysis to model damage progress (based on self-similar matrix crack multiplication) in general composite laminates. Their simple analysis was able to capture, in general, the damage trends in AS4/3501-6 laminates of three different lay-ups: $[0_4/45_4/90_4/-45_4]_s$, $[0_2/45_2/90_2/-45_2]_s$ and $[0_2/60_2/-60_2]_s$. This simple shear-lag theory is a fairly good first approximation of the damage growth in the laminate. However for a more detailed analysis of the damage state the analysis is ineffective since, it does not include damage growth in the form of delaminations. Su *et al* [31] used a combined FEA/ECM to predict micro-crack densities in IM7/977-2 graphite epoxy laminate of lay-up $[0/45/90/-45]_s$ for uniform matrix crack multiplication. Although their predictions compared reasonably well with the experimental data from Donaldson *et al* [37], the method is computationally expensive to use as a design tool.

The determination of the crack opening displacement (COD) is closely related to the damage state in a composite. Properties such as permeability, largely depends on the crack opening of its individual layers. Hence, it is important to understand the variation of crack opening with applied load and also to functionalize the COD in terms of geometry and damage parameters of the laminate. Varna *et al* [32] predicted average COD based on shear-lag model and variational approach and found that the stiffness reduction in the uncracked layer influences COD of the interior layer. Roy and Benjamin [33] developed a simple shear-lag model to determine COD. Noh and Whitcomb [34, 35] developed analytical expressions for calculating the crack opening volume (COV) and studied the effects of various parameters such as adjacent ply orientation, material

properties of the cracked and surrounding plies on its value. More recently, they used 3-D FEA to determine the growth of delamination and calculated the resulting delaminated crack opening displacement (DCOD) at the intersection of transverse matrix cracks (TMC) [35]. Roy and Benjamin [36] were able to extend the first order shear deformable plate model proposed by Armanios *et al* [20] and Zhang *et al* [21] to study the DCOD in the 90˚ ply of the laminate configuration $[\phi_l / \varphi_m / .../ \theta_n / 90_r]_s$ subjected to mechanical and/or thermal load(s). This model was subsequently verified for cross-ply laminates using 2-D FEA, representing damage states that included transverse matrix cracks as well as delaminations.

Any one of the damage model for composites suggested above can be used to predict the permeability of damaged composite when subjected to mechanical and/or temperature fields. However, experimental setups for permeability prediction are hard to design and use effectively. The challenge involved in inducing cracks in undamaged laminates and reliably studying their permeability characteristics has motivated many researchers to study this problem intently. References [37]-[41] list the major experimental work currently in progress in this area. Donaldson *et al* [37] were able to induce damage in IM7/977-2 composite samples of lay-up $[0/45/90/-45]_s$ through mechanical cycling in cryogenic condition. Grenoble and Gates [40] induced micro-cracks in IM7/977-2 laminates through mechanical cycling at room temperature and then tested them for permeability at both room and cryogenic temperature. They observed that the damage develops quicker in the off-axis plies near the top and/or bottom surface of the laminate. They also observed that the permeability depended strongly on the crack density, loading conditions and test temperature. Bechel [38, 41] was able to induce

damage in IM7/5250-4, IM7/977-2 and IM7/977-3 of laminate stacking sequences: $[0/90]_{2s}$, $[0/90/45/-45]_s$, and $[0/45/-45/90]_s$. The experimental setup was designed based on the setup by Henaff-Gardin *et al* [28]: the biaxial thermal fatigue in the composite caused through thermal cycling between a high temperature (~177˚C) and liquid nitrogen temperature (-196˚C) induces matrix cracks to develop in the composite. They studied and reported in particular the permeation characteristics of the $[0/45/-45/90]_s$ IM7/5250-4 laminate since it was found to be the most susceptible to permeation. Aoki *et al* [39] observed that the chief difference between the cracks in a composite with off-axis plies and cross-ply laminates were the existence of short "stitch" cracks in the off-axis cracked layer(s). They observed that the cracks in angle plies do not usually develop through the width of the lamina; instead they tend to accumulate around the junctions with the crack in the adjacent layer. They referred to the through-thickness cracks in the 0 (or 90) plies as long cracks since the cracks in these layers usually extend through the width, and referred to the partially extended through the width cracks as stitch cracks. They further, observed from a study of laminates with varying off-axis ply lay-ups that the stitch cracks were dominant in the cracked ply as its orientation moved away from orthotropic configurations. Bechel *et al* [41] verified the existence of stitch cracks in the off-axis (±45) layers of the $[0/90/45/-45]_s$, and $[0/45/-45/90]_s$ laminates that were thermally cycled.

Peddiraju *et al* [42] predicted the experimental observations made by Gates *et al* [38] using an analytical model. They used the crack opening and crack spacing data from experiments to describe the geometry of the cracked laminate and then made predictions for the leak rate after modeling the geometry in a commercial fluid analysis code. Roy

and Benjamin [36] proposed an analytical model based on Darcy's law to predict permeability. This analytical model was not validated against any experimental data.

In this thesis, the damage analysis model proposed by Roy and Benjamin [36] will be first extended to determine the crack opening distribution through the thickness of a generic configuration of plies, and then used to verify the analytical permeability model in [36] using experimental results from Bechel *et al* [41].

Of the various models that have been reviewed in this chapter, the first order shear deformable plate theory has been chosen to analyze damaged laminates. The ability of this analytical model to give approximate two-dimensional solutions of longitudinal displacements of the laminate in the presence of TMC and delaminations makes it an ideal candidate for simple COD analysis.

The model presented in Roy and Benjamin [36] uses the first order plate theory\ECM to predict the COD in cross-ply laminates for a given crack density under the influence of mechanical and/or thermal loads. This two dimensional analysis model considers uniformly spaced through thickness transverse matrix cracks along with delaminations that extend from the tips of each matrix crack. Since, cross-ply laminates have limited application in most aerospace structures the model will be extended, as presented in this thesis, to include analysis of cracks in off-axis cracked plies which can be located at any position along the thickness. Zhang *et al* [22], suggested a similar analytical model that solves for pure matrix crack growth in a general configuration laminate. However, since the solution procedure requires the determination of eigen values of a 10x10 system matrix, the method is computationally demanding and can be solved only numerically. However, with the extended model suggested in this thesis the

system matrix is reduced to a 3x3 system, which is significantly easier to solve. The model analysis in this thesis simplifies the multi-layer cracking model of [22], by the assumption that there is no interaction between the cracks in adjacent layers. Hence, for each instance of crack analysis there will be unique ECM associated with that crack (with or without delamination) in which, all other sublaminates will be intact. Further, the inclusion of the delamination damage model to the analysis makes this model more sophisticated. Also, a simple methodology to model stitch cracks is proposed to address experimental observations. The extended model (which is the input for the permeability analysis) will include this model for the stitch cracks. The extended model proposed in this thesis will also be used to determine the strain energy release rates associated with mode I (matrix crack multiplication, self-similar crack growth) and mode II (interlaminar delamination) for a laminate of any given lay-up. The damage evolution will be verified using 2-D FEA.

It is anticipated that when this model is implemented and verified, it can be used as a screening tool in the design of cryogenic composite propellant tanks subjected to mechanical and/or temperature loads, within the limits of a first order approximation, without recourse to labor extensive three-dimensional FEA.

CHAPTER 3

THE FIVE LAYER MODEL

3.1. Delaminated Crack Opening Displacement

The most common damage modes of a composite under the action of thermal and or mechanical loading are transverse matrix cracks and delaminations. Transverse matrix cracks is typically the initial damage mode observed and is enhanced with increasing load, however, due to the high local stresses that develop at crack tips, damage mode soon switches from matrix cracks to delamination. The delaminated crack opening displacement (DCOD) for a cracked composite sublaminate is defined as the minimum crack opening distance between the two faces of the transverse matrix crack in the sublaminate. In this thesis a five layer model (FLM) has been suggested to determine the DCOD of the cracked laminate. The FLM is a 2-D model based on the governing equations from classical lamination theory (CLT). In order to simulate the transverse shear in the laminate, the equations from CLT are modified with first order shear deformable plate theory assumptions.

The delaminated crack opening displacement (DCOD) determined from this model is a critical input to the permeability model (discussed later in chapter 7). Also, since the model will be used in the study of damage evolution (chapter 6) in the cracked layer, it is important to build a model that can accurately describe the variation of the crack opening as a function of applied mechanical load and/or applied temperature excursion.

The FLM presented in this thesis is an extension to the model suggested by Roy and Benjamin [36]. The extension is provided in the manner of cracks in sublaminate 5 and sublaminate 6 of the FLM. Fig. 3.1, shows the typical 3-D repeating volume element (RVE) of a cracked laminate symmetric about its mid-plane. Also shown in the figure shows are the various cracked sublaminate configurations that will be addressed using FLM.

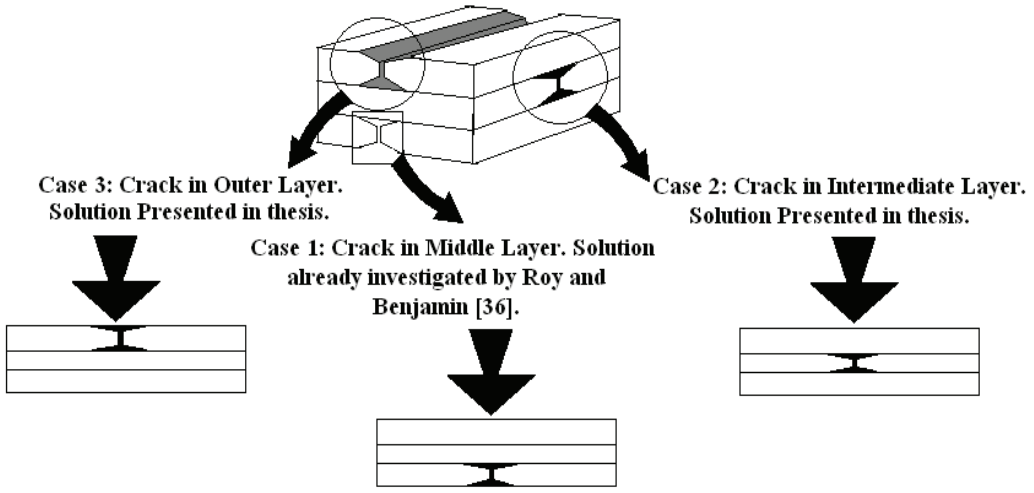

Fig. 3.1. Illustration of crack RVE and the corresponding mathematical models

As shown in the figure above, a unique analysis model is suggested to handle each specific case of cracked configuration. The focus of this thesis will be to superpose

the sublaminate models to analyze a laminate with cracks in objective plies of any orientation. In the section to follow (section 3.2), the three FLM cases for cracked 90 plies are introduced. Later, in section for the extended FLM (section 3.5), the analyses are generalized for a cracked layer of any orientation.

3.2. Introduction to FLM

In this section, analytical expressions to determine the DCOD for crack positions in sublaminates 5 and 6 are studied. Also, a summary of the work by Roy and Benjamin [36], where the motivation was to determine the crack opening displacement for the delaminated layer 3 of the FLM, has been included in the interest of completeness. Since the models presented in this thesis are an extension to [36], the notations and symbols used in [36] will be retained.

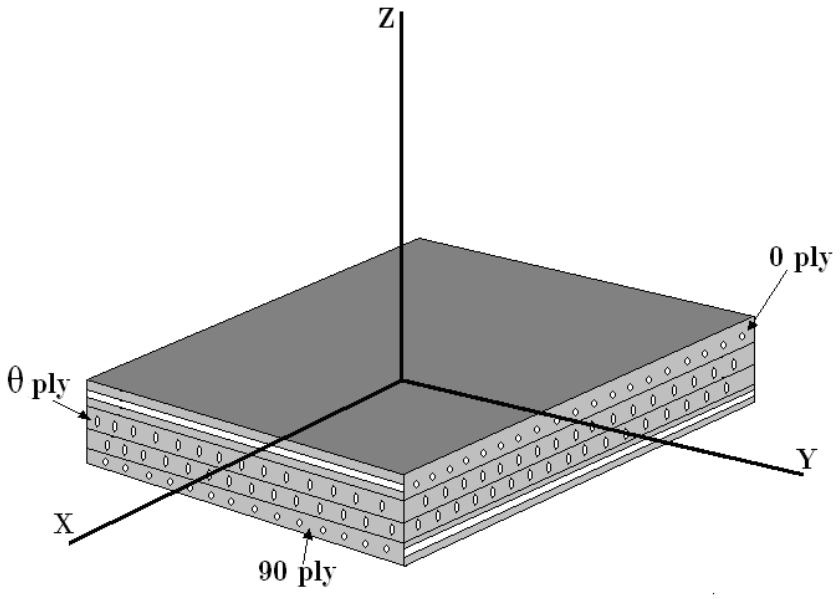

Fig. 3.2. The global XYZ axis for the composite

Before we proceed to the detailed analysis and solution of each case of crack position, the governing equations of the FLM are introduced.

The two-dimensional FLM model is assumed to lie in the Y-Z plane, with the principle axis of the 0˚ ply group coinciding with the global Y axis (refer Fig. 3.2). A plain strain condition is assumed to exist in the X-direction of the laminate. In addition to the global axis a sublaminate-wise local axis is also used inorder to describe displacements and rotations of the sublaminate (e.g., see Fig. 3.3(b)). Since the model employs a first order shear deformation plate theory, the displacements in y (v) and z (w) direction are assumed to be of the form:

$$v^{(i)}(y,z) = V^{(i)}(y) + z\beta^{(i)}(y) \tag{3.1a}$$

$$w^{(i)}(y) = W^{(i)}(y) \tag{3.1b}$$

Where, V(y) is the mid-plane displacement in the y-direction and β(y) is the slope of the normal to the mid-plane of the sublaminate in the y-direction. Note that, the displacement in the z-direction, W(y), does not vary through the thickness.

The equilibrium equations of the model are listed below in the order of force balance in the y-direction, moment balance along the x axis and force equilibrium in the z-direction. Assuming plain strain conditions to exist in the x-direction of the model, we get, for each sublaminate,

$$N_{,y} + T_t - T_b = 0 \tag{3.2a}$$

$$M_{,y} - Q + \frac{h}{2}(T_t + T_b) = 0 \tag{3.2b}$$

$$Q_{,y} + P_t - P_b = 0 \tag{3.2c}$$

Where, N, M and Q are the axial force, bending moment and shear resultants, while P and T denote the inter-laminar peel and shear stresses associated with the with top (t) and bottom (b) surfaces. The constitutive relations for each sublaminate are: (the subscript 'm' denotes "mechanical" or applied load)

$$N_M = A_{22}V_{,y} + B_{22}\beta_{,y} - \bar{Q}_{22}h\int_{T_{ref}}^{T_f} \bar{\alpha}_y dT \tag{3.3a}$$

$$M_M = B_{22}V_{,y} + D_{22}\beta_{,y} - \bar{Q}_{22}h\bar{Z}\int_{T_{ref}}^{T_f} \bar{\alpha}_y dT \tag{3.3b}$$

$$Q = A_{44}(\beta + W_{,y}) \tag{3.3c}$$

Where, A_{22}, B_{22}, D_{22} & A_{44} are components of the A, B and D stiffness matrices from classical lamination theory (CLT), h is the thickness of the lamina, $\bar{Z}$ is the centroidal distance of the lamina from laminate mid-plane, $\bar{\alpha}_y$ is the coefficient of thermal expansion in y-direction. Substituting in (3.3a – 3.3c) into (3.2a – 3.2c) we have the governing equations,

$$A_{22}V_{,yy} + B_{22}\beta_{,yy} + T_t - T_b = 0 \tag{3.4a}$$

$$\left(D_{22} - \frac{B_{22}^2}{A_{22}}\right)\beta_{,yy} - A_{44}(\beta + W_{,y}) + \left(\frac{h}{2} - \frac{B_{22}}{A_{22}}\right)T_t - \left(\frac{h}{2} + \frac{B_{22}}{A_{22}}\right)T_b = 0 \tag{3.4b}$$

$$A_{44}(\beta_{,y} + W_{,yy}) + P_t - P_b = 0 \tag{3.4c}$$

The governing equations above can be modified as required by the lamina (or sublaminate) boundary conditions. In the sections to follow, the 'i' superscript will be attached to the displacements and rotations to describe the displacements in i^{th} sublaminate.

3.2.1. Case 1: Crack in Sublaminate 4

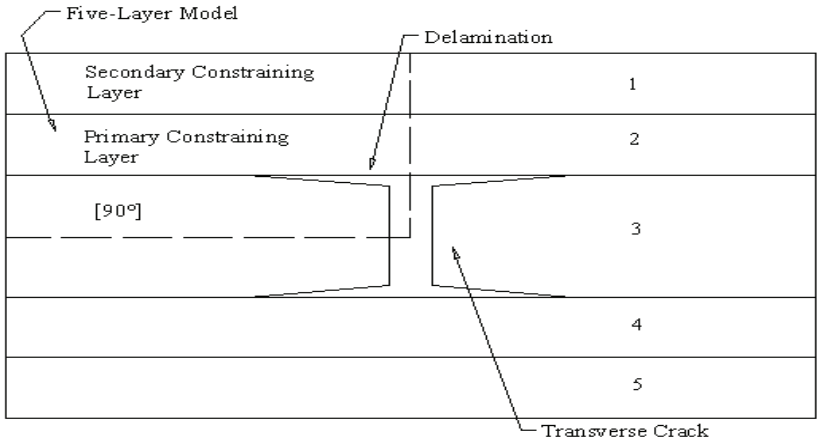

Fig. 3.3(a). The Five-Layer Model for Case 1

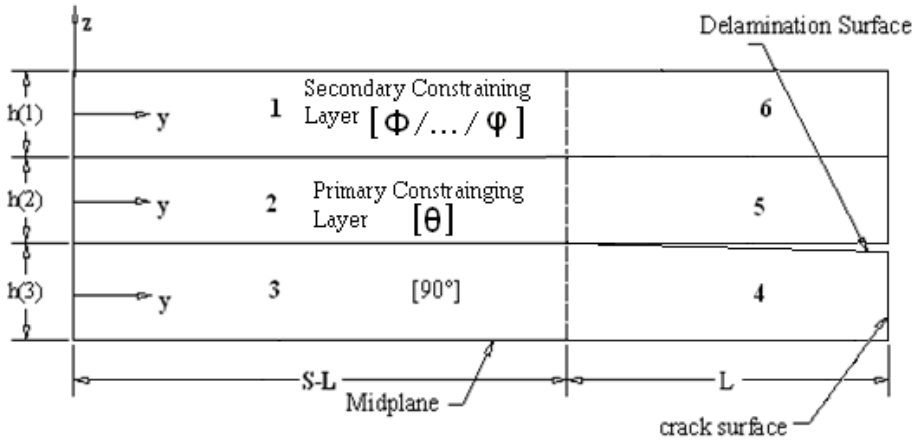

Fig. 3.3(b). One quarter repeating interval of the FLM (Case 1)

The solutions for this case are already listed in Roy and Benjamin [36]. Using this baseline case we can solve for the DCOD in a symmetric laminate with the general configuration $[\phi_l/.../\varphi_m/\theta_n/90_r]_s$, with the crack in the 90˚ ply. The transverse matrix cracks are assumed to have a uniform spacing of '2S', while delaminations are assumed to initiate and grow in a symmetric manner from tips of each matrix crack and extend a length "L" from the crack tip. The Fig. 3.3(a) shows the FLM for the case of crack in a middle layer. Fig. 3.3(b) shows the RVE developed from Fig. 3.3(a) after invoking conditions of symmetery in load and geometry. Note that the FLM for this case takes into account the effect of a primary and secondary constraining layer Zhang *et al* [21] on the delaminated crack opening (see Fig. 3.3(a)). From [36], the solutions for this case of crack configuration are:

$$v^{(4)}(y,z) = V^{(4)}(y) + z^{(3)}\beta^{(4)}(y) \tag{3.5}$$

$$v^{(5)}(y,z) = V^{(5)}(y) + z^{(2)}\beta^{(5)}(y) \tag{3.6}$$

$$\text{Where, } V^{(4)} = \psi_3 y + \psi_4 \tag{3.7}$$

$$V^{(5)} = -k_1(\theta_1 e^{\omega y} + \theta_2 e^{-\omega y}) + \theta_5 y + \theta_7 \tag{3.8}$$

$$\beta^{(4)} = \psi_1 e^{\omega_1 y} + \psi_2 e^{-\omega_1 y} \tag{3.9}$$

$$\beta^{(5)} = q(\theta_1 e^{\omega y} + \theta_2 e^{-\omega y}) + \theta_3 y + \theta_4 \tag{3.10}$$

The detailed procedure for obtaining the constants for the case of mechanical and/or thermal loading can be found in Roy and Benjamin [36].

Using equations (3.5 – 3.10), the delaminated crack opening displacement calculated at the interface of sublaminate 4 and 5 at y=S for a given delamination length L and crack density 1/2S is,

$$\text{DCOD} = v^{(5)}(S, \frac{-h^{(2)}}{2}) - v^{(4)}(S, \frac{h^{(3)}}{2}) \tag{3.11}$$

3.2.2. Case 2: Crack in Sublaminate 5

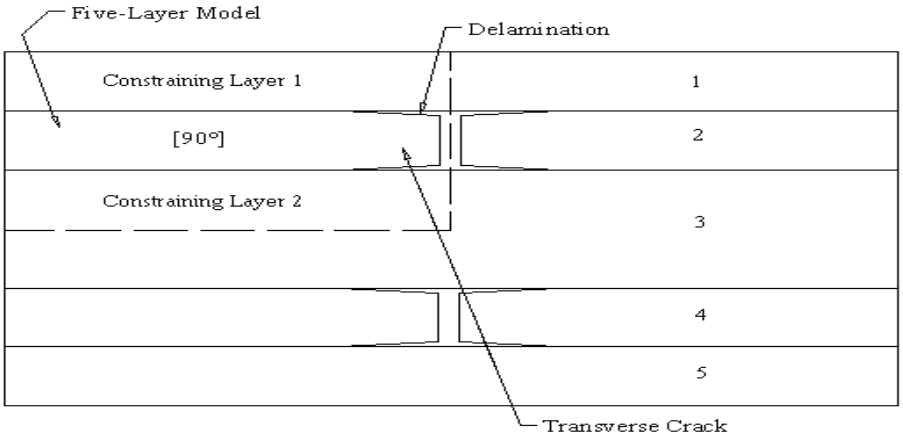

Fig. 3.4(a). The Five-Layer Model for Case 2

We next consider the case for crack in layers 2, 4 of the FLM (Fig. 3.3(a)), or sublaminate 5 of the quarter repeating model (Fig. 3.4(b)). The model solves DCOD for the general case of $[\phi_l / .../ \theta_m / 90_n / \varphi_p / .../ \psi_q]_s$, with the crack located in the 90° ply. The geometry and material parameters follow the same notation and meaning as before (see Fig. 3.4(b)).

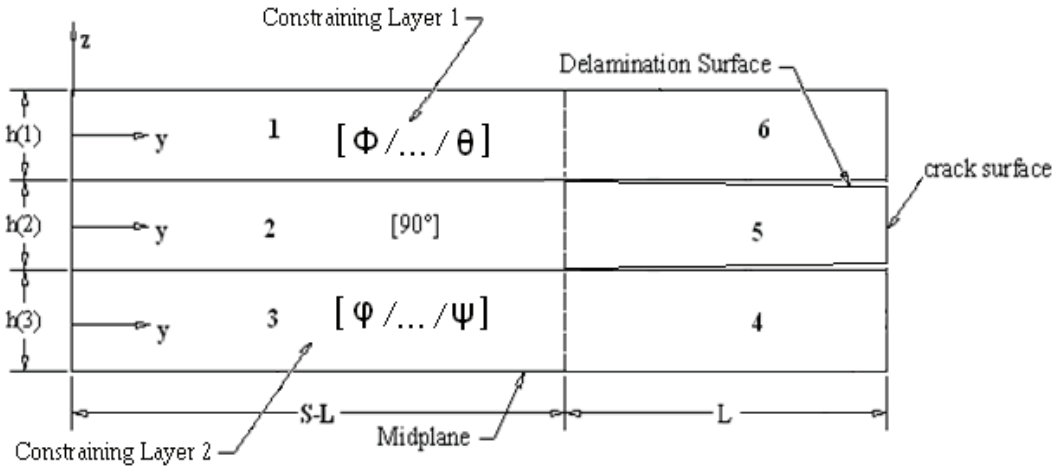

Fig. 3.4(b). One quarter repeating interval of the FLM (Case 2)

As can be seen from the Fig. 3.4(b) above, the model has been generalized to have unsymmetric sublaminates (in this case the sublaminate groups $[\phi_l/.../\theta_m]$ & $[\varphi_p/.../\psi_q]_s$) surround the cracked ply. Since only the effective "smeared" properties of the uncracked sublaminate groups are considered the model does not capture the effect of an immediate constraining layer. The analysis can easily be modified to include the effect of the constraining plies, but that will result in equations that can only be solved numerically (e.g., Zhang *et al* [22]). A detailed derivation for the individual mid-plane displacements and rotations for Case 2 are presented in Appendix A.

From first order shear deformation assumptions we have the following relations,

$$v^{(4)}(y,z) = V^{(4)}(y) + z^{(3)}\beta^{(4)}(y) \tag{3.12}$$

$$v^{(5)}(y,z) = V^{(5)}(y) + z^{(2)}\beta^{(5)}(y) \tag{3.13}$$

$$v^{(6)}(y,z) = V^{(6)}(y) + z^{(1)}\beta^{(6)}(y) \tag{3.14}$$

The solutions for the displacements and rotations are given by,

$$V^{(6)} = \theta_6 y + \theta_8 \tag{3.15}$$

$$\beta^{(6)} = \theta_3 y + \theta_4 \tag{3.16}$$

$$V^{(5)} = \psi_3 y + \psi_4 \tag{3.17}$$

$$\beta^{(5)} = \psi_1 e^{\omega_1 y} + \psi_2 e^{-\omega_1 y} \tag{3.18}$$

$$V^{(4)} = \theta_5 y + \theta_7 \tag{3.19}$$

$$\beta^{(4)} = \theta_1 y + \theta_2 \tag{3.20}$$

Using equations (3.12 – 3.20), the delaminated crack opening displacement (DCOD) for sublaminate 5 in Fig. 3.3(b) at y=S for a given delamination length L and crack density 1/2S can be determined,

From the boundary conditions for the sublaminate, we see that the relative displacement calculated at the interface of sublaminates 4 and 5 (or, sublaminates 5 and 6) at y=S will be the same, since $V^{(4)}(S) = V^{(6)}(S)$ and $\beta^{(4)}(S)=0$, $\beta^{(6)}(S)=0$ (refer Appendix A).

$$\text{DCOD}= v^{(5)}(S, \frac{-h^{(2)}}{2}) - v^{(4)}(S, \frac{h^{(3)}}{2}) \tag{3.21}$$

$$\text{Or, DCOD}= v^{(5)}(S, \frac{h^{(2)}}{2}) - v^{(6)}(S, \frac{-h^{(1)}}{2}) \tag{3.22}$$

3.2.3. Case 3: Crack in Sublaminate 6

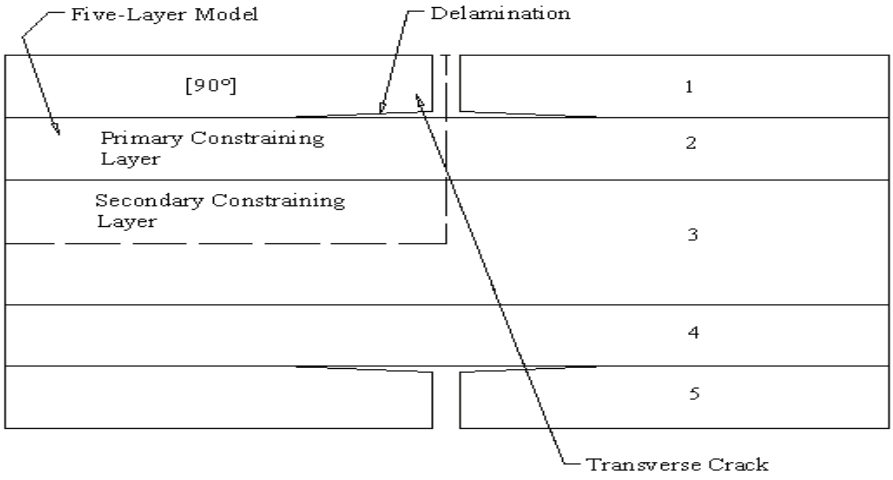

Fig. 3.5(a). The Five-Layer Model for Case 3

The configuration of FLM considers the crack to be at the outer most layers of the laminate (i.e., layer 6 in Fig. 3.5(b)). This model includes the effect of the primary and secondary constraining layers of the FLM (Fig. 3.5(b)).

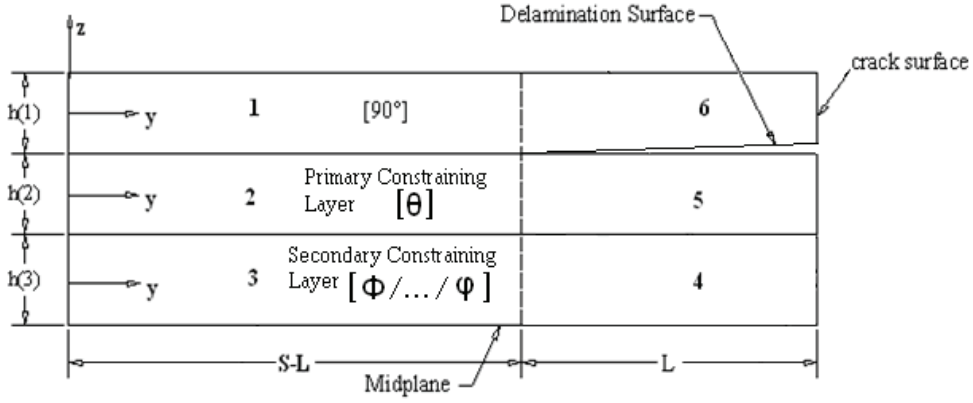

Fig. 3.5(b). One quarter repeating interval of the FLM (Case 3)

The solution for displacements and rotations are given in detail in Appendix B. From first order shear deformable plate theory assumptions,

$$v^{(5)}(y,z) = V^{(5)}(y) + z^{(2)}\beta^{(5)}(y) \tag{3.23}$$

$$v^{(6)}(y,z) = V^{(6)}(y) + z^{(1)}\beta^{(6)}(y) \tag{3.24}$$

Solving the set of governing equations for this case (Appendix B) gives,

$$V^{(6)} = \psi_3 y + \psi_4 \tag{3.25}$$

$$V^{(5)} = k_3(\theta_1 e^{\omega y} + \theta_2 e^{-\omega y}) + \theta_5 y + \theta_7 \tag{3.26}$$

$$\beta^{(6)} = \psi_1 e^{\omega_1 y} + \psi_2 e^{-\omega_1 y} \tag{3.27}$$

$$\beta^{(5)} = \theta_1 e^{\omega y} + \theta_2 e^{-\omega y} + \theta_3 y + \theta_4 \tag{3.28}$$

Using equations (3.23 – 3.28), the delaminated crack opening displacement calculated in layer 6 (Fig. 3.5(b)) at y=S for a given delamination length L and crack density 1/2S is given by,

$$\text{DCOD} = v^{(6)}(S, \frac{-h^{(1)}}{2}) - v^{(5)}(S, \frac{h^{(2)}}{2}) \tag{3.29}$$

3.3. Issues regarding FLM

Although the suggested models compare well with 2-D FEA results (see, section 8.1) there are however analytical modeling issues such as discontinuity of rotations at the interfaces that are not fully accounted for. Specifically, if we look at the boundary conditions that are satisfied for the FLM – case 2 (Appendix A), we see that the mid-plane rotations between sublaminate 3 and 4 are not included (i.e., $\beta^{(3)}(s-l) \neq \beta^{(4)}(s-l)$)

since, there were inadequate number of constants available to satisfy all the boundary conditions. This problem of discontinuity was probably one of the sources of error while computing the strain energy of the model. However, this issue does not affect the solution for mid-plane displacements, as seen from FEA results. The critical problem is however, the method employed to solve the governing equations for sublaminate-4 in the FLM Cases 2 and 3. In particular, the solution for $\beta^{(4)}$ is the cause of errors in the derivation of FLM – Cases 2 and 3. Consider for instance the solution of sublaminate 4 in FLM – Case 2 (Refer Fig. 3.4(b)). Following our assumptions of no lateral displacement (i.e., $W^{(4)}(y)=0$, from symmetry) and no surface shear tractions for sublaminate 4 (due to the delamination on top and model symmetry at the bottom) we arrive at the two governing equations involving $b^{(4)}$ for this sublaminate,

$$\left(D_{22}^{(3)} - \frac{B_{22}^{(3)2}}{A_{22}^{(3)}} \right) \beta_{,yy}^{(4)} + A_{44}^{(3)} \beta^{(4)} = 0 \tag{3.30}$$

$$A_{44}^{(3)} \beta_{,y}^{(4)} - P_b^{(4)} = 0 \tag{3.31}$$

Solving eq. (3.30) we get: $\beta^{(4)} = \psi_1 e^{\omega y} + \psi_2 e^{-\omega y}$, where $\omega = \sqrt{\dfrac{A_{44}^{(3)}}{D_{22}^{(3)} - \dfrac{B_{22}^{(3)2}}{A_{22}^{(3)}}}}$.

Following this solution procedure we see that the governing equation for shear, eq. (3.31), is not satisfied since, the function $P_b^{(4)}$, the peel-stress at the bottom of sublaminate-4, is unknown. While this does not affect the solutions of FLM – Case 1, the solutions of FLM – Cases 2 and 3 depend on the manner in which sublaminate 4 is

solved. In other words, the solutions for these two cases are coupled to solution of sublaminate 4 (refer to Appendix A & B for details).

From 2-D FEA simulations it is observed that this error in formulation only affects the solutions for mid-plane rotation and displacement of sublaminate 2 (Fig. 3.4(b)) (i.e. $\beta^{(2)}(y)$ and $V^{(2)}(y)$). Since these functions are important to the determination of the crack opening displacement, we can "suppress" the error by simply omitting the terms in $V^{(2)}(y)$ that has contributions from the terms from $\beta^{(2)}(y)$, i.e., We have the solution $\beta^{(2)}(y) = \sum_{j=1}^{3} \alpha_j P_j^{(2)} \sinh(\lambda_j y)$, while, $V^{(2)}(y) = \sum_{j=1}^{3} \alpha_j \gamma_j^{(2)} \sinh(\lambda_j y) + \alpha_5 y$. Hence, The corrected solution for $V^{(2)}(y)$ now becomes a simple expression: $V^{(2)}(y) = \alpha_5 y$.

By neglecting the contribution from the summation term in the solution for $V^{(2)}(y)$ the solutions for DCOD were closer to the results from 2-D FEA (section 8.1).

Going back to our exponential solutions for $\beta^{(4)}$, we see that the parameter 'w' is susceptible to numerical instabilities. It can be seen that when $A_{44}^{(3)} >> D_{22}^{(3)} - \frac{B_{22}^{(3)2}}{A_{22}^{(3)}}$, the solution for $\beta^{(4)}$ approaches physically unrealistic values at y=S, the axis along which the DCOD is computed. In Appendix A, an alternate solution is proposed to suppress this instability. In this solution, it is assumed that the shear force in the sublaminate 4 is zero. It is further assumed that $W^{(4)} \neq 0$ and $P_b^{(4)} = 0$. The boundary conditions for the sublaminate along with the above assumptions yield solutions similar to sublaminate 6, for the FLM - Case 2 (refer to Appendix A).

While, only the errors in the solution for the FLM – Case 2 are documented in this section, similar errors were seen in FLM – Case 3 for which identical methods were adopted to suppress errors and instabilities (Appendix B).

Another flaw that exists in the current (and previous, Roy and Benjamin [36]) FLM is in the modeling of the cracked sublaminate, for all cases of FLM. While, the solutions in the cracked sublaminate for all cases could adequately ensure continuity in displacements and force, it does not handle the variation of moment within the cracked sublaminate, i.e., since the cracked end at y=S in the delaminated portion of the laminate is a free surface, the moment must go to zero at the cracked surface. However in the current formulation of the cracked sublaminate the moment in the cracked lamina increases as $y \to S$. In the following section, a novel method is proposed to simulate the variation of moment with in the cracked sublaminate accurately.

3.4. Elastic Foundation

In this section an alternate solution for the cracked sublaminate is suggested. In this approach, we assume that the cracked sublaminate to be supported by a system of springs representing an elastic foundation (see Fig. 3.6), with the spring stiffness equal to $E_3/h^{(k)}$, where E_3 is the modulus of the composite in the direction normal to the mid-plane of the laminate, while $h^{(k)}$ is the thickness of the cracked layer.

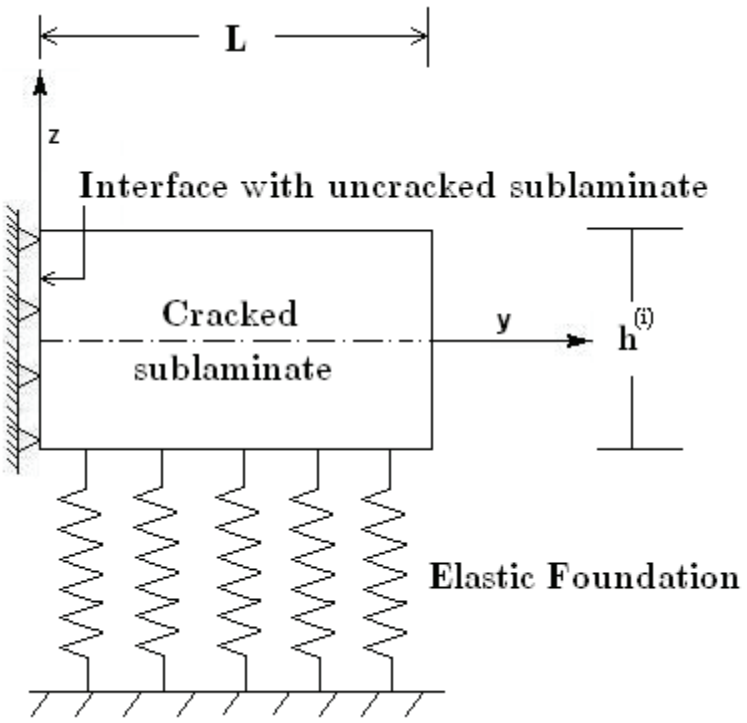

Fig. 3.6. Elastic foundation model

It is argued that through this foundation of elastic springs we can enforce the moment and shear forces with in the laminate to go to zero at the cracked surface (i.e., at y=S).

In Fig. 3.6, a general cracked sub-laminate of length L (the delamination length) is shown. The thickness of this layer is assumed to be $h^{(i)}$ (where, i = 4, 5 or 6). For the derivation that follows, we consider the case of crack in sublaminate 4 (i.e. i = 4), in which case the sublaminate is supported at the mid-plane (see Fig. 3.3(a) & (b)), so that $h^{(i)}=h^{(3)}/2$. A distributed spring system is setup at the bottom of the sublaminate such that, $P_b^{(4)} = \frac{2E_3}{h^{(3)}} W^{(4)}$. We also assume that $W^{(4)}(y) \neq 0$. Using these assumptions and the

application of the appropriate traction boundary conditions ($T_t^{(4)} = T_b^{(4)} = 0$), the governing equations for this sublaminate reduce to:

$$A_{22}^{(3)} V_{,yy}^{(4)} = 0 \tag{3.32}$$

$$D_{22}^{(3)} \beta_{,yy}^{(4)} - A_{44}^{(3)} (\beta^{(4)} + W_{,y}^{(4)}) = 0 \tag{3.33}$$

$$A_{44}^{(3)} (\beta_{,y}^{(4)} + W_{,yy}^{(4)}) - \frac{2E_3}{h^{(3)}} W^{(4)} = 0 \tag{3.34}$$

Since, the solution for eq. (3.32) is not affected with the introduction of the elastic foundation, we first consider the solution to the coupled system of equations, eqs. (3.33) and (3.34). Eliminating one of the functions in terms of another, we get the following governing equation for this sublaminate (refer to Appendix C for details).

$$D_{22}^{(3)} A_{44}^{(3)} \frac{d^4 \beta^{(4)}}{dy^4} - \frac{2D_{22}^{(3)} E_3}{h^{(3)}} \frac{d^2 \beta^{(4)}}{dy^2} + \frac{2E_3 A_{44}^{(3)}}{h^{(3)}} \beta^{(4)} = 0 \tag{3.35}$$

Assuming the solution to be of the form $\beta^{(4)} = e^{\omega y}$, we arrive at the following eigen values (4 in number) to the characteristic equation (Appendix C).

$$\omega_{(1,2,3 \text{ or } 4)} = \pm \left[\frac{E_3}{h^{(3)} A_{44}^{(3)}} \left(1 \pm \sqrt{1 - \frac{2h^{(3)} A_{44}^{(3)2}}{D_{22}^{(3)} E_3}} \right) \right]^{\frac{1}{2}} \tag{3.36}$$

If $\frac{2h^{(3)} A_{44}^{(3)2}}{D_{22}^{(3)} E_3} > 1$, then we get,

$$\beta^{(4)} = e^{C_1 y} (\psi_1 \cos C_2 y + \psi_2 \sin C_2 y) + e^{-C_1 y} (\psi_3 \cos C_2 y + \psi_4 \sin C_2 y) \tag{3.37}$$

else,

$$\beta^{(4)} = \psi_1 e^{\omega_1 y} + \psi_2 e^{-\omega_1 y} + \psi_3 e^{\omega_2 y} + \psi_4 e^{-\omega_2 y} \tag{3.38}$$

The four constants (ψ_1, ψ_2, ψ_3 & ψ_4) are solved using the following four boundary conditions,

(i) $\beta^{(3)}(S-L) = \beta^{(4)}(S-L)$
(ii) $M_M^{(3)}(S-L) = M_M^{(4)}(S-L)$
(iii) $M_M^{(4)}(S) = 0$
(iv) $Q^{(4)}(S) = 0$

Through the use of these boundary conditions, the spurious moment and the shear force at the end of the sublaminate, are effectively suppressed.

Analogously, For the FLM Cases 2 and 3, the boundary conditions are changed to suppress the high values of mid-plane rotations due to discontinuities in the FLM formulation (see section 3.2). In order to do so, the boundary condition in shear, (iv) $Q^{(i)}(S) = 0$, is replaced with $\beta^{(i)}(S) = 0$ (where, i is the cracked sublaminate). All the other equations remain unchanged ensuring that the appropriate cracked sublaminate moment and rotation continuities are enforced.

3.5. The extended FLM

Since the FLM was proposed to solve for cracks in a 90˚ oriented layer for any position of crack, the equations derived for the 90˚ cases have to be modified in-order to solve for the cracks in a general configuration of plies.

Consider a laminate configuration: $[0/\theta/90]_s$, which has the number of cracks in the layer, specified through the thickness, subjected to a mechanical and/or thermal load. Fig. 3.7, shows the angle-ply lamina (the θ oriented ply) in the global XYZ axis. The crack in 90º can be solved using the FLM case 1, while the crack in 0 and the θ ply can be analyzed using Cases 2 and 3 respectively. However, a slightly modified procedure will have to be applied to study the cracks in the 0 and θ oriented plies. Consider for now, the crack in the θ ply in-order to develop the equations for the extended FLM. The crack in this ply can be analyzed using the second case of FLM, since, the crack is located in the middle layer. However, to use the FLM Case 2 the coordinate system has to be rotated such that the orientation of the cracked layer becomes 90˚. In other words, the laminate has to be rotated such that the local axis of the θ ply coincides with the reference axis $x'y'z'$, the principle axis of the ply (see Fig. 3.7).

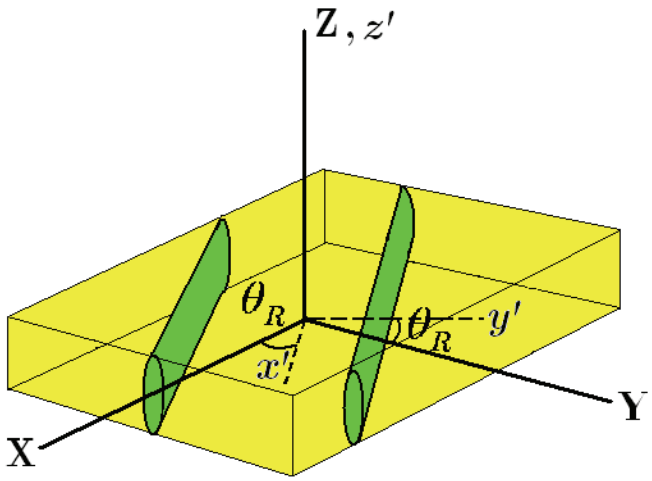

Fig. 3.7. The global XYZ and the rotated $x'y'z'$ reference frames for the angle-ply.

Through this rotation the θ ply becomes the 90 oriented ply and to which we can now use the equations developed in FLM Case 2 to solve for its DCOD. The equations below give the appropriate transformations in applied loads and material properties of the lamina (or the sublaminate). The rotation angle of the lamina, θ_R (see Fig. 3.7) is given by,

$$\theta_R = 90 - \theta \tag{3.39}$$

Since, the laminate is to be rotated about the Z axis of the global reference frame, the new orientation of the layers will be given by,

$$\phi'^{(k)} = \phi^{(k)} + \theta_R \tag{3.40}$$

Where, $\phi'^{(k)}$ is the orientation of the k^{th} ply in the $x'y'z'$ frame. $\phi^{(k)}$ is the orientation of the k^{th} ply in the XYZ frame, while θ_R is the rotation angle. It is easily seen that, if we substitute $\phi^{(k)} = \theta$ in the above equation, the angle of this ply in the $x'y'z'$ frame will be 90°. Similarly, if we substitute, $\phi^{(k)} = 0$, we will get $\theta_R = 90$ i.e., the laminate has to be rotated by 90° in-order to view the 0 as the cracked ply.

The loads (both thermal and mechanical) will also need to be transformed using the following force transformations,

$$N'_x = N_x \cos\theta_R + N_y \sin\theta_R \tag{3.41}$$

$$N'_y = N_y \cos\theta_R - N_x \sin\theta_R \tag{3.42}$$

Where,

$$N_x = N_x\,(mechanical) + N_x\,(thermal) \tag{3.43}$$

$$N_y = N_y\,(mechanical) + N_y\,(thermal) \tag{3.44}$$

In-plane shear load Nxy is ignored. The DCOD obtained in this frame (say, Δ^{xyz}) after the appropriate FLM analysis, needs to be transformed back to the original frame XYZ in-order to determine the actual value of the opening (Δ^{XYZ}). This transformation is given by,

$$\Delta^{XYZ} = \Delta^{xyz} \sin\theta_R \tag{3.45}$$

Using these equations for the extended FLM, we can now analyze a laminate of any configuration.

CHAPTER 4

THE STITCH CRACK MODEL

4.1. Introduction to Stitch Cracks

Until now it was assumed that the cracks in the composite extend though the thickness of the individual layer and that it also spans the entire width of the laminate.

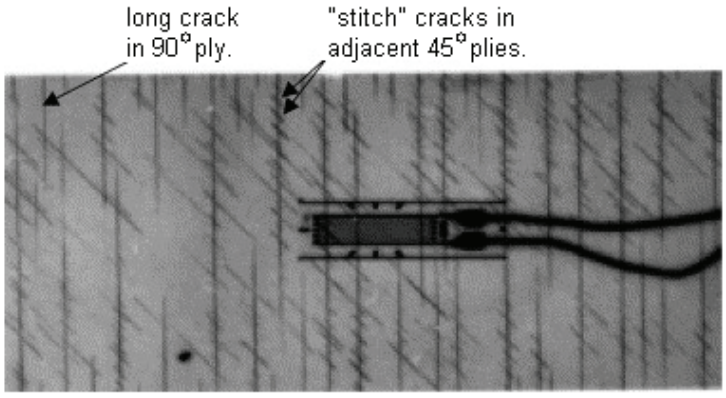

Fig. 4.1. Experimental[†] observation of stitch-cracks in a 45˚ laminate, with through (or long cracks) in the 90˚ ply.

[†] Yokozeki, T., Aoki, T., Ogasawara, T., and Takashi, I., "Effects of layup angle and ply-thickness on matrix crack interaction in contiguous plies of composite laminates", *Composites Part A: Applied Science and Manufacturing,* Vol. 36, 2005, pp. 1229-1235

However, recent experimental observations [39,41] have shown that although most cracks extend through the thickness of the ply, they do not necessarily span the entire width of the laminate. Instead, they tend to form short cracks concentrated along the intersections of the crack with the cracks in adjacent layer (see Fig. 4.1).

Aoki *et al* [39] compared cracked composites samples of orientations of 0˚, 30˚, 45˚, 60˚, 90˚. They observed that while there are long cracks (cracks that extend through the width of the lamina) in the orthotropic layers, as the fiber orientation moves away from an orthotropic configuration the cracks show a greater tendency to accumulate as stitches around the intersections with cracks in the adjacent layers. They observed that the stitch cracks typically do not extend through the width of the ply, even though they might extend through thickness of the lamina (see Fig. 4.1). Bechel *et al* [41] had made similar observations for the cracks in $[0/45/-45/90]_s$. They observed that the majority of the cracks in the off axis plies (i.e., +45 and -45) fit the description of stitch cracks.

Due to this stitch like pattern of the cracks within the lamina, there will be significantly more resistance offered by the laminate to permeation than if these were long cracks. The FLM, on the other hand, considers the cracks to extend through the width of the lamina, hence the permeability predicted by a FLM analysis will be higher. The stitch crack model proposed below, provides a sample methodology to simulate this 3-D phenomena within the framework of 2-D FLM.

4.2. The FLM Stitch Crack

The idea of the FLM stitch crack model will be to simulate the overall reduction in crack opening displacement (COD) in the laminate due to the presence of stitch cracks in the place of long cracks. Fig. 4.2, depicts the top view of stitch cracks in a generic angle-ply lamina with orientation angle θ, with long cracks in the adjacent 0˚ ply. As shown in the schematic, the cracks in the angle ply do not develop through the full extent of the width of the laminate, and usually end up as stitches concentrated along the seam of a 0˚ (or 90˚) ply.

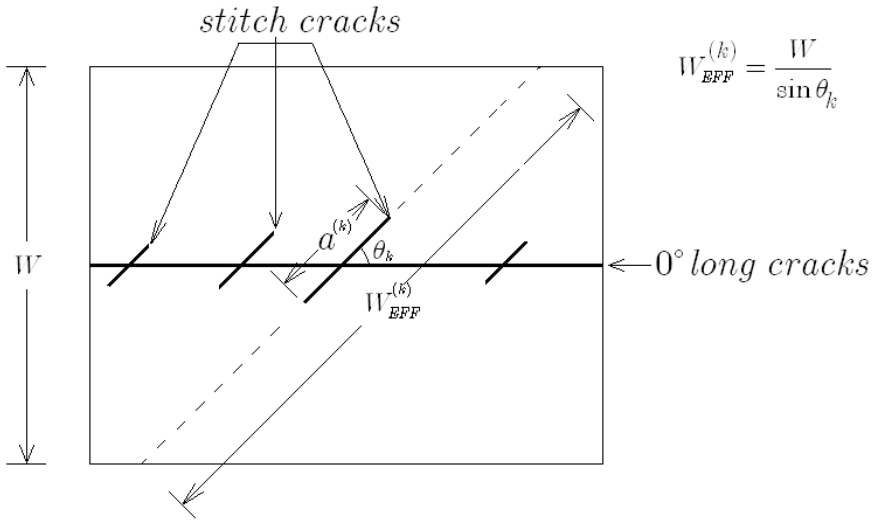

Fig. 4.2. Top view sketch of stitch-cracks in the angle-ply laminate, with through (or long) cracks in the 0˚ ply.

To model this phenomenon, a linear spring at the end of the cracked surface to represent the effective stiffness of the un-cracked ligament in the cracked sublaminate is employed (see Fig. 4.3). This implies that the DCOD for a stitch crack in an angle ply

lamina will be less than that for a long crack due to the constraining effect of the uncracked ligament(s). We could simply write the effective spring stiffness ' $K_{spring}^{(k)}$ ' as,

$$K_{spring}^{(k)} = \varepsilon^{(k)} A_{22}^{(k)} \tag{4.1}$$

with,

$$\varepsilon^{(k)} = \frac{W_{EFF}^{(k)} - a^{(k)}}{W_{EFF}^{(k)}} \tag{4.2}$$

Where, $W_{EFF}^{(k)}$ is the effective width of a fully developed (long) crack in the kth angle-ply (see Fig. 4.2), 'a$^{(k)}$' is the total length of the stitch cracks (i.e. summation of individual lengths). $A_{22}^{(k)}$ is the extensional stiffness of the cracked ply perpendicular to the crack plane. It can be seen that when $\varepsilon^{(k)} = 0$ stitch cracks have coalesced into a "long crack", while, $\varepsilon^{(k)} = 1$ implies that the lamina is uncracked.

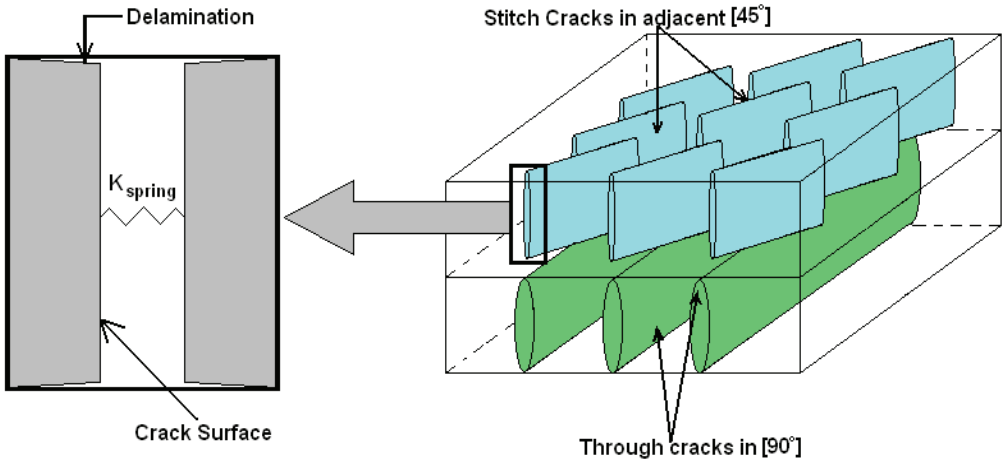

Fig. 4.3. 3-D view of stitch cracks in a 45° ply, with the equivalent FLM spring model

Fig. 4.3, depicts the configuration of the effective "spring" within the cracked sublaminate. Appendix D has the derivation of the solutions for the spring model. The effective spring model was verified using 2-D FEA and then implemented in the permeation prediction model as well.

CHAPTER 5

STRAIN ENERGY RELEASE RATE

5.1. Introduction to Strain Energy Release Rate

In this section a generalized model to determine the damage evolution parameters for the FLM subjected to general loading is developed. The model for the strain energy release rate (SERR) for matrix cracking and delamination growth is determined for the FLM based on the equivalent constraint model (ECM) by Zhang *et al* [21]. As per the assumptions of the ECM, the laminate is assumed to be a perfectly bonded set of damaged laminates. Zhang *et al* [15, 21] has proposed the use of an in-situ damage effective function (IDEF) to evaluate the degradation in stiffness of the laminate system as a function of the loss of load carrying capacity of the cracked 90˚ plies. The model presented in this thesis will follow the idea of ECM, however, unlike [21], whose focus was to define the damage growth in the model in terms of the IDEF, the damage parameters will follow the classical definition. In this report, the matrix crack evolution is assumed to be self-similar and uniform, hence the Griffith's energy balance equation is employed to model this phenomenon. For delamination growth, the model is developed based on the stiffness degradation of the laminate with increasing delamination length to

which we can use the basic definitions of energy release rate to evaluate the damage growth. Also, the damage model suggested in [21] has been extended to include the effect of thermal loads on the damaged laminate. Note that in the sections to follow, the 'd' superscript will be used to represent a damage state variable.

5.2. Potential Energy

Following Zhang *et al* [18], the potential energy for the damaged system is derived in terms of the stiffness reduction parameters. To simplify the formulation, only the reduction in extensional stiffness of the laminate is considered.

From Zhang *et al* [18, 21] we define, the overall or total strain of the laminate as,

$$\varepsilon_y = \frac{V^{(k)}(S)}{S} \tag{5.1}$$

Where, $V^{(k)}(S)$ is the displacement of the uncracked sublaminate at y=S, e.g., for the FLM Case 2, k=4 or 6. Now, define N as the applied mechanical load and N_T as the total thermal load given by,

$$N_T = 2\left(\bar{Q}_{22}^{(1)} h^{(1)} \int_{T_{ref}}^{T_f} \bar{\alpha}_y^{(1)} dT + \bar{Q}_{22}^{(2)} h^{(2)} \int_{T_{ref}}^{T_f} \bar{\alpha}_y^{(2)} dT + \bar{Q}_{22}^{(3)} h^{(3)} \int_{T_{ref}}^{T_f} \bar{\alpha}_y^{(3)} dT \right) \tag{5.2}$$

From [18], we have the constitutive law for the laminate for the ECM as,

$$\{\mathbf{N}\} = [\mathbf{A}](\{\bar{\boldsymbol{\varepsilon}}\} - \{\bar{\boldsymbol{\varepsilon}}^{\mathbf{p}}\}) \tag{5.3}$$

Where, $\{\mathbf{N}\}$ is the load force vector, $[\mathbf{A}]$ is the extensional stiffness matrix of the damaged laminate, $\{\bar{\boldsymbol{\varepsilon}}\}$ is the macro-strain vector [18] of the laminate, while $\{\bar{\boldsymbol{\varepsilon}}^{\mathbf{p}}\}$ is defined as,

$$\{\bar{\boldsymbol{\varepsilon}}^{\mathbf{p}}\} = [\mathbf{A}]^{-1}(\{\mathbf{N}^{\mathbf{T}}\} + \{\mathbf{N}^{\mathbf{H}}\}) - [\mathbf{A}^{0}]^{-1}(\{\mathbf{N}^{0\mathbf{T}}\} + \{\mathbf{N}^{0\mathbf{H}}\}) \tag{5.4}$$

Where, $\{\mathbf{N}^{\mathbf{T}}\}$, $\{\mathbf{N}^{\mathbf{H}}\}$ and $\{\mathbf{N}^{0\mathbf{T}}\}$, $\{\mathbf{N}^{0\mathbf{H}}\}$ are the effective damaged and undamaged thermal and hygro load vectors, respectively, calculated using the appropriate reduced stiffnesses in the resultant thermal and hygro-force equations from classical lamination theory (Jones [46]).

The derivation in this thesis, does not consider the effect of moisture diffusion. Hence, ignoring the hygro-loads, assuming plain strain conditions in the laminate width direction and neglecting the shear coupling terms in eq. (5.4) we get the expression,

$$N = A_{22}^{d}\left(\varepsilon_y - \frac{N_T}{A_{22}^{d}} + \int_{T_{ref}}^{T_f} \bar{\alpha}_y dT\right)$$

$$\Rightarrow A_{22}^{d} = \frac{N + N_T}{\varepsilon_y + \int_{T_{ref}}^{T_f} \bar{\alpha}_y dT} = \frac{N + N_T}{\varepsilon} \tag{5.5}$$

Where, $\varepsilon = \varepsilon_y + \int_{T_{ref}}^{T_f} \bar{\alpha}_y dT$, $\bar{\alpha}_y$ is the effective thermal coefficient of expansion of the laminate in the global 'y' direction. Note that the undamaged total thermal load N_T is used instead of N_T^d (the total thermal load calculated using the damaged stiffnesses of the laminas). This was done to reduce the complexity of the final equations. As a result of

this assumption the damaged stiffness of the laminate predicted by eq. (5.5) will always be higher than the actual damaged stiffness of the laminate. It can be seen that when there is no thermal load on the laminate eq. (5.5) reduces to the case presented in [21]:

$$A_{22}^{d} = \frac{N}{\varepsilon_{y}} \tag{5.6}$$

From [18] and [21], for a specimen of gage length 2S and unit width, we have the strain energy (U) of the laminate as,

$$U = \frac{1}{2}(A_{22}^{d}\varepsilon^{2}) \cdot (2S) = A_{22}^{d}\varepsilon^{2}S \tag{5.7}$$

The work done by the external applied load 'N' will be (from [18] and [21]),

$$W = N\varepsilon_{y}2S \tag{5.8}$$

The potential energy (π) of the laminate can be now calculated using the equation below.

$$\pi(S, L, N, \Delta T) = U - W \tag{5.9}$$

5.3. Strain Energy Release Rate for Matrix Cracks

The matrix crack multiplication in the cracked ply is assumed to occur in a self-similar manner. Shown in Fig. 5.1, is the self-similar initiation of the crack within the cracked ply.

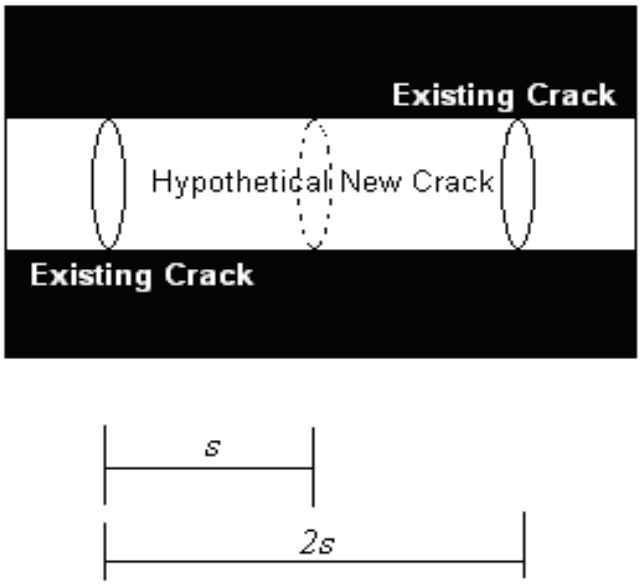

Fig. 5.1. Model of the two systems with existing and hypothetical cracks

If it is assumed that cracks exist within the cracked ply are equally spaced at 2S, then the new crack will be formed at y=S, i.e., half-way between the two existing cracks. The new cracked surface area formed will be, $(2h^{(k)})*(1)$, assuming unit width (under plain strain conditions) with, $h^{(k)}$ as the thickness of the k^{th} cracked ply.

Mcmanus and Maddocks [30] used a shear-lag type analysis and the self-similar crack formation concept to evaluate the mode I release rate. Extending the Griffiths energy balance criterion for self similar crack formation (under fixed load conditons), we have the SERR for the k^{th} cracked ply as,

$$G_I^{(k)} = -\frac{2\pi(S/2) - \pi(S)}{2h^{(k)}} \tag{5.10}$$

Where, $\pi(S)$ is the potential energy of the system with the crack spacing of 2S while $\pi(S/2)$ is the potential energy of the laminate system with a crack spacing of S.

The potential is evaluated keeping the applied load(s) and delamination length constant. The results from this analysis are compared and verified with results from 2-D finite element analysis (FEA) in Section 8.4.

5.3. Strain Energy Release Rate for Delamination Growth

The delamination propogation is assumed to occur at the interface between the cracked and uncracked ply under pure mode II conditions. 2-D FEA solutions (section 6.4) show that the above assumption is correct for a 2-D delamination analysis. The mode II strain energy release rate is defined as the first partial derivative of the potential energy of the system with respect to the total delaminated crack surface area, with the applied load kept constant. We can write the SERR in mode II for the k^{th} cracked ply as,

$$G_{II}^{(k)} = -\frac{1}{4}\frac{\partial \pi}{\partial L}\bigg|_{N,\Delta T} \tag{5.11}$$

The model has been compared and verified using 2-D FEA. The results to the verification are tabulated in section 8.4.

CHAPTER 6

FINITE ELEMENT MODELING

6.1. Introduction

The finite element analysis (FEA) was used to verify the analytical solutions for crack opening and strain energy release rates derived in earlier chapters. The analysis was done using the commercially available FEA code, ABAQUS®. The non-linear solver available in ABAQUS, was used in all the analyses. The benchmark FEA models for all problems were 2-D. Even though ABAQUS has an option to create 2-D models of composite laminas, it was not used. Instead, the analysis employed the orthotropic and anisotropic elastic material models available in ABAQUS, because of the 3-D nature of the problems solved with respect to the orientation of the plies and the applied load. In all FEA models, contact controls were used at the interface of the delaminations, in-order to prevent the inter-penetration of the two surfaces that came into contact during the analysis.

6.2. Delaminated Crack Opening Displacement

The delaminated crack opening displacement (DCOD) obtained from the 3 cases of FLM was verified for the quasi-isotropic configuration $[0/45/-45/90]_s$. The verification was run for the cases of crack in each of the four individual plies of the above laminate. It should be noted that, the verification for the outer (0) and middle (±45) plies were done for their rotated counterparts (refer section 3.4 for details) of the FLM, since the modeling of these cracks as inclined to the loading direction would have been complicated. The verification for the 90 ply is straight forward since the FLM case 1 can be directly used with out any further rotation. In order to simulate FLM conditions, the FEA models were constructed assuming that there is only a single cracked ply and all the other plies remain intact and that there are no interactions between cracks in adjacent layers.

The delamination and matrix cracks were modeled by manipulation of the input file to ABAQUS. At the required position of matrix crack (or delamination) a line of duplicate nodes with identical coordinates were created and the connectivity of the associated elements were changed to create the crack model. Fig. 6.1., illustrates this idea. Two dimensional, 8 node, plain-strain quadrilateral elements were used to discretize the geometry (available in ABAQUS as CPE8R).

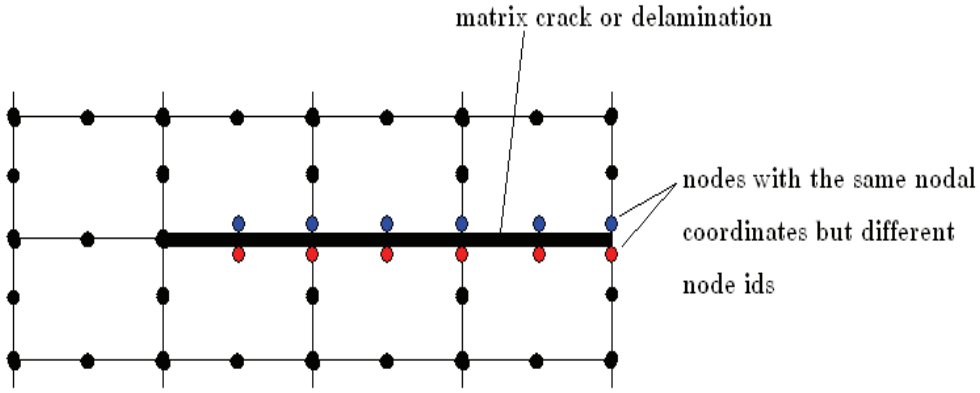

Fig.6.1. FEA model of crack

Figures 6.2 – 6.5, show the two-dimenesional FEA models associated with each case of FLM verification. Due to mid-plane symmetry only one-half of the laminate geometry was modeled. For the case of cracks in 0, +45 and -45, the layers were rotated using the equations from the extended FLM (section 3.4). In the figures below, the rotated orientations of each layer for the respective case of FLM are indicated. Fig. 6.2, is the model to verify the FLM case 1, Fig. 6.3 and Fig. 6.4 is to verify FLM case 2, while Fig. 6.5 is the model to verify the results from FLM case 3.

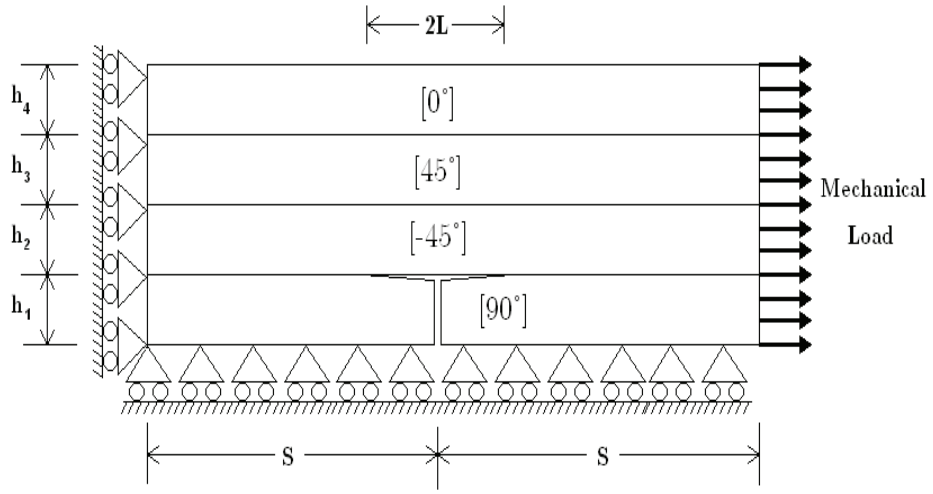

Fig. 6.2. FEA model for FLM case 1 (crack in 90˚)

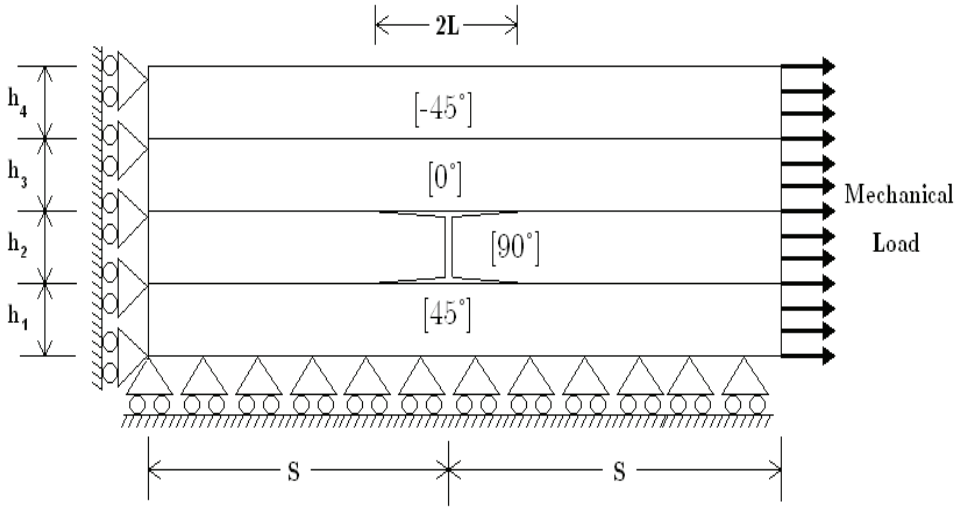

Fig. 6.3. FEA model for FLM case 2 (crack in -45˚)

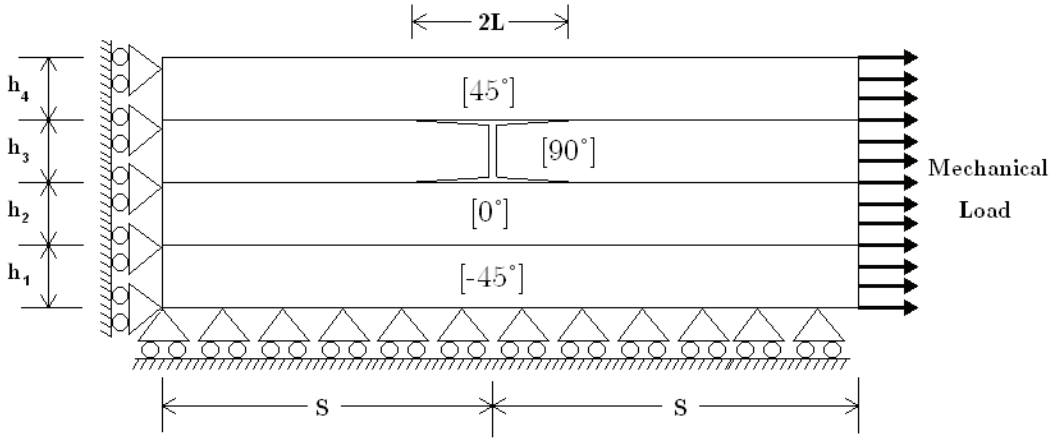

Fig. 6.4. FEA model for FLM case 2 (crack in +45˚)

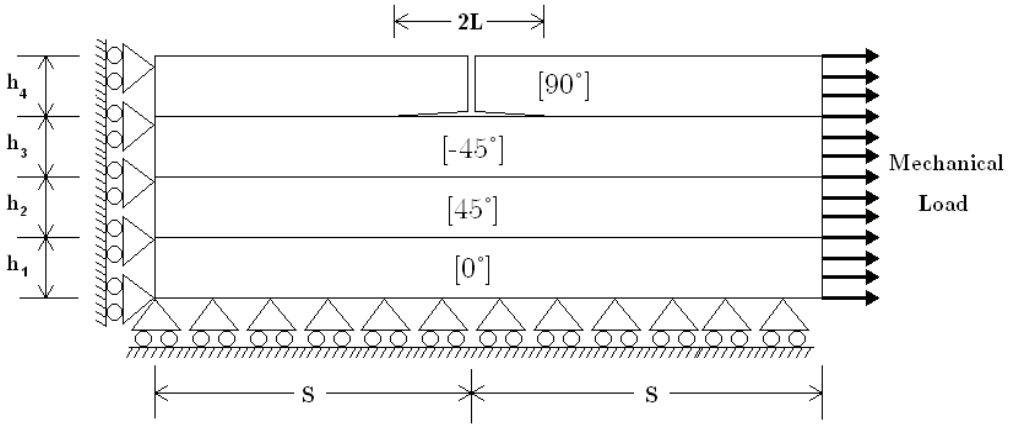

Fig. 6.5. FEA model for FLM case 2 (crack in 0˚)

The thicknesses for all the plies were the same (h_1= h_2= h_3= h_4=0.003”). A crack density of 2.5 cracks per inch (S=0.2 inches) was assumed. The delamination length (L) was 0.03 inches. The material used was IM7/5250-4 graphite-epoxy composite (see Table for properties). The mechanical load was applied as a surface traction on the edge as shown in the figures. The magnitude of the applied surface traction = $\frac{N}{2\cdot(h_1+h_2+h_3+h_4)}$

lbs/inch^2, where N=500 lbs/inch, applied in the direction as shown in the schematic. For the thermal case, a constant through the thickness temperature field was applied to the model. The field had an initial value equal to zero and a final value equal to the ΔT applied to FLM. The results of the thermal and mechanical load analysis are given in section 8.1.

6.2. Stitch Crack

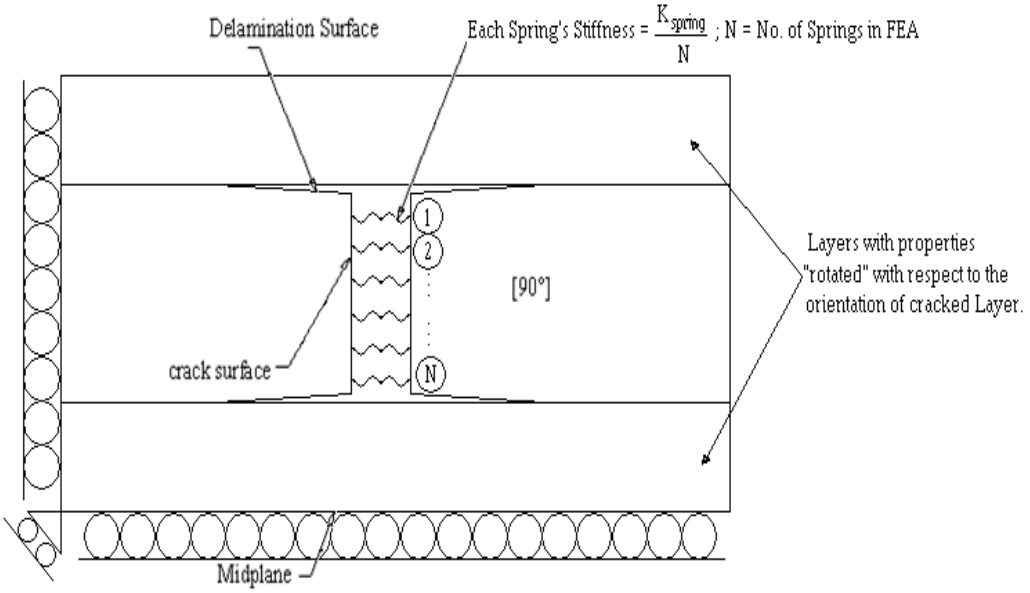

Fig. 6.6. 2-D FEA model of Spring Crack Model

Fig. 6.6, shows the 2-D FEA model constructed to verify the FLM-Spring Model. The material chosen was IM7/5250-4 with the $[0/45/-45/90]_s$ lay-up. As mentioned before, since the stitch cracks tend to form only in the angle-plies, the DCOD values was only verified for the ±45˚ layers. A crack spacing of 0.2 inches with a delamination length of 0.03 inches was used as geometry input to the FLM. As can be seen from Fig.

6.6, a distributed spring system was chosen in the FEA model to simulate the single spring in FLM inorder to prevent local distortions to the crack face in FEA model. The spring system in the FEA simulation was chosen so that it was equivalent to the single spring used in FLM (the stiffness of each FEA spring was = K_{spring}/N, where N is the number of springs in the FEA model). Section 8.3 describes the results to the variation of DCOD with decreasing spring stiffness in a thermal loading condition (ΔT=-760.8˚F) and applied mechanical load condition (N=500lbs/inch) for the cases of stitch cracks in 45 and -45.

6.3. Strain Energy Release Rate for Matrix Cracking

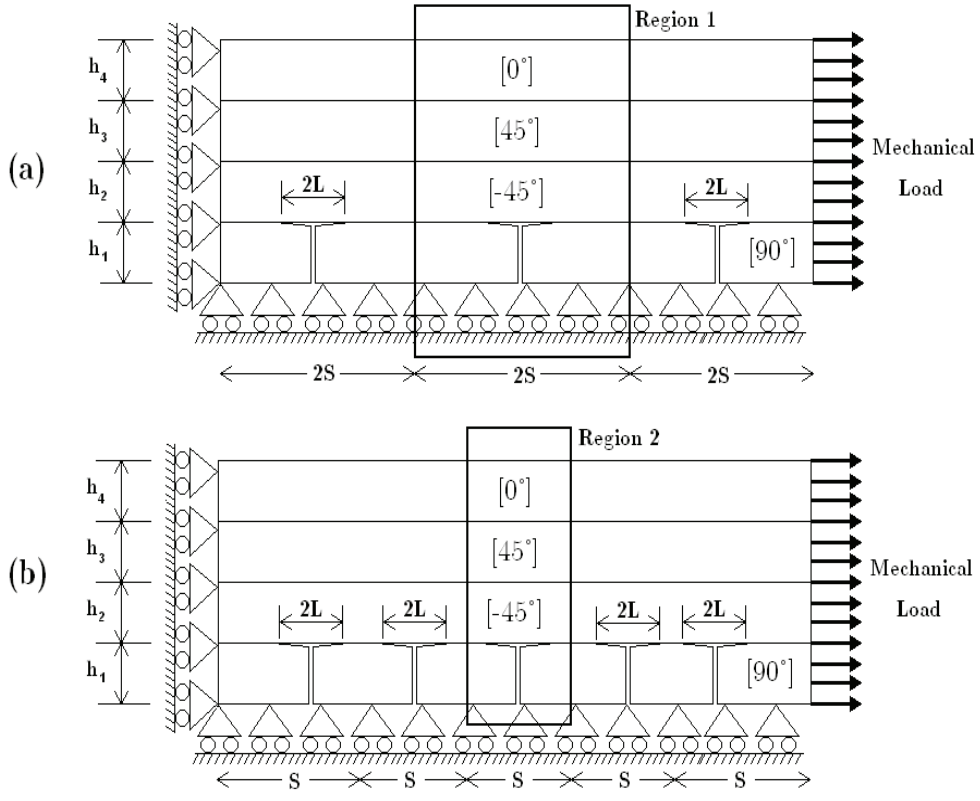

Fig. 6.7. FEA models for SERR: Matrix Cracking

The strain energy release rate (SERR) for matrix cracking was determined from FEA using the self-similar crack growth concept used in FLM (refer to section 5.3). The SERR solutions for the cracking of the mid 90 ply group of the $[0/45/-45/90]_s$ configuration was determined and compared with FEA. From symmetry, only half the geometry was modeled for analysis.

In the first step, the model is assumed to have an array of cracks with a crack spacing 2S that corresponds to the initial crack density (Fig. 6.7(a)). The FEA is then performed with an applied mechanical load (or applied thermal field). In the second step, a second model is created with reduced crack spacing, S, and FEA simulation is run again, with the applied loads remaining the same. The total strain energy is then computed for the two models in region 1, $U_{\text{REGION 1}}$ (in Fig. 6.7(a)) and region 2, $U_{\text{REGION 2}}$ (in Fig. 6.7(b)), The strain energy release rate can be then determined from the Griffith's energy balance equation,

$$G_I = \frac{4U_{\text{REGION 2}} - 2U_{\text{REGION 1}}}{2h_3} \tag{6.1}$$

If $G_I < G_{Ic}$ the critical strain energy release rate for mode I matrix crack, the load is increased and the analysis is performed again. The process is repeated until we reach the critical applied load, i.e. the load at which, $G_I = G_{Ic}$. Fig. 6.8, has the logic for the above described iterative technique.

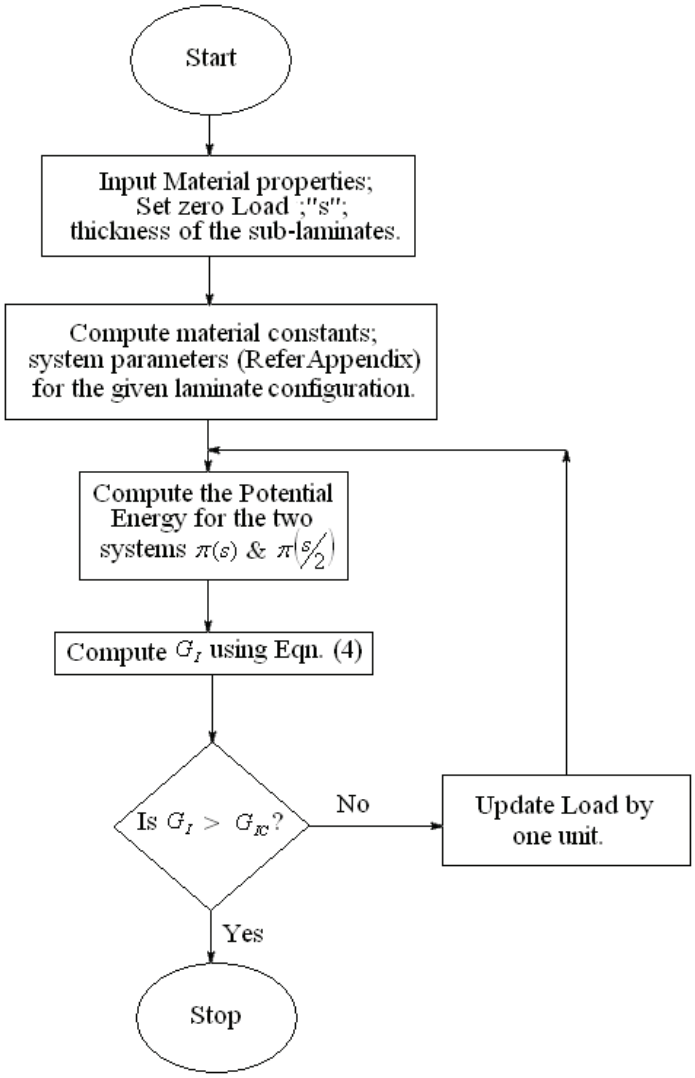

Fig. 6.8. Flow chart for determination of critical applied load.

The applied critical load (in both mechanical and thermal loading conditions) for the crack densities: 2.5 and 5 cracks per meter were determined using FLM and verified using the process discussed above. Section 8.4 has the results to the verification.

6.4. Strain Energy Release Rate for Delamination Growth

The delamination growth predicted by the FLM case 1, for the crack in the 90 ply of a $[0/45/-45/90]_s$ composite was compared with the values from 2-D FEA. Unlike the model for matrix crack formation, the delamination growth is assumed to be continuous and propagating within the cracked and uncracked ply interface (in this example at the interface between -45 and 90 layers). We assume that the delamination growth is primarily a mode II phenomenon, and thus it is dominated by the shear forces acting at the crack tip. The FEA solutions show that this assumption of mode II crack growth is correct for the delamination lengths considered in this study. Fig. 6.9, is the schematic of the FEA model used.

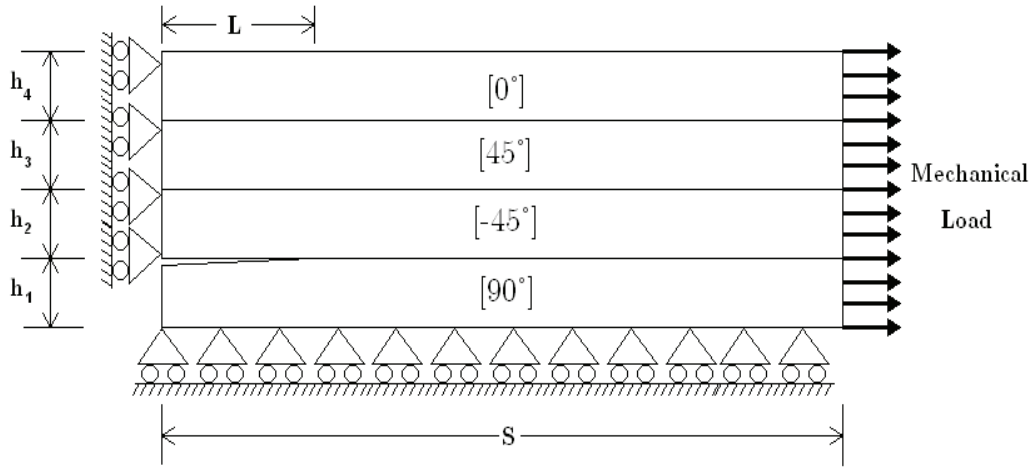

Fig. 6.9. FEA model for Delamination Growth

The FEA model for delamination analysis uses the quarter symmetry model for analysis, since there is a need for a highly refined mesh at the crack tip. Fig. 6.10, shows the FEA mesh used for the analysis.

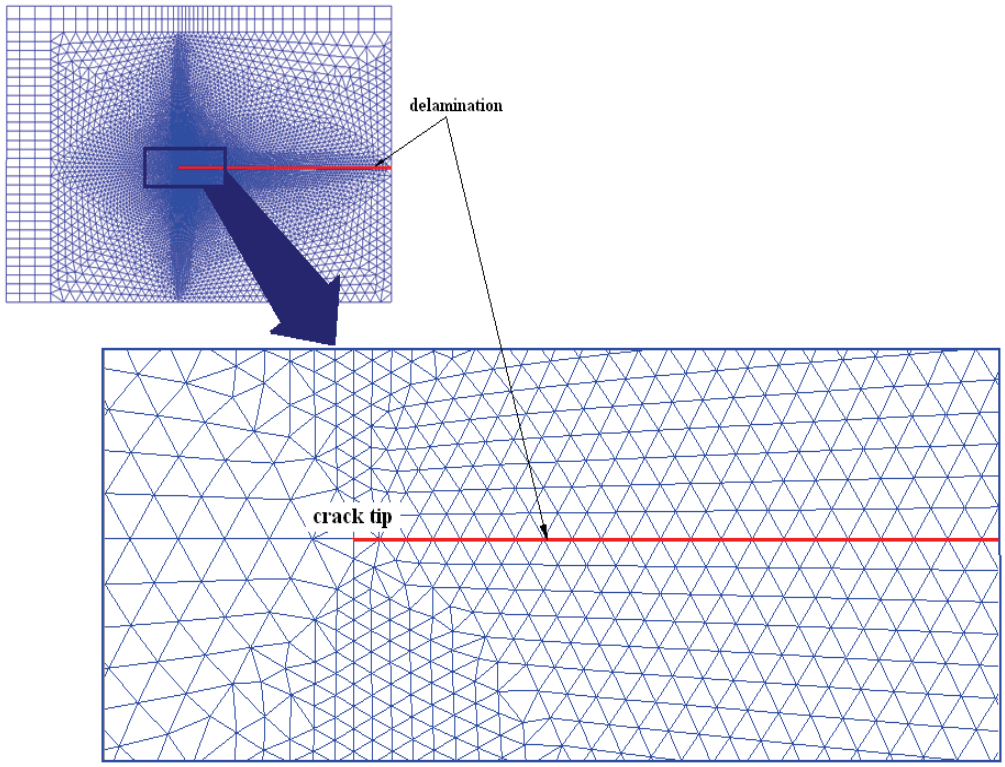

Fig. 6.10. FEA mesh for delamination

From Fig. 6.10, we can see that the mesh is non-uniform and refined at the crack tip. The modified one-step virtual crack closure technique (VCCT) Krueger [45] was used to evaluate the mode II SERR at the crack-tip. As per the self-similar crack growth assumptions of the virtual crack closure technique, we assume that energy released when the crack is extended from L+ΔL to L+2ΔL, is the same as the energy required to close the cracks from node m to node k (refer to Fig. 6.11). The modified crack closure further assumes that the extension of the crack from node i to node k (or from node k to node m) does not significantly alter the displacements behind the crack (or the forces at the crack tip), i.e., the displacements behind node k is approximately equal to the displacements behind the original crack at node i.

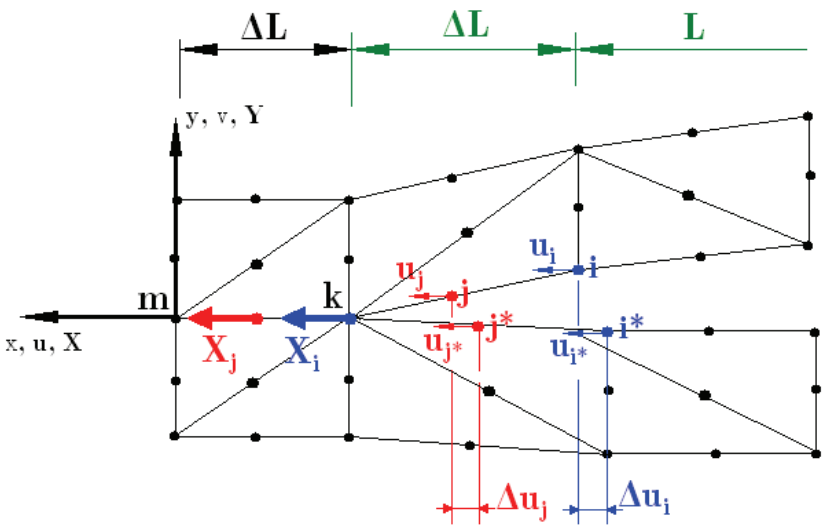

Fig. 6.11. The one step VCCT

From VCCT, we have the energy release rate as,

$$G_{II} = -\frac{1}{2\Delta L}\left(X_i(u_i - u_{i^*}) + X_j(u_j - u_{j^*})\right) = -\frac{1}{2\Delta L}\left(X_i\Delta u_i + X_j\Delta u_j\right) \tag{6.2}$$

It is evident that this modified one-step procedure is only applicable for refined meshes, since a coarse mesh at the crack tip would invalidate the assumptions of the VCCT. The mesh used in FEA model had non-uniform lengths for elements around the crack tip. Hence, the eq. (6.2) has to be modified slightly to include this non-uniformity of element lengths. From [45], we have the modified formula for energy release rate as,

$$G_{II} = -\frac{1}{2\Delta L_1}\left(X_i\Delta u_i + X_j\Delta u_j\right)\sqrt{\frac{\Delta L_1}{\Delta L_2}} \tag{6.3}$$

Where, ΔL_1 is the element length behind the crack tip (the distance between node i and k) while ΔL_2 is the the element length ahead of the crack tip (the distance between

node m and k). The value of L=0.005m was used for the analysis. Note that the delamination length used is large but, was employed in the interest of theoretical validation. The G_{II} values from FEA and FLM was verified for four crack densities: 2.5, 5, 10 cracks per meter, for the same delamination length and keeping the load applied in FEA and FLM the same. Comparison of solutions for G_{II} from the thermal case and mechanical case are given in Section 8.4.

CHAPTER 7

PERMEATION MODEL

7.1. Introduction

In the recent past, much scientific effort has been spent to learn the permeation characteristics of damaged composite structures. Extensive experimental work [38-42, 44] has been performed in this area to characterize permeation in composites according to the damage state in the composite and permeant leakage. In this section, the extended FLM discussed earlier (section 3.4) will be used to calculate the delaminated crack opening displacement (DCOD) distribution through the thickness of a cracked composite laminate of given damage state and loading condition (mechanical and/or thermal), which will be subsequently input into the permeability model to calculate the permeability of the cracked composite.

The permeability model presented in this thesis is the work already reported by Roy and Benjamin [36]. However, the model presented in [36] lacked experimental verification and was only used to theoretically study the permeation characteristics of IM7/PETI-5 orthotropic laminates. In this thesis the model is extended to study a generic configuration plies and is verified through comparison with experimental data provided

by Bechel [40]. Since, the model here is an extension to the one presented in [36], only the more important equations of the analysis are repeated here.

7.2. Permeability modeling

The analytical model for permeation follows Darcy's assumptions for flow through porous media. From the assumptions of Darcy's law we have the mass flow rate (U) through the composite damaged laminate given by,

$$U = C_{total}\Delta P \tag{7.1}$$

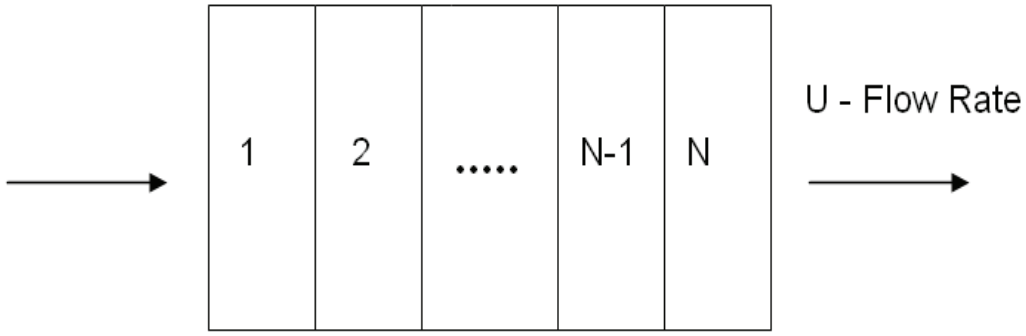

Fig. 7.1. Conductance through composite laminate

Where, C_{total} is the total conductance of the damaged laminate in the thickness direction and ΔP is the total pressure drop across the thickness of the laminate. Further the conductance (C_{total}) for a series of damaged plies (see Fig. 7.1) is given by,

$$C_{total} = \left[\sum_{K=1}^{N}\left(\frac{1}{C_K}\right)\right]^{-1} \tag{7.2}$$

Where, C_K is the conductance of the K^{th} layer, of a composite with N plies. With these assumptions we can now derive the equations for the micro-crack permeation model. Fig. 7.2 is the top view of the junction of two idealized intersecting micro-cracks in the K^{th} and $K+1^{th}$ plies.

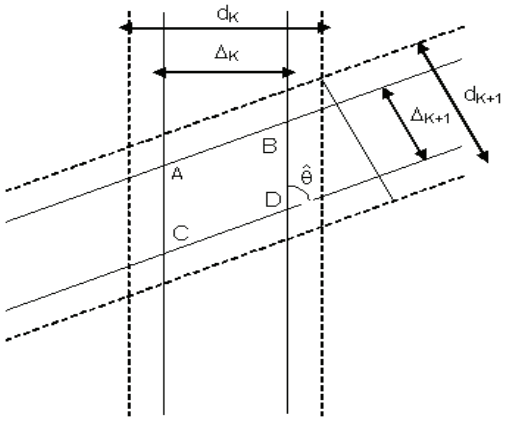

Fig. 7.2. Top view of two intersecting micro-cracks in a laminate

From the figure above we see that the area formed from the intersection of the two cracks is given by the trapezoid ABCD. That is the overlap area for the K^{th} interface will be,

$$\text{area } \overline{\text{ABCD}} = \frac{\Delta_K . \Delta_{K+1}}{\sin\hat{\theta}} \tag{7.3}$$

Where, Δ_K and Δ_{K+1} are the delaminated crack opening diplacements (DCOD) of the K^{th} and $K+1^{th}$ ply, and $\hat{\theta}$ is the angle between the fiber directions of the K^{th} and $K+1^{th}$ ply. As see from the derivations for the FLM in chapter 3 we know that the DCOD Δ_K and Δ_{K+1} are functions of the delamination lengths d_K and d_{K+1} (shown in Fig. 7.2) of its respective layer, i.e., $\Delta_K = \Delta_K(d_K)$ while $\Delta_{K+1} = \Delta_{K+1}(d_{K+1})$.

For a given crack density in the K^{th} ply (N_K) and the $K+1^{th}$ ply (N_{K+1}), we can write the total overlap area (Ω_K) as,

$$\Omega_K = \frac{N_K N_{K+1} \Delta_K \Delta_{K+1}}{\sin\hat{\theta}} \tag{7.4}$$

Assuming that the conductance at the interface is proportional to the DCOD overlap area [44] we have for the K^{th} cracked layer,

$$C_K = \hat{C}\Omega_K \tag{7.5}$$

Where, $\hat{C}$ is a material constant that needs to be characterized from experimental data. Hence, from eq. (7.4), (7.5) and using relation (7.2) for total conductance we get,

$$C_{total} = \hat{C}\left[\sum_{K=1}^{N}\left(\frac{\sin\hat{\theta}}{N_K N_{K+1}\Delta_K\Delta_{K+1}}\right)\right]^{-1} \tag{7.6}$$

From (7.1) and (7.6) we get,

$$U = \hat{C}\left[\sum_{K=1}^{N}\left(\frac{\sin\hat{\theta}}{N_K N_{K+1}\Delta_K\Delta_{K+1}}\right)\right]^{-1}\Delta P \tag{7.7}$$

From Darcy's law for isothermal, viscous flow of gases through porous media we have,

$$\rho u = \frac{-B_o M}{RT\eta} P \frac{dP}{dX} \tag{7.8}$$

Where, r is the density of the fluid (or the permeant), B_o is the permeability of the material, h is the viscosity of the fluid, P the pressure, M the molecular weight of the gas, T is the temperature and R is the universal gas constant. Assuming that the flow is in the X-direction (with 'X' denoting the thickness direction) and u is the velocity component in the X-direction we get 'ρu' as the mass flow per unit area in the X-direction. In other words we have, $U = \rho u$, by definition.

Integrating eq. (7.8) [36, 43] and applying the pressure boundary conditions of P_1 at $X = X_1$ and P_2 at $X = X_2$, we get,

$$U = \rho u = \left(\frac{-B_o M P_{AVG}}{RT\eta h} \right) \Delta P \tag{7.9}$$

Where, P_{AVG} is the average pressure $\left(= \frac{P_1 + P_2}{2} \right)$ and $\Delta P = P_2 - P_1$, the pressure differential, while h is the layer thickness ($h = X_2 - X_1$). Comparing eq. (7.7) and (7.9) we obtain,

$$B_o = C \left[\sum_{K=1}^{N} \left(\frac{\sin \hat{\theta}}{N_K N_{K+1} \Delta_K \Delta_{K+1}} \right) \right]^{-1} \tag{7.10}$$

Where, $$C = \frac{\hat{C} RT\eta h}{M P_{AVG}}$$

Using eq. (7.10) we can determine the permeability B_o for any composite with known crack density and delamination data, subjected to thermo-mechanical loads.

The analytical model for permeability was verified using experimental data from Bechel [40] for the IM7/5250-4 composite laminate of lay-up $[0/45/-45/90]_s$. The

characterization of the material constant C was obtained for this material using a combination of experimental and analytical results. The same material constant C was then used to predict the permeability of the composite laminate. The detailed procedure for the characterization of C and the experimental verification of the permeability predictions are discussed in section 8.5.

CHAPTER 8

RESULTS AND DISCUSSION

8.1. FLM

The finite element analysis models to determine the DCOD(s) for the [0/45/-45/90]s carbon/epoxy composite was created as described in section 6.1. The laminate has equal thickness plies of 0.003 inch. The material used is IM7/5250-4 (see Table 8.1 for properties). All cases of the FLM were verified for mechanical load (N=500lbs/inch) and thermal load (ΔT=-760.8˚F). The results to the mechanical analysis are tabulated in Table 8.2, while the thermal case results are given in Table 8.3. Fig. 8.1 to 8.4 show the DCOD profile comparisons for each individual ply in the $[0/45/-45/90]_s$ laminate from FLM and 2-D FEA for the mechanical case. Fig. 8.5 to 8.8, are the DCOD profiles from the thermal analysis. Equations from Elastic foundation (section 3.4) were used in the analysis of the cracked layers, in which the rotation and moment at the boundary of the delaminated portion were set to zero. As a result of these boundary conditions, the DCOD profiles for the crack face will always be a straight line, as can be seen from the Figures 8.1 – 8.8. We can see from the results that the FLM compares very well with FEA for each ply, for the mechanical loading case. However for the thermal case, since the FLM

is linear through-the-thickness it is unable to capture the non-linear deformation of the delaminated beam at y=S, as depicted in Fig. 8.5 to 8.8.

Table 8.1. Material properties of IM7/5250-4 (Bechel *et al* [41])

E_1 (GPa)	174
E_2 (GPa)	11
G_{12} (GPa)	5.5
ν_{12}	0.31
α_1 (x 10^{-6} ε/°C)	0.25
α_2 (x 10^{-6} ε/°C)	25

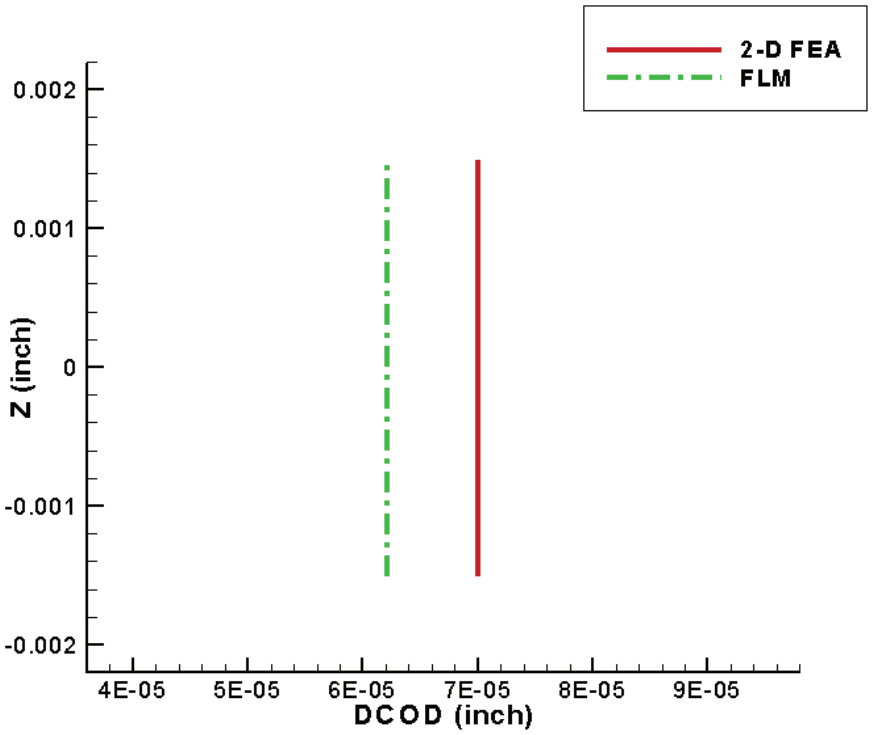

Fig. 8.1. Crack Profile Comparison FLM – 2-D FEA for $[0/45/-45/90]_S$ IM7/5250-4 laminate with crack in 0˚ layer: N = 500 lbs/inch, L=0.03", S=0.20"

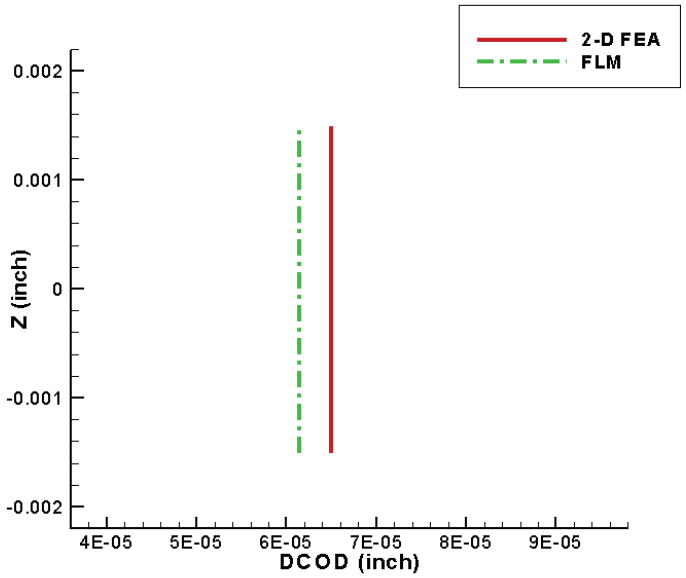

Fig. 8.2. Crack Profile Comparison FLM – 2-D FEA for $[0/45/-45/90]_S$ IM7/5250-4 laminate with crack in 45˚ layer: N = 500 lbs/inch, L=0.03”, S=0.20”

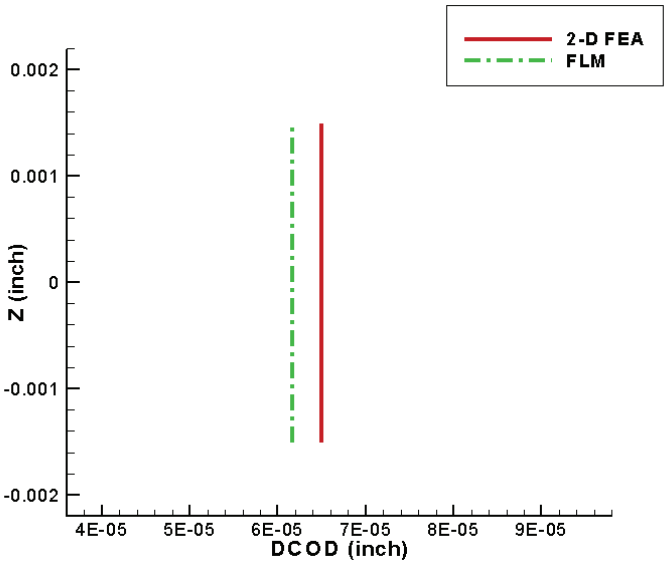

Fig. 8.3. Crack Profile Comparison FLM – 2-D FEA for $[0/45/-45/90]_S$ IM7/5250-4 laminate with crack in -45˚ layer: N = 500 lbs/inch, L=0.03”, S=0.20”

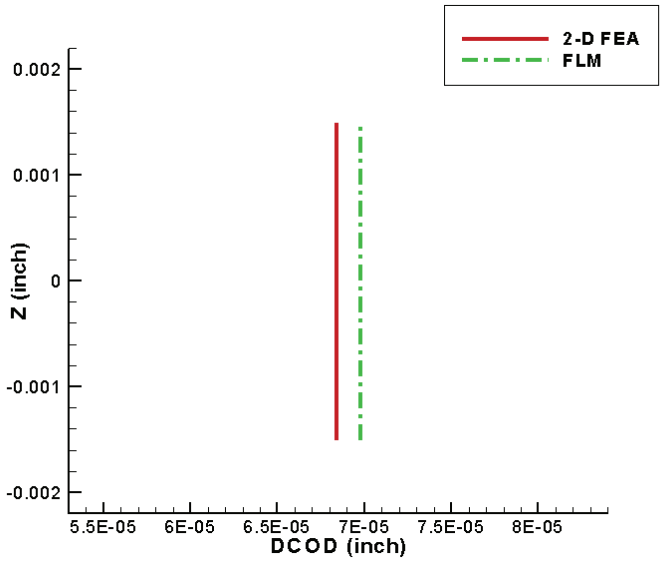

Fig. 8.4. Crack Profile Comparison FLM – 2-D FEA for $[0/45/-45/90]_S$ IM7/5250-4 laminate with crack in 90˚ layer: N = 500 lbs/inch, L=0.03", S=0.20"

Table 8.2. DCOD Predictions: Enhanced FLM – 2-D FEA $[0/45/-45/90]_s$ laminate, under mechanical load

$[0/45/-45/90]_S$ IM7/5250-4	**S** 0.20 inch **L** 0.03 inch	
N= 500 lb/inch		
Layer	**FLM DCOD Inch**	**2D FEA DCOD Inch**	**% Error**
0°	6.217×10^{-05}	7.002×10^{-05}	-11.21
45°	6.141×10^{-05}	6.498×10^{-05}	-5.49
-45°	6.167×10^{-05}	6.503×10^{-05}	-5.16
90°	6.981×10^{-05}	6.843×10^{-05}	2.02

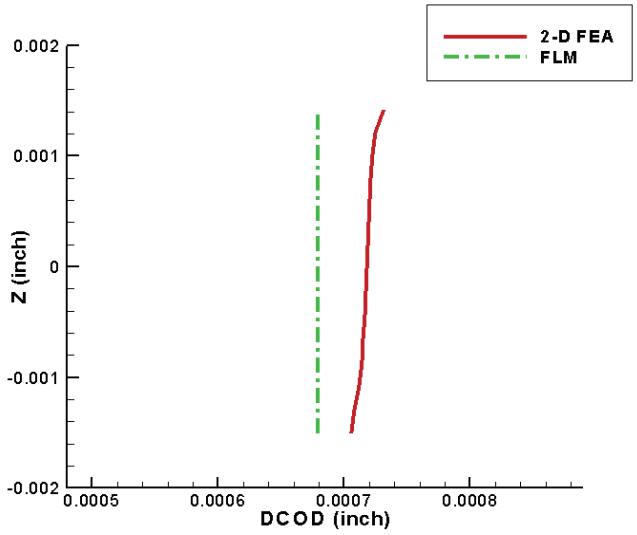

Fig. 8.5. Crack Profile Comparison FLM – 2-D FEA for $[0/45/-45/90]_S$ IM7/5250-4 laminate with crack in 0˚ layer: ΔT = -760.8˚F, L=0.03”, S=0.20”

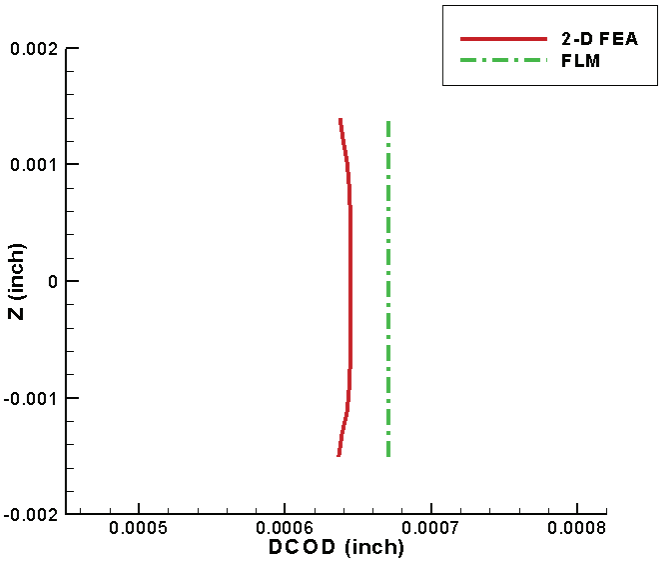

Fig. 8.6. Crack Profile Comparison FLM – 2-D FEA for $[0/45/-45/90]_S$ IM7/5250-4 laminate with crack in 45˚ layer: ΔT = -760.8˚F, L=0.03”, S=0.20”

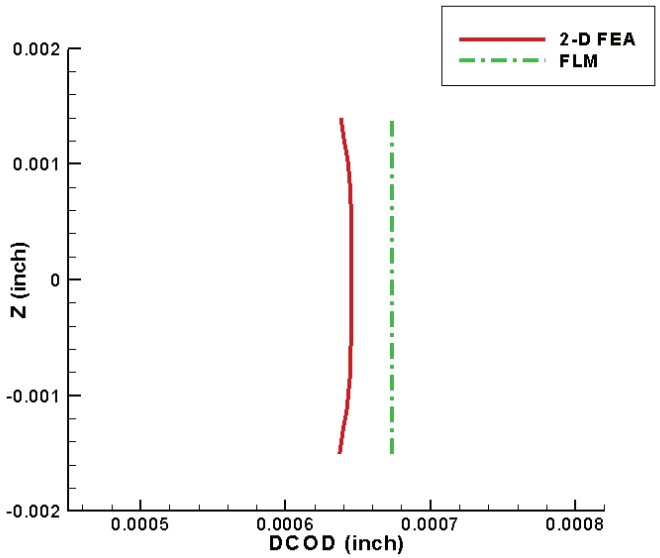

Fig. 8.7. Crack Profile Comparison FLM – 2-D FEA for $[0/45/-45/90]_S$ IM7/5250-4 laminate with crack in 0˚ layer: ΔT = -760.8˚F, L=0.03”, S=0.20”

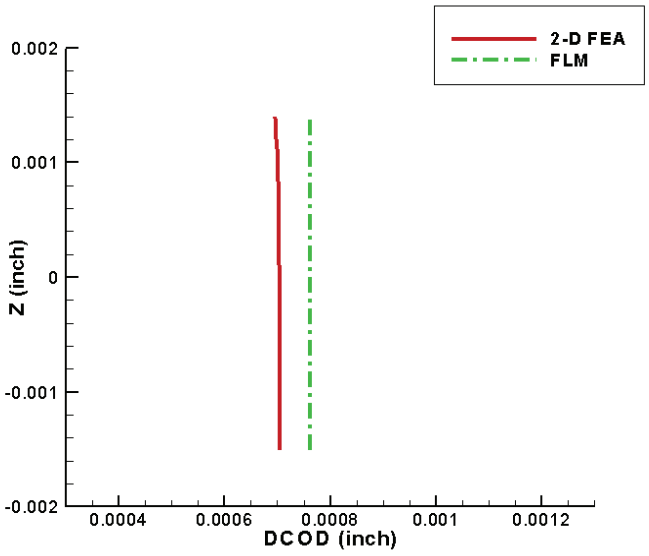

Fig. 8.8. Crack Profile Comparison FLM – 2-D FEA for $[0/45/-45/90]_S$ IM7/5250-4 laminate with crack in 0˚ layer: ΔT = -760.8˚F, L=0.03”, S=0.20”

Table 8.3. DCOD Predictions: Enhanced FLM – 2-D FEA
$[0/45/-45/90]_s$ laminate, under thermal load.

$[0/45/-45/90]_S$ IM7/5250-4	**S = 0.20 inch L = 0.03 inch**		
$\Delta T = -760.8\ ^0F$			
Layer	**FLM DCOD Inch**	**2D FEA DCOD Inch**	**% Error**
0°	6.792×10^{-04}	7.059×10^{-04}	-3.77
45°	6.709×10^{-04}	6.369×10^{-04}	5.34
-45°	6.738×10^{-04}	6.372×10^{-04}	5.74
90°	7.627×10^{-04}	6.949×10^{-04}	9.75

8.2. Stitch Crack

Figures 8.9-8.12 are plots comparing the results from the extended FLM analysis with stitch cracks (Chapter 4) and 2-D FEA. The stitch crack model was applied to five cases of laminate width. As per the spring crack formulation in FLM, the percentage of through cracked can be converted to an equivalent spring stiffness, using equations discussed in Chapter 4. The analysis was performed for the ±45˚ plies of the $[0/45/-45/90]_S$ IM7/5250-4 laminate (S=0.2", L=0.03"), for both thermal (ΔT = -760.8˚F) and mechanical (N=500lbs/in) cases. Fig. 8.9 and 8.10 are the results from comparison of the FLM-2-D FEA for +45 and -45 ply for mechanical loading, while Fig. 8.11 and 8.12 are the results for +45 and -45 from thermal load case, respectively.

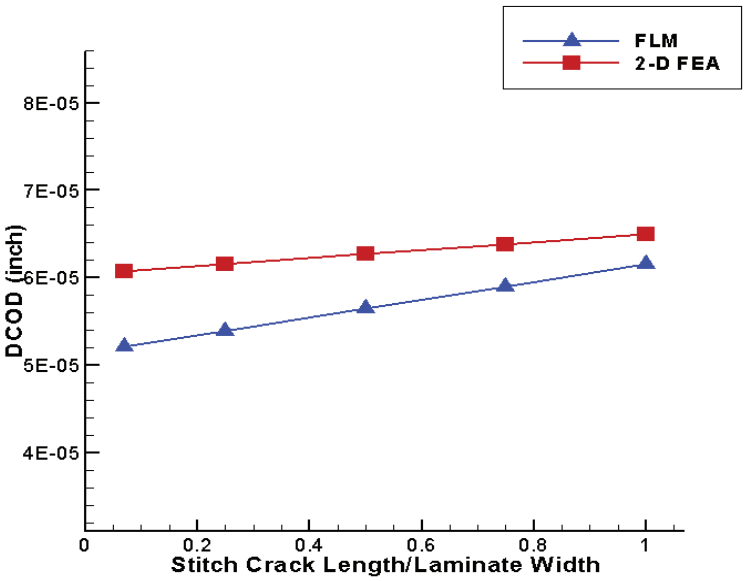

Fig. 8.9. DCOD vs. Stitch Crack Length for cracks in +45 Mechanical load, N=500lbs/in, L=0.03", S=0.20".

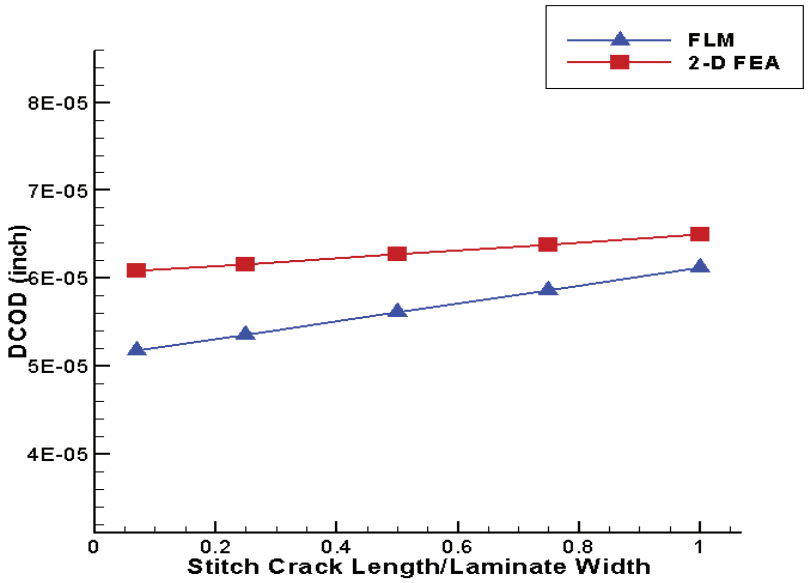

Fig. 8.10. DCOD vs. Stitch Crack Length for cracks in -45 Mechanical load, N=500lbs/in, L=0.03", S=0.20".

Table. 8.4. DCOD comparisons FLM-FEA for stitch crack model, Mechanical load case

	DCOD for +45 for N=500lbs/in, L=0.03", S=0.20"			DCOD for -45 for N=500lbs/in, L=0.03", S=0.20"		
a/W	FLM (inch)	2-D FEA (inch)	%Error	FLM (inch)	2-D FEA (inch)	%Error
0.07	$5.21x10^{-05}$	$6.08x10^{-05}$	-14.24	$5.18x10^{-05}$	$6.09x10^{-05}$	-14.98
0.25	$5.39x10^{-05}$	$6.16x10^{-05}$	-12.40	$5.35x10^{-05}$	$6.16x10^{-05}$	-13.09
0.50	$5.65 x10^{-5}$	$6.27x10^{-05}$	-9.91	$5.61x10^{-05}$	$6.27x10^{-05}$	-10.62
0.75	$5.90 x10^{-5}$	$6.38x10^{-05}$	-7.50	$5.86x10^{-05}$	$6.38x10^{-05}$	-8.23
1	$6.16x10^{-05}$	$6.50x10^{-05}$	-5.18	$6.12x10^{-05}$	$6.50x10^{-05}$	-5.93

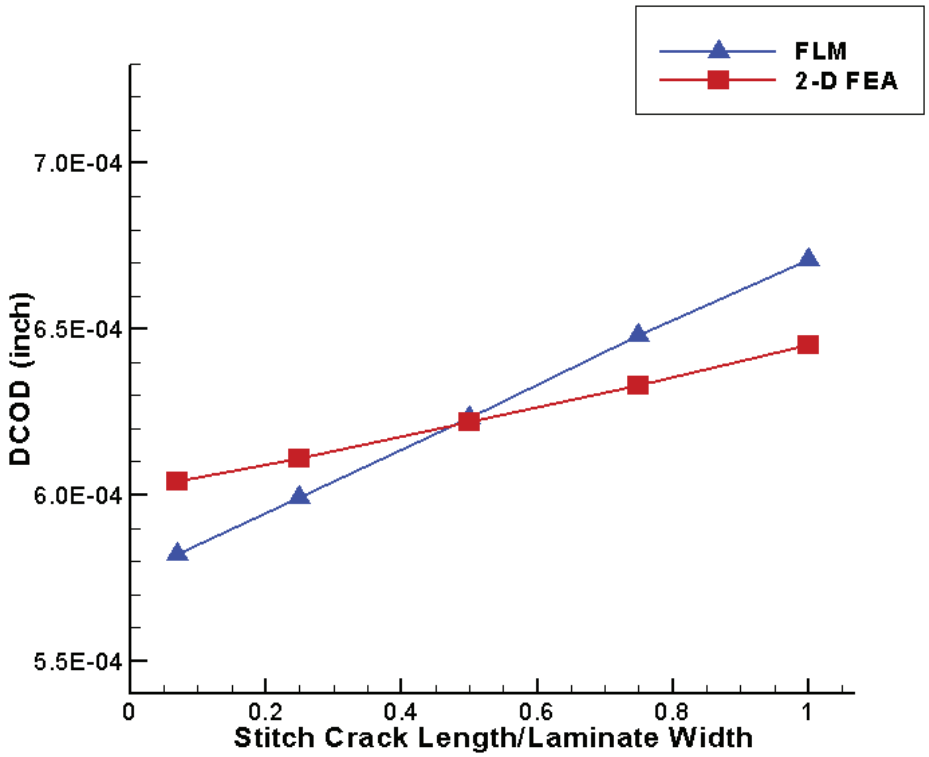

Fig. 8.11. DCOD vs. Stitch Crack Length for cracks in +45 Mechanical load, ΔT = -760.8˚F, L=0.03", S=0.20".

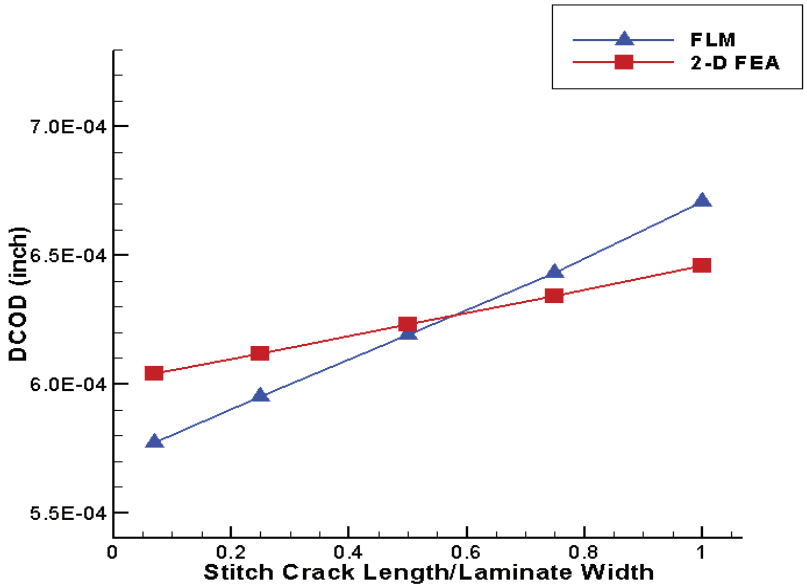

Fig. 8.12. DCOD vs. Stitch Crack Length for cracks in -45 Mechanical load, ΔT = -760.8˚F, L=0.03", S=0.20".

Table. 8.5. DCOD comparisons FLM-FEA for stitch crack model, Thermal load case

	DCOD for +45 for ΔT = -760.8˚F, L=0.03", S=0.20"			DCOD for -45 for ΔT = -760.8˚F, L=0.03", S=0.20"		
a/W	FLM (inch)	2-D FEA (inch)	%Error	FLM (inch)	2-D FEA (inch)	%Error
0.07	$5.82\text{x}10^{-04}$	$6.04\text{x}10^{-04}$	-3.63	$5.77\text{x}10^{-04}$	$6.04\text{x}10^{-04}$	-4.39
0.25	$5.99\text{x}10^{-04}$	$6.11\text{x}10^{-04}$	-2.00	$5.95\text{x}10^{-04}$	$6.12\text{x}10^{-04}$	-2.77
0.50	$6.23\text{x}10^{-04}$	$6.22\text{x}10^{-04}$	0.20	$6.19\text{x}10^{-04}$	$6.23\text{x}10^{-04}$	-0.59
0.75	$6.48\text{x}10^{-04}$	$6.33\text{x}10^{-04}$	2.32	$6.43\text{x}10^{-04}$	$6.34\text{x}10^{-04}$	1.51
1	$6.71\text{x}10^{-04}$	$6.45\text{x}10^{-04}$	5.34	$6.74\text{x}10^{-04}$	$6.46\text{x}10^{-04}$	5.74

The crack openings given above are not the actual openings, The true or projected opening for the laminate can be calculated by multiplying the above values with √2 (refer section 3.5 for details). As can be seen from the plots above, the FLM-spring model has the same the trends for both the mechanical and thermal load cases.

8.3. Strain Energy Release Rate

The FEA models discussed in section 6.3 and 6.4 were employed to compare with the results from FLM for both mode I and mode II energy release rate. As before the material used is IM7/5250-4 laminate of lay-up $[0/45/-45/90]_S$. The mode I and mode II SERR were compared for the case of crack in the 90 ply of the above composite (FLM Case 1).

For mode I, the critical load (the applied load at which the energy release rate is equal to G_{IC}, the critical energy release rate) was computed for crack densities of 0.0635 and 0.127 cracks/inch (2.5 and 5 cracks/m), using Griffith's energy balance equation [eq.(5.9)] for both thermal and mechanical load cases. The delamination length for both these cases were kept constant at L=0.197 inch (0.005 m), for all cases of crack density (CD). Given in Table 8.6 are comparisons of FLM with FEA, for the mode I critical applied load assuming G_{IC}=1.6 lbs/inch (280 N/m) (from Bechel *et al* [39],[41]).

Table 8.6. Critical Applied Load comparisons FLM – 2-D FEA

	Critical Mechanical load			Critical Thermal Load		
Crack Density (cracks/inch)	FLM (lbs/inch)	2-D FEA (lbs/inch)	%Error	FLM (˚F)	2-D FEA (˚F)	%Error
0.0635	16559.44	18272.48	-9.37	-213.88	-183.82	16.35
0.127	16559.44	18272.48	-9.37	-213.88	-183.82	16.35

As observed from the results for mode I, we see that the FLM under predicts the critical mechanical load and over-predicts the critical applied thermal load. While, under-prediction in load cases can be considered conservative with respect to the crack-initiation, over prediction of the critical thermal load implies that the number of cracks

formed in this layer as predicted by FLM, will likely be lower in comparison with the actual experimental results. However, since the mode I model has been verified only with numerical simulation it is recommended that the results be checked against monotonic-tensile loaded composite specimens to verify the solutions from the current mode I damage model.

For the verification of mode II, the laminate was considered with three different cases of crack spacing: S=1.97 inch (0.05m), S=3.94 inch (0.1m) and S=7.87 inch (0.2m). The energy release rate from FLM was found by solving (eq.5.11) numerically. The virtual crack closure technique (VCCT) was used to evaluate the energy release rate from 2-D FEA. Identical loads were applied both to the FLM and FEA models and the resulting mode II energy release rate from the two analyses were compared. The results from the comparisons are tabulated in Table 8.7, indicating reasonable agreement, with FEA with FLM predictions consistently conservative.

Table 8.7. G_{II} comparisons FLM – 2-D FEA

	G_{II} for Mechanical load ($N=18.3x10^3$ lbs/inch)			G_{II} for Thermal Load ($\Delta T = -184^{\circ}F$)		
Crack Density (cracks/inch)	FLM (N/m)	2-D FEA (N/m)	%Error	FLM (N/m)	2-D FEA (N/m)	%Error
0.0635	0.343	0.249	37.83	0.218	0.173	25.79
0.127	0.343	0.255	34.54	0.218	0.181	20.56
0.254	0.343	0.255	34.39	0.218	0.204	7.06

The damage model verified above, was subsequently used to study the variation of critical applied load for both the mechanical and thermal loading cases. Fig. 8.13 and 8.14, show the variation of crack density in the 90˚ layer of a [0/45/-45/90]s IM7/5250-4

composite for mechanical and thermal loading cases. The effect of delamination length on the crack initiation is also presented in Fig. 8.13 and 8.14.

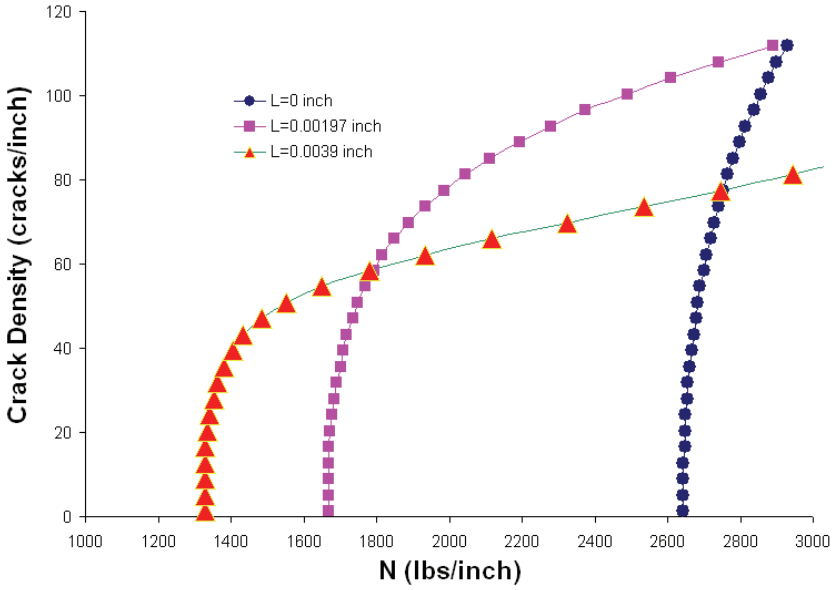

Fig. 8.13. Crack Density vs. Critical Applied Mechanical load

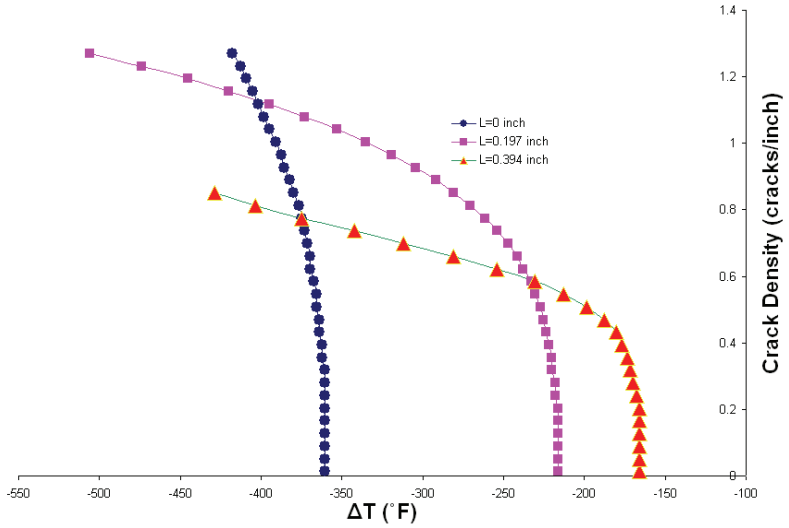

Fig. 8.14. Crack Density vs. Critical Applied Thermal Load

From the figures above, a similarity in the trends for the pure mechanical and pure thermal loading cases can be observed. First we see that for lower crack densities the applied load initially remains constant until a critical crack spacing is reached after which

the cracks within the system increases exponentially with linear increase in load. This was also observed in shear-lag solutions of Mcmanus and Maddocks [30]. Initially, for lower crack densities, the cracks spacing is wide enough so that the critical stress required to initiate the crack at the required position (refer section 5.1) is always available. However, as the cracks get closer, for the same applied load, the critical stress midway between any two cracks decreases, and therefore the crack initiation load increases.

However, with increase in delamination length the mechanics behind crack multiplication changes. With increase in delamination length the load transferred to the adjacent uncracked ply is decreased, Hence, sufficient strain energy is still available for the crack to initiate and that too at a lower load (with respect to an un-delaminated laminate).

8.4. Permeability

In this section, the permeability model proposed in Chapter 7, is validated using experimental data from Bechel *et al* [41] for the IM7/5250-4 composite of lay-up: $[0/45/-45/90]_s$. The laminate is of thickness 0.13 mm, with equal thickness plies. Bechel *et al* induced cracks in the composite laminate through thermal cycling (See Ref. [28],[38],[41]). Bechel *et al* [41], has compiled data for cycling composite laminates, and provided crack density data for every 250 cycles starting from 750 through to 1250 for three different temperature profiles (-196˚C to 177˚C, -196˚C to 120˚C and -196˚C to room temperature) and also measured the permeability of the damaged composite for each temperature profile at both cryogenic temperature (in liquid nitrogen, -196˚C) and

room temperature. Table 8.8 shows the average crack density data from their thermal-cycling experiments, while Table 8.9 is the permeability of the damaged cycled composite laminates measured by Bechel *et al* [41] at both room temperature and liquid nitrogen temperature. The permeation data for the composite samples cycled from -196˚C to room temperature (RT) are not reported since, they did not to experience appreciable permeation at both room and cryogenic temperatures.

Table 8.8. Crack densities in IM7/5250-4 $[0/45/-45/90]_s$ vs. thermal cycle profile

Cycling profiles :		-196˚C to 177˚C (cracks/cm)	-196˚C to 120˚C (cracks/cm)	-196˚C to RT (cracks/cm)
750 cycles	plies 1, 8	12.08	9.03	4.33
	plies 2, 7	6.92	2.82	0.1
	plies 3, 6	0.63	0.04	0
	plies 4, 5	1.13	0.34	0.2
1000 cycles	plies 1, 8	12.21	9.84	5.97
	plies 2, 7	10.45	3.93	0.1
	plies 3, 6	4.08	0.14	0
	plies 4, 5	6.66	0.34	0.2
1250 cycles	plies 1, 8	13.41	10.36	not tested
	plies 2, 7	13.76	4.91	not tested
	plies 3, 6	6.89	0.42	not tested
	plies 4, 5	6.52	0.44	not tested

Table 8.9. Permeability vs. thermal cycle profile (Bechel *et al* [41])

Cycles	Permeability at Room Temperature	
	-196˚C to 177˚C (scc/s-cm^2)	-196˚C to 120˚C (scc/s-cm^2)
750	5.49 x10^{-08}	1.15 x10^{-09}
1000	5.28 x10^{-06}	1.47 x10^{-08}
1250	1.75 x10^{-05}	1.80 x10^{-07}
Cycles	Permeability at LN_2 Temperature	
	-196˚C to 177˚C (scc/s-cm^2)	-196˚C to 120˚C (scc/s-cm^2)
750	6.23 x10^{-07}	1.15 x10^{-09}
1000	6.87 x10^{-05}	4.11 x10^{-07}
1250	2.75 x10^{-04}	3.60 x10^{-06}

In this thesis, crack densities from the -196˚C to 177˚C range thermal cycling was input to the extended FLM proposed in Chapter 3, to predict the DCOD distribution through the thickness of the $[0/45/-45/90]_s$ laminate. Since, considerable permeation only occured for experiments at liquid nitrogen temperature conditions, the experimental data from the cryogenic tests (Bechel *et al* [41]) for this temperature profile were used to validate the model. For the FLM, a thermal load of -760.8˚F was applied to simulate the temperature drop from cure ($T_{initial}$=440˚F) to test (T_{final}=-320.8˚F) temperature. The material properties (listed in Table 8.1) were assumed not to vary with temperature although, the FLM non-linear (NL), in which the material property varies with temperature, could be used as easily, once we know the variation of the material properties with temperature.

Table 8.10. Assumed delamination lengths in IM7/5250-4 $[0/45/-45/90]_s$ vs. thermal cycle profile

Cycling profiles : -196˚C to 177˚C		Delamination length (in inch)
750 cycles	plies 1, 8	0
	plies 2, 7	0
	plies 3, 6	0.0109
	plies 4, 5	0
1000 cycles	plies 1, 8	0.0010
	plies 2, 7	0.0011
	plies 3, 6	0.0029
	plies 4, 5	0.0018
1250 cycles	plies 1, 8	0.0018
	plies 2, 7	0.0017
	plies 3, 6	0.0034
	plies 4, 5	0.0036

Since experimental measurements of the delamination lengths were not available and because delamination length is an important input parameter to the FLM, an evolving delamination distribution that increases with number of cycles was assumed. It was assumed for the 750 cycles the 0˚(Plies 1 and 8) , 45˚(Plies 2 and 7) and 90˚(Plies 4 and 5) do not have any delaminations with the exception of the -45 (Plies 3 and 6) where the delamination was assumed to be 3.5% of its crack spacing (crack spacing 'S'=1/(2CD), where CD is the crack density). For the 1000 and 1250 cycles, the delaminations of each layer was assumed, respectively, to be 6% and 12% of the crack spacing (S) of that layer, respectively. Table 8.10 shows the delamination lengths assumed in each ply for the three cycles.

The FLM was then used to evaluate the normalized permeability (B_o/C) for the 750, 1000, 1250 cycles. The model was also run for different percentages of through cracks in the ±45 plies (both plies having the same amount of stitch cracks), starting from 7, 25, 50, 75 and 100%. This was done in order to conduct a parametric sensitivity study on the effect of the length of stitch cracks on the permeability of the laminate. The stitch crack model (Chapter 4) was used in the extended FLM to calculate the DCOD for the ±45 plies. An estimation for the conductance 'C' was made using the experimental value for permeability at 1000 cycles and the value for (B_o/C) from the FLM with 7% through cracks at 1000 cycles, i.e.:

For the case of 7% through cracked, $(B_o/C)_{FLM}$ for 1000 cycles = $3.022\text{x}10^{-07}$.

From Table 8.9, the experimental value of $(B_o)_{1000}$ at LN_2 temperature = $6.870\text{x}10^{-05}$ scc/s-cm^2.

Hence, $C = \dfrac{(B_o)_{1000}}{(B_o/C)_{FLM}} = \dfrac{6.870\text{x}10^{-05}}{3.022\text{x}10^{-07}} = 2273.103$ scc/s-cm^2.

The value calculated for the conductance 'C' was then used to predict the permeability for the 750 and 1250 cycles (for various lengths of stitch cracks). Fig. 8.15, is the plot of permeability calculated from FLM compared with the experimental data from Bechel *et al* [41].

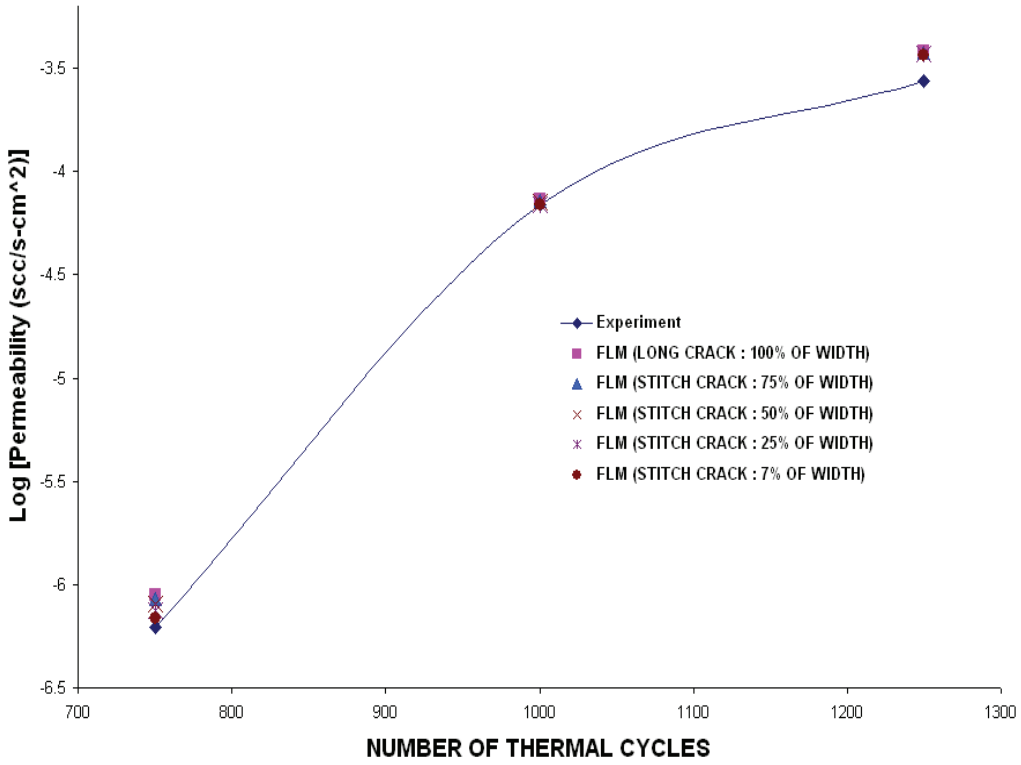

Fig. 8.15. Log [Permeability (scc/s-cm^2)] vs. Number of thermal cycles

Table 8.11, tabulates the relative errors (in percentage) between the predicted analytical result and the corresponding experimental result. As can be observed, the analytical predictions for permeability are conservative and within acceptable error limits. It is also evident that the error in predictions decreases with the decrease in the length of stitch cracks in the angle plies, the reduction in error becoming more obvious in the prediction of permeability for the 750 cycles, underscoring the significance of including the stitch crack model in FLM.

The relative insensitivity of the stitch crack model in the prediction for 1250 cycles could be attributed to the fact that, the permeability measured at 1000 and 1250 cycles do not undergo as big an increase (the permeability increased by a single order of

magnitude) as compared with the one between 750 and 1000 cycles (where, the values increase roughly by 11,000%).

If the permeability were measured at cycles that were more spread apart, the drop would have been much more significant.

Table 8.11. Permeability predictions using FLM compared with experimental data (Bechel *et al* [41])

100% THROUGH CRACKED			
Cycles	Bo (Experiment)	Bo (FLM)	%Error
750	6.230×10^{-07}	8.872×10^{-07}	42.40
1250	2.750×10^{-04}	3.791×10^{-04}	37.87
75% THROUGH CRACKED			
Cycles	Bo (Experiment)	Bo (FLM)	%Error
750	6.230×10^{-07}	8.522×10^{-07}	36.78
1250	2.750×10^{-04}	3.756×10^{-04}	36.58
50% THROUGH CRACKED			
Cycles	Bo (Experiment)	Bo (FLM)	%Error
750	6.230×10^{-07}	8.074×10^{-07}	29.60
1250	2.750×10^{-04}	3.720×10^{-04}	35.28
25% THROUGH CRACKED			
Cycles	Bo (Experiment)	Bo (FLM)	%Error
750	6.230×10^{-07}	7.482×10^{-07}	20.09
1250	2.750×10^{-04}	3.684×10^{-04}	33.98
7% THROUGH CRACKED			
Cycles	Bo (Experiment)	Bo (FLM)	%Error
750	6.230×10^{-07}	6.921×10^{-07}	11.09
1250	2.750×10^{-04}	3.658×10^{-04}	33.03

CHAPTER 9

CONCLUSIONS

An analytical model was developed to find the crack opening displacements in composites with transverse matrix cracks and delaminations subjected to mechanical and/or thermal loads. Verification using finite element analysis has shown that the model could be used to analyze laminates of any general configuration. The introduction of stitch crack model and subsequent verification with experimental data for permeation indicate that the experimental observations can be closely simulated using this simple model.

The model was used to predict the permeability of thermo-cycled damaged composite specimens. Good agreement in the results from experiment and theoretical analysis suggest that the model proposed in this thesis could be used as a tool in the initial design of composite structures subjected to thermal and mechanical load. However, In the interest of future enhancement of the model a few points are suggested below:

- Although a damage evolution model was proposed and verified with finite element analysis, the applicability of this model to design can only be evaluated through verification with experimental results. It is suggested that the damage evolution model be verified with results from experiments for composites under monotonic tension (for the mechanical case) and a uniform thermal field (for the case of thermal load).
- The FLM in this thesis, is based on a linear model for which certain boundary conditions are not satisfied (refer section 3.3). These issues could be addressed with a model based on higher order deformation theory. By using, a higher order model the non-linearity in the deformation of the delaminated ply could also be captured. However, the higher order model will require a numerical the solution process.
- The model under predicts the crack initiation under mechanical load and over predicts the critical thermal load. Since, under prediction of critical load is conservative and amenable to a good design tool, the over-prediction in thermal load is not favorable especially if the model is to be used in the analysis of composites in cryogenic environments. For this, the damage evolution model proposed for the thermal case, suggested in Chapter 5, should be modified to superpose the effects of each individual ply group, instead of the effective method in use currently. However, this would complicate the equations considerably.
- Finally, the COD from the model should be compared with actual COD data from experiments. The permeability predictions in this thesis were performed

after assuming trends in the input parameters (i.e., crack density, delamination length). A more comprehensive validation would be if these parameters were confirmed using experimental observations.

References

1. Talreja, R., "Transverse Cracking and Stiffness reduction in Composite Laminates", *Journal of Composite Materials,* Vol. 19, 1985, pp. 355-375.
2. Allen, D.H., Harris, C.E. and Groves, S.E., "A Theoretical Constitutive Theory for Elastic Composite with Distributed Damage – I: Theoretical Development", *International Journal of Solids and Structures,* Vol. 23, 1987, pp. 1301-1318.
3. Allen, D.H., Harris, C.E. and Groves, S.E., "A Theoretical Constitutive Theory for Elastic Composite with Distributed Damage – II: Application to matrix cracking in laminated composites", *International Journal of Solids and Structures,* Vol. 23, 1987, pp. 1319-1338.
4. Berthelot, J.M., Leblond, P. and El Mahi, A., "2D and 3D numerical models of Transverse Cracking in Cross-Ply Laminates", *Composite Science and Technology*, Vol. 56, 1996, pp. 793-796.
5. Hashin, Z., "Analysis of Cracked Laminate: A Variational Approach", *Mechanics of Materials*, Vol. 4, 1985, pp. 121-136.
6. Nairn, J.A., "The Strain Energy Release Rate of Composite Micro-cracking: A Variational approach", *Journal of Composite Materials,* Vol. 23, 1989, pp. 1106-1129.
7. Nairn, J.A. and Hu, S., "The Initiation and Growth of Delaminations induced by Matrix Microcracks in Laminated Composites", *International Journal of Fracture,* Vol. 57, 1992, pp. 1-24.

8. Schoeppner, G.A. and Pagano, N.J., "Stress Fields and Energy Release Rates in Cross-Ply Laminates", *International Journal of Solids and Structures*, Vol. 35, 1998, pp. 1025-1055.
9. McCartney, L.N., "Theory of Stress Transfer in a 0˚-90˚-0˚ Cross-Ply Laminate Containing a Parallel Array of Transverse Cracks", *Journal of Mechanics and Physics of Solids*, Vol. 40, 1992, pp. 27-68.
10. McCartney, L.N., "The Prediction of Cracking in Biaxially Loaded Cross-Ply Laminates having Brittle Matrices", *Composites*, Vol. 24, 1993, 84-92.
11. McCartney, L.N., Schoeppner, G.A. and Becker, W., "Comparison of Models for Transverse Ply Cracks in Composite Laminates", *Composites Science and Technology*, 2000, Vol. 60, pp. 2347-2359.
12. Hong, C.S. and Lim, S.G., "Effect of Transverse Cracks on the Thermomechanical Properties of Cross-Ply Laminated Composites", *Composites Science and Technology,* Vol. 34, 1989, pp. 145-162.
13. Han, Y.M. and Hahn, H.T., "Ply Cracking and Property Degradations of Symmetric Balanced Laminates under General In-Plane Loading", *Composite Science and Technology,* Vol. 35, 1989, pp. 377-397.
14. Henaff-Gardin, C., Lafarie-Frenot, M.C. and Gamby, D., "Doubly Periodic Cracking in Composite Laminates Part 1: General In-Plane Loading", *Composite Structures*, Vol. 36, 1996, 113-130.
15. Fan, J. and Zhang, J., "In-situ Damage Evolution and Micro/Macro Transition for Laminated Composites", *Composite Science and Technology*, Vol. 47, 1993, pp. 107-118.

16. Zhang, J., Fan, J. and Soutis, C., "Analysis of Multiple Matrix Cracking in $[\pm\theta_m/90_n]_s$ Composite Laminates Part 1:In-plane Stiffness Properties", *Composites*, Vol. 23, 1992, pp. 291-298.
17. Zhang, J., Fan, J. and Soutis, C., "Analysis of Multiple Matrix Cracking in $[\pm\theta_m/90_n]_s$ Composite Laminates Part 2:Development of Transverse Ply Cracks", *Composites*, Vol. 23, 1992, pp. 299-304.
18. Zhang, J., Soutis, C. and Fan, J., "Strain Energy Release Rates associated with Local Delaminations in Cracked Composite Laminates", *Composites*, Vol. 25, 1994, pp. 851-862.
19. Kashtalayan, M. and Soutis, C., "Stiffness degradation in cross-ply laminates damaged by transverse cracking and splitting", *Composites Part A: Applied Science and Manufacturing*, Vol. 31, 2000, pp. 335-351.
20. Armanios, E.A., Sriram, P. and Badir, A.M., "Fracture Anlaysis of Transverse Crack-Tip and Free-Edge Delamination in Laminated Composites", *Composite Materials: Fatigue and Fracture,* ASTM STP 1110, 1991, pp. 269-286.
21. Zhang, J., Fan, J., and Herrmann, K.P., "Delaminations Induced by Constrained Transverse Cracking in Symmetric Composite Laminates", *International Journal of Solids and Structures,* Vol. 36, 1999, pp. 813-846.
22. Zhang, J., Fan, J., and Herrmann, K.P., "Stiffness degradation by multilayer intralaminar cracking in composite laminates", *Composites Part A: Applied Science and Manufacturing,* Vol. 30, 1999, pp. 683-706.

23. O'Brien, T.K. and Hooper, S.J., "Local delamination in laminates with angle-ply matrix cracks: Part I Tension tests and stress analysis", NASA Technical Memorandum 104055 AVSCOM Technical report 91-B-010, 1991.
24. O'Brien, T.K., "Local delamination in laminates with angle-ply matrix cracks: Part II Delamination fracture analysis and fatigue characterization", NASA Technical Memorandum 104076 AVSCOM Technical report 91-B-011, 1991.
25. Salpekar, S.A., O'Brien, T.K. and Shivakumar, K.N., "Analysis of local delaminations caused by angle-ply matrix cracks", *Journal of Composite Materials*, Vol. 30, 1996, pp. 418-440.
26. Kashtalayan, M. and Soutis, C., "Analysis of local delaminations in composite laminates with angle-ply matrix cracks", *International Journal of Solids and Structures*, Vol. 39, 2002, pp. 1515-1537.
27. Varna, J., Joffe, R., Akshantala, N.V. and Talreja, R., "Damage in composite laminates with off-axis plies", *Composite Science and Technology,* Vol. 59, 1999, pp. 2139-2147.
28. Henaff-Gardin, C., Lafarie-Frenot, M.C. and Gamby, D., "Doubly Periodic Cracking in Composite Laminates Part 2: Thermal bi-axial Loading", *Composite Structures*, Vol. 36, 1996, 131-140.
29. Takeda, N., McCartney, L.N. and Ogihara, S., "The application of a ply-refinement technique to the analysis of microscopic deformation in interlaminar-toughned laminates with transverse cracks", *Composite Science and Technology*, Vol. 60, 2000, pp. 231-240.

30. McManus, H.L. and Maddocks, J.R., "On Micro-Cracking in Composite Laminates under Thermal and Mechanical Loading", *Polymers and Polymer Composites*, Vol. 4, 1996, pp. 304-314.
31. Su, X., Abdi, F. and Kim, R.Y., "Prediction of Micro-crack Densities in IM7/977-2 Polymer Composite Laminates under Mechanical Loading at Room and Cryogenic Temperatures", *AIAA paper,* Austin, TX, April 2005, AIAA-2005-2226.
32. Varna, J., Berglund, L., Talreja, R., and Jacovics, A., "A Study of the Opening Displacement of Transverse Cracks in Cross-Ply Laminates", *International Journal of Damage Mechanics*, Vol. 2, 1993, pp. 272-289.
33. Roy, S. and Benjamin, M., "Modeling of Opening Displacement of Transverse Cracks in Graphite-Epoxy Laminates using Shear Lag Analysis", *American Society for Composites*, Lafayette, IN, October 2002, Paper 023.
34. Noh, J. and Whitcomb, J., "Effect of Laminate Design and Loads on Crack Opening Volume in Laminates used in Cryogenic Tanks", *AIAA paper,* Denver, CO, April 2002, AIAA-2002-1415.
35. Noh, J. and Whitcomb, J., "Prediction of Delamination Growth and Opening near Intersection of Transverse Matrix Cracks and Delamination", *AIAA paper,* Norfolk, VA, April 2003, AIAA-2003-1602.
36. Roy, S. and Benjamin, M., "Modeling of Permeation and Damage in Graphite/Epoxy laminates for Cryogenic Fuel Storage", *Composites Science and Technology,* Vol. 64, 2004, 2051-2065.

37. Donaldson, S.L., Kim, R.Y. and Trejo, R.E., "Damage Development in Laminates Mechanically cycled at Cryogenic Temperatures", *AIAA paper*, Palm Springs, CA, AIAA-2004-1774.

38. Bechel, V.T. and Kim, R.Y., "Damage Trends in Cryogenically Cycled Carbon/Polymer Composites", *Composites Science and Technology,* Vol. 64, 2004, pp. 1773-1784.

39. Yokozeki, T., Aoki, T., Ogasawara, T., and Takashi, I., "Effects of layup angle and ply-thickness on matrix crack interaction in contiguous plies of composite laminates", *Composites Part A: Applied Science and Manufacturing,* Vol. 36, 2005, pp. 1229-1235.

40. Gates, T.S. and Grenoble, R.W., "Hydrogen Permeability of Polymer Matrix Composites at Cryogenic Temperatures", *AIAA paper,* Austin, TX, April 2005, AIAA-2005-2086.

41. Bechel, V.T., "Permeability and Damage in Unloaded Cryogenically Cycled PMCs", *AIAA paper,* Austin, TX, April 2005, AIAA-2005-2156.

42. Peddiraju, P., Grenoble, R., Fried, K., Gates, T. and Lagoudas, D.C. "Analytical Predictions and Experimental Measurements of Hydogen Permeability in a Microcrack Damaged Composite", *AIAA paper,* Austin, TX, April 2005, AIAA-2005-2087.

43. McManus, H.L., Faust, A. and Uebelhart, S., "Gas Permeability of Thermally Cycled Graphite-Epoxy Composites," *American Society for Composites*, Blacksburg, VA, Sept 9-12, 2001, Paper 092.

44. Yozeki, T., Aoki, T. and Ishikawa, T., "Gas Permeability of Micro-cracked Laminates under Cryogenic Conditions", *AIAA paper,* Seattle, WA, April 2001, AIAA-2001-1218.

45. Krueger, R., "The Virtual Crack Closure Technique: History, Approach and Applications", NASA/CR-2002-211628 ICASE Report No. 2002-10.

46. Jones, R.M., "Mechanics of Composite Materials", Taylor & Francis, Philadelphia, 1999.

APPENDIX A

FIVE-LAYER MODEL ANALYSIS (CASE 2)

In this section, the governing equations for the five-layer model (FLM) are presented and solved for the case of laminate with the generalized ply orientation $[\phi_l/.../\theta_m/90_n/\varphi_p/.../\psi_q]_s$. Fig. A.1. shows the quarter model selected from the FLM (Fig. 3.4(a)) from symmetry of load and boundary conditions.

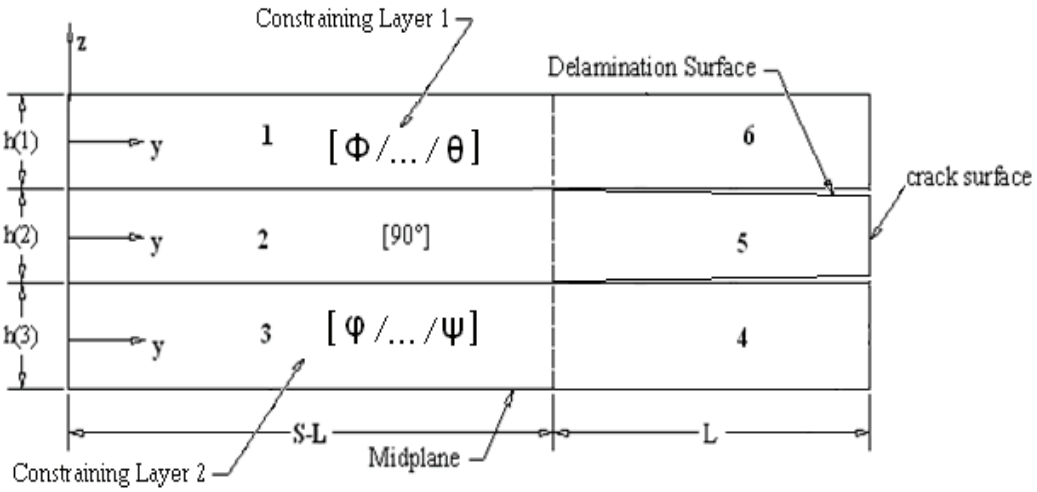

Fig. A.1. One quarter repeating interval of the FLM (Case 2)

The quarter symmetry model is divided into 6 sublaminate groups. Sublaminates 1, 2 and 3 are intact and extend from y=0 to y=S-L. Sublaminate group 6 and 4 are a continuation of plies 1 and 3 respectively and are unbroken. Sublaminate 5 represents the

delaminated portion, extending from y=S-L to y=S. Since, sublaminates 1, 2 and 3 are intact their solutions will be determined first. The derivation for these sublaminates are based on the derivation presented earlier by [21, 36], extended to include asymmetric configuration of plies in sublaminate 3.

From first order shear deformation theory assumptions we have the displacement field as,

$$v^{(i)}(y,z) = V^{(i)}(y) + z\beta^{(i)}(y) \tag{A.1a}$$

$$w^{(i)}(y) = W^{(i)}(y) \tag{A.1b}$$

Where, V(y) is the mid-plane displacement in the y-direction, β(y) is the slope of the normal to the mid-plane of the sublaminate in the y-direction. Note that, the displacement in the z-direction, W(y) does not vary through the thickness.

The governing equations for each sublaminate are,

$$N_{,y} + T_t - T_b = 0 \tag{A.2a}$$

$$M_{,y} - Q + \frac{h}{2}(T_t + T_b) = 0 \tag{A.2b}$$

$$Q_{,y} + P_t - P_b = 0 \tag{A.2c}$$

Where, N, M and Q are the Axial Force, Bending Moment and Shear resultants, while P and T denote the inter-laminar peel and shear stresses with t and b denote the top and bottom surfaces. The constitutive relations are: (the 'm' subscripts denote the "mechanical")

$$N_M = A_{22}V_{,y} + B_{22}\beta_{,y} - \bar{Q}_{22}h\int_{T_{ref}}^{T_f} \bar{\alpha}_y dT \tag{A.3a}$$

$$M_M = B_{22}V_{,y} + D_{22}\beta_{,y} - \bar{Q}_{22}h\bar{Z}\int_{T_{ref}}^{T_f} \bar{\alpha}_y dT \tag{A.3b}$$

$$Q = A_{44}(\beta + W_{,y}) \tag{A.3c}$$

Where, A_{22}, B_{22}, D_{22} & A_{44} are components of the A, B and D stiffness matrices from classical lamination theory, h is the thickness of the lamina, $\bar{Z}$ is the centroidal distance of the lamina from laminate mid-plane, $\bar{\alpha}_y$ is the coefficient of thermal expansion in y-direction. Plugging in (A.3a – A.3c) into (A.2a – A.2c) we have the governing equations,

$$A_{22}V_{,yy} + B_{22}\beta_{,yy} + T_t - T_b = 0 \tag{A.4a}$$

$$\left(D_{22} - \frac{B_{22}^2}{A_{22}}\right)\beta_{,yy} - A_{44}(\beta + W_{,y}) + \left(\frac{h}{2} - \frac{B_{22}}{A_{22}}\right)T_t + \left(\frac{h}{2} + \frac{B_{22}}{A_{22}}\right)T_b = 0 \tag{A.4b}$$

$$A_{44}(\beta_{,y} + W_{,yy}) + P_t - P_b = 0 \tag{A.4c}$$

In the sections to follow, the governing equations listed above will be modified as required by the lamina (or sublaminate) boundary conditions.

A.1. Laminated Portion: Sublaminate 1, 2 and 3 ($0 \le y \le S\text{-}L$)

Since the sublaminates are intact the following conditions of continuity must be satisfied.

$$V^{(1)}(y) - \frac{h^{(1)}}{2}\beta^{(1)}(y) = V^{(2)}(y) + \frac{h^{(2)}}{2}\beta^{(2)}(y) \tag{A.5a}$$

$$V^{(2)}(y) - \frac{h^{(2)}}{2}\beta^{(2)}(y) = V^{(3)}(y) + \frac{h^{(3)}}{2}\beta^{(3)}(y) \tag{A.5b}$$

From eqs. (A.4a) and (A.4b) and using the zero shear tractions on free surface of sublaminate 1($T_t^{(1)}=0$) and the bottom of sublaminate 3 ($T_b^{(3)}=0$) due to mid plane symmetry, the governing equations for the individual sublaminates are,

$$A_{22}^{(1)}V_{,yy}^{(1)}+B_{22}^{(1)}\beta_{,yy}^{(1)}-T_b^{(1)}=0 \tag{A.6a}$$

$$A_{22}^{(2)}V_{,yy}^{(2)}+T_t^{(2)}-T_b^{(2)}=0 \tag{A.6b}$$

$$A_{22}^{(3)}V_{,yy}^{(3)}+B_{22}^{(3)}\beta_{,yy}^{(3)}+T_b^{(3)}=0 \tag{A.6c}$$

And,

$$\left(D_{22}^{(1)}-\frac{B_{22}^{(1)2}}{A_{22}^{(1)}}\right)\beta_{,yy}^{(1)}-A_{44}^{(1)}\beta^{(1)}+\left(\frac{h^{(1)}}{2}+\frac{B_{22}^{(1)}}{A_{22}^{(1)}}\right)T_b^{(1)}=0 \tag{A.7a}$$

$$D_{22}^{(2)}\beta_{,yy}^{(2)}-A_{44}^{(2)}\beta^{(2)}+\frac{h^{(2)}}{2}(T_t+T_b)=0 \tag{A.7b}$$

$$\left(D_{22}^{(3)}-\frac{B_{22}^{(3)2}}{A_{22}^{(3)}}\right)\beta_{,yy}^{(3)}-A_{44}^{(3)}\beta^{(3)}+\left(\frac{h^{(3)}}{2}-\frac{B_{22}^{(3)}}{A_{22}^{(3)}}\right)T_b^{(3)}=0 \tag{A.7c}$$

Using the continuity in displacement, eqs. (A.5a) and (A.5b) and the continuity of surface tractions, i.e., $T_b^{(1)}=T_t^{(2)}$ and $T_b^{(2)}=T_t^{(3)}$, we can solve for the quantities $V_{,yy}^{(1)}$, $V_{,yy}^{(2)}$ and $V_{,yy}^{(3)}$ from eqs. (A.6a), (A.6b) and (A.6c).

$$\begin{aligned}V_{,yy}^{(1)}=\frac{1}{A_{22}}\Big\{&[h^{(1)}(A_{22}^{(2)}+A_{22}^{(3)})-2B_{22}^{(1)}]\beta_{,yy}^{(1)}\\&+h^{(2)}(A_{22}^{(2)}+2A_{22}^{(3)})\beta_{,yy}^{(2)}+(h^{(2)}A_{22}^{(3)}-2B_{22}^{(3)})\beta_{,yy}^{(3)}\Big\}\end{aligned} \tag{A.8a}$$

$$\begin{aligned}V_{,yy}^{(2)}=-\frac{1}{A_{22}}\Big\{&(h^{(1)}A_{22}^{(2)}+2B_{22}^{(1)})\beta_{,yy}^{(1)}+h^{(2)}(A_{22}^{(1)}-A_{22}^{(3)})\beta_{,yy}^{(2)}\\&-(h^{(2)}A_{22}^{(3)}-2B_{22}^{(3)})\beta_{,yy}^{(3)}\Big\}\end{aligned} \tag{A.8b}$$

$$V^{(3)}_{,yy} = -\frac{1}{A_{22}}\Big\{(h^{(1)}A^{(1)}_{22} + 2B^{(1)}_{22})\beta^{(1)}_{,yy} + h^{(2)}(2A^{(1)}_{22} + A^{(2)}_{22})\beta^{(2)}_{,yy} + [2B^{(3)}_{22} + h^{(3)}(A^{(1)}_{22} + A^{(2)}_{22})]\beta^{(3)}_{,yy}\Big\} \tag{A.8c}$$

Where, $A_{22} = 2(A^{(1)}_{22} + A^{(2)}_{22} + A^{(3)}_{22})$, is the total extensional stiffness of the laminate.

Using equations above (A.8a) – (A.8c), along with the eqs. (A.6a) – (A.6c) for the surface tractions we can solve for the surface tractions,

$$T^{(1)}_b = T^{(2)}_t = \frac{1}{A_{22}}\Big\{(A^{(2)}_{22} + A^{(3)}_{22})(h^{(1)}A^{(1)}_{22} + 2B^{(1)}_{22})\beta^{(1)}_{,yy} + h^{(2)}A^{(1)}_{22}(A^{(2)}_{22} + 2A^{(3)}_{22})\beta^{(2)}_{,yy} + A^{(1)}_{22}(h^{(3)}A^{(3)}_{22} - 2B^{(3)}_{22})\beta^{(3)}_{,yy}\Big\} \tag{A.9}$$

$$T^{(1)}_b = T^{(2)}_t = \frac{1}{A_{22}}\Big\{A^{(3)}_{22}(h^{(1)}A^{(1)}_{22} + 2B^{(1)}_{22})\beta^{(1)}_{,yy} + h^{(2)}A^{(3)}_{22}(2A^{(1)}_{22} + A^{(2)}_{22})\beta^{(2)}_{,yy} + (A^{(1)}_{22} + A^{(2)}_{22})(h^{(3)}A^{(3)}_{22} - 2B^{(3)}_{22})\beta^{(3)}_{,yy}\Big\} \tag{A.10}$$

Substituting the eqs. (A.9) and (A.10) into (A.7a) – (A.7c), we arrive at the following system of coupled differential equations,

$$\begin{bmatrix} a_{11} & a_{12} & a_{13} \\ a_{12} & a_{22} & a_{23} \\ a_{13} & a_{23} & a_{22} \end{bmatrix}\begin{Bmatrix} \beta^{(1)}_{,yy} \\ \beta^{(2)}_{,yy} \\ \beta^{(3)}_{,yy} \end{Bmatrix} = \begin{bmatrix} A^{(1)}_{44} & 0 & 0 \\ 0 & A^{(2)}_{44} & 0 \\ 0 & 0 & A^{(3)}_{44} \end{bmatrix}\begin{Bmatrix} \beta^{(1)} \\ \beta^{(2)} \\ \beta^{(3)} \end{Bmatrix} \tag{A.11}$$

The expressions for a_{ij} has been defined in Appendix E. The solution for this set of equations follows the approach developed in Zhang *et al* [21]. Using the method in [21], we get,

$$\beta^{(i)} = \sum_{j=1}^{3} \alpha_j P^{(i)}_j \sinh(\lambda_j y) \tag{A.12}$$

Where, i=1, 2 and 3, while,

$$\begin{Bmatrix} P_j^{(1)} \\ P_j^{(2)} \end{Bmatrix} = \frac{\lambda_j^*}{(a_{11}\lambda_j^* - A_{44}^{(1)})(a_{22}\lambda_j^* - A_{44}^{(2)}) - a_{12}^2\lambda_j^{*2}} \begin{Bmatrix} a_{13}A_{44}^{(2)} - (a_{22}a_{13} - a_{12}a_{23})\lambda_j^* \\ a_{23}A_{44}^{(1)} - (a_{11}a_{13} - a_{12}a_{23})\lambda_j^* \end{Bmatrix} \quad \text{(A.13)}$$

with, $P_j^{(3)} = 1$ and λ_j^* is one of the three real positive solutions to the following cubic characteristic equation ($\lambda_j = \sqrt{\lambda_j^*}$),

$$\begin{aligned} &(a_{11}a_{22}a_{33} + 2a_{12}a_{13}a_{23} - a_{33}a_{12}^2 - a_{11}a_{23}^2 - a_{22}a_{13}^2)\lambda^{*3} \\ &-(a_{11}a_{22}A_{44}^{(3)} + a_{33}a_{22}A_{44}^{(1)} + a_{33}a_{11}A_{44}^{(2)} - a_{12}^2A_{44}^{(3)} - a_{23}^2A_{44}^{(1)} - a_{13}^2A_{44}^{(2)})\lambda^{*2} \\ &+(a_{11}A_{44}^{(2)}A_{44}^{(3)} + a_{22}A_{44}^{(1)}A_{44}^{(3)} + a_{33}A_{44}^{(2)}A_{44}^{(1)})\lambda^* - A_{44}^{(1)}A_{44}^{(2)}A_{44}^{(3)} = 0 \end{aligned} \quad \text{(A.14)}$$

Substituting (A.12) into (A.8a) – (A.8c), and integrating we get (after applying condition of no transalations at y=0),

$$V^{(i)} = \sum_{j=1}^{3} \alpha_j \gamma_j^{(i)} \sinh(\lambda_j y) + \alpha_{3+i} y \quad \text{(A.15)}$$

From (A.3a) and (A.3b), we have the force and moment resultants as,

$$N_M^{(i)} = \sum_{j=1}^{3} \alpha_j \eta_j^{(i)} \cosh(\lambda_j y) + A_{22}^{(i)}\alpha_{3+i} - \bar{Q}_{22}^{(i)}h^{(i)} \int_{T_{ref}}^{T_f} \bar{\alpha}_y^{(i)} dT \quad \text{(A.16)}$$

$$M_M^{(i)} = \sum_{j=1}^{3} \alpha_j \xi_j^{(i)} \cosh(\lambda_j y) + B_{22}^{(i)}\alpha_{3+i} - \bar{Q}_{22}^{(i)}h^{(i)}\bar{Z}^{(i)} \int_{T_{ref}}^{T_f} \bar{\alpha}_y^{(i)} dT \quad \text{(A.17)}$$

The constants $\gamma_j^{(i)}$, $\eta_j^{(i)}$ and $\xi_j^{(i)}$ have been listed in Appendix E.

A.2. Laminated Portion: Sublaminate 6 (S-L ≤ y ≤ S)

The sublaminate 6 is an intact ply group, unsymmetric about its mid-plane (Fig. A.1). Assuming that $W^{(6)} \neq 0$ and applying the traction boundary conditions $T_t^{(6)} = 0$,

$T_b^{(6)} = 0$, $P_t^{(6)} = 0$ and $P_b^{(6)} = 0$ to the sublaminate, we get the governing equations for this sublaminate as,

$$A_{22}^{(1)} V_{,yy}^{(6)} + B_{22}^{(1)} \beta_{,yy}^{(6)} = 0 \tag{A.18a}$$

$$\left(D_{22}^{(1)} - \frac{B_{22}^{(1)2}}{A_{22}^{(1)}} \right) \beta_{,yy}^{(6)} - A_{44}^{(1)} (\beta^{(6)} + W_{,y}^{(6)}) = 0 \tag{A.18b}$$

$$A_{44}^{(1)} (\beta_{,y}^{(6)} + W_{,yy}^{(6)}) = 0 \tag{A.18c}$$

Integrating, (A.18c) once and applying the boundary condition $Q^{(6)}(S)=0$ (from symmetry of FLM), we get,

$$A_{44}^{(1)} (\beta^{(6)} + W_{,y}^{(6)}) = 0 \tag{A.18d}$$

From (A.18b) and (A.18d) we get,

$$\beta_{,yy}^{(6)} = 0$$

$$\text{or, } \beta^{(6)} = \theta_3 y + \theta_4 \tag{A.19}$$

Similarly, from (A.18a) and (A.19) we get,

$$V^{(6)} = \theta_6 y + \theta_8 \tag{A.20}$$

Solving (A.18d), we get,

$$W^{(6)} = -\theta_3 \frac{y^2}{2} - \theta_4 y + \theta_9 \tag{A.21}$$

Using the constitutive relations listed (A.3a) and (A.3b) we have the relations for resultant force and moment for the sublaminate as,

$$N_M^{(6)} = A_{22}^{(1)}\theta_6 + B_{22}^{(1)}\theta_3 - \bar{Q}_{22}^{(1)}h^{(1)}\int_{T_{ref}}^{T_f}\bar{\alpha}_y^{(1)}dT \tag{A.22}$$

$$M_M^{(6)} = B_{22}^{(1)}\theta_6 + D_{22}^{(1)}\theta_3 - \bar{Q}_{22}^{(1)}h^{(1)}\bar{Z}^{(1)}\int_{T_{ref}}^{T_f}\bar{\alpha}_y^{(1)}dT \tag{A.23}$$

A.3. Laminated Portion: Sublaminate 4 (S-L ≤ y ≤ S)

The sublaminate 4 is an intact ply group, unsymmetric about its mid-plane (Fig. A.1). Due to the problems faced in modeling sublaminate 4 with $W^{(4)}=0$ (refer section 3.3), a modified solution for sublaminate 4 is suggested here. Assume $W^{(6)}\neq 0$ and the peel stress at the bottom of the sublaminate $P_b^{(4)} = 0$. Now applying the traction boundary conditions $T_t^{(6)} = 0$, $T_b^{(6)} = 0$ to the sublaminate, the governing equations for this sublaminate will be,

$$A_{22}^{(3)}V_{,yy}^{(4)} + B_{22}^{(3)}\beta_{,yy}^{(4)} = 0 \tag{A.24a}$$

$$\left(D_{22}^{(3)} - \frac{B_{22}^{(3)2}}{A_{22}^{(3)}}\right)\beta_{,yy}^{(4)} - A_{44}^{(3)}(\beta^{(4)} + W_{,y}^{(4)}) = 0 \tag{A.24b}$$

$$A_{44}^{(3)}(\beta_{,y}^{(4)} + W_{,yy}^{(4)}) = 0 \tag{A.24c}$$

Since, $Q^{(6)}(S)=0$, the solutions for sublaminate 4 and 6 will be similar. Following a solution procedure similar to that for sublaminate 6, we get,

$$\beta^{(4)} = \theta_1 y + \theta_2 \tag{A.25}$$

$$V^{(4)} = \theta_5 y + \theta_7 \tag{A.26}$$

$$W^{(4)} = -\theta_1 \frac{y^2}{2} - \theta_2 y + \theta_{10} \tag{A.27}$$

$$N_M^{(4)} = A_{22}^{(3)}\theta_5 + B_{22}^{(3)}\theta_1 - \bar{Q}_{22}^{(3)}h^{(3)} \int_{T_{ref}}^{T_f} \bar{\alpha}_y^{(3)} dT \tag{A.28}$$

$$M_M^{(4)} = B_{22}^{(3)}\theta_5 + D_{22}^{(3)}\theta_1 - \bar{Q}_{22}^{(3)}h^{(3)}\bar{Z}^{(3)} \int_{T_{ref}}^{T_f} \bar{\alpha}_y^{(3)} dT \tag{A.29}$$

A.4. Delaminated Portion: Sublaminate 5 (S-L ≤ y ≤ S)

The solution for rotations in the delaminated portion is solved using the elastic foundation solutions described in Section 3.4. Since, the cracked layer is decoupled from the solution to the rest of the laminate we can discuss the solution for rotations and displacements separately.

The equilibrium equation for the cracked lamina is,

$$A_{22}^{(5)} V_{,yy}^{(5)} = 0 \tag{A.30}$$

Solving the above equation we get,

$$V^{(5)} = \psi_5 y + \psi_6 \tag{A.31}$$

From, the above solution we can derive the solution for mechanical load in the cracked sublaminate as,

$$N_M^{(5)} = A_{22}^{(2)} V_{,y}^{(5)} - \bar{Q}_{22}^{(2)}h^{(2)} \int_{T_{ref}}^{T_f} \bar{\alpha}_y^{(2)} dT = A_{22}^{(2)}\psi_5 - \bar{Q}_{22}^{(2)}h^{(2)} \int_{T_{ref}}^{T_f} \bar{\alpha}_y^{(2)} dT \tag{A.32}$$

Hence, we need to specify 18 boundary conditions to solve for the 18 constants ($\alpha_1, \alpha_2, ..., \alpha_6, \theta_1, \theta_2, ..., \theta_{10}, \psi_5, \psi_6$).

A.5. Solutions for constants: $\alpha_1, \alpha_2, ..., \alpha_6, \theta_1, \theta_2, ..., \theta_{10}, \psi_5, \psi_6$

The boundary conditions that need to be satisfied are,

$$\beta^{(4)}(S) = 0 \tag{A.33a}$$

$$\beta^{(6)}(S) = 0 \tag{A.33b}$$

$$V^{(6)}(S) = V^{(4)}(S) \tag{A.33c}$$

$$N_M^{(5)}(S) = 0 \tag{A.33d}$$

$$\beta^{(1)}(S-L) = \beta^{(6)}(S-L) \tag{A.33e}$$

$$\beta^{(3)}(S-L) = \beta^{(4)}(S-L) \tag{A.33f}$$

$$V^{(1)}(S-L) = V^{(6)}(S-L) \tag{A.33g}$$

$$V^{(2)}(S-L) = V^{(5)}(S-L) \tag{A.33h}$$

$$V^{(3)}(S-L) = V^{(4)}(S-L) \tag{A.33i}$$

$$W^{(1)}(S-L) = W^{(6)}(S-L) \tag{A.33j}$$

$$W^{(3)}(S-L) = W^{(4)}(S-L) \tag{A.33k}$$

$$N_M^{(1)}(S-L) = N_M^{(6)}(S-L) \tag{A.33l}$$

$$N_M^{(2)}(S-L) = N_M^{(5)}(S-L) \tag{A.33m}$$

$$N_M^{(3)}(S-L) = N_M^{(4)}(S-L) \tag{A.33n}$$

$$M_M^{(1)}(S-L) = M_M^{(6)}(S-L) \tag{A.33o}$$

$$M_M^{(3)}(S-L) = M_M^{(4)}(S-L) \tag{A.33p}$$

$$N_M^{(1)}(0) + N_M^{(2)}(0) + N_M^{(3)}(0) = \frac{N}{2} \tag{A.33q}$$

The above 17 boundary conditions and the two continuity equations (A.5a, b) (19 boundary conditions in total) have to be satisfied. However, the unavailability of constants (only 18 in number) implies that one of the boundary conditions have to be dropped. Due to this restraint, the eq. (A.33e) : the boundary condition for continuity in rotation is omitted. Problems that may arise from this solution procedure has been discussed in Section 3.3. Also note that here, the axial load ta the boundary of the cracked layer (the free surface) has been set to zero in eq. (A.33d). However, in the stitch crack model this will be modified to include the spring force at the end of the delaminated beam. Hence, the appropriate changes have to be made in the equations for 'ψ_5' and 'ψ_6' to be made, depending on the model.

Substituting the solutions to rotations and displacements from the sections before, we get,

$$\theta_1 S + \theta_2 = 0 \tag{A.34a}$$

$$\theta_3 S + \theta_4 = 0 \tag{A.34b}$$

$$\theta_6 S + \theta_8 = \theta_5 S + \theta_7 \tag{A.34c}$$

$$A_{22}^{(2)} \psi_5 - \bar{Q}_{22}^{(2)} h^{(2)} \int_{T_{ref}}^{T_f} \bar{\alpha}_y^{(2)} dT = 0 \tag{A.34d}$$

$$\sum_{j=1}^{3} \alpha_j P_j^{(1)} \sinh(\lambda_j (S-L)) = \theta_3 (S-L) + \theta_4 \tag{A.34e}$$

$$\sum_{j=1}^{3} \alpha_j \sinh(\lambda_j (S-L)) = \theta_1 (S-L) + \theta_2 \tag{A.34f}$$

$$\sum_{j=1}^{3} \alpha_j \gamma_j^{(1)} \sinh(\lambda_j (S-L)) + \alpha_4 (S-L) = \theta_6 (S-L) + \theta_8 \tag{A.34g}$$

$$\sum_{j=1}^{3} \alpha_j \gamma_j^{(2)} \sinh(\lambda_j (S-L)) + \alpha_5 (S-L) = \psi_5 (S-L) + \psi_6 \tag{A.34h}$$

$$\sum_{j=1}^{3} \alpha_j \gamma_j^{(3)} \sinh(\lambda_j (S-L)) + \alpha_6 (S-L) = \theta_5 (S-L) + \theta_7 \tag{A.34i}$$

$$-\theta_3 \frac{(S-L)^2}{2} - \theta_4 (S-L) + \theta_9 = 0 \tag{A.34j}$$

$$-\theta_1 \frac{(S-L)^2}{2} - \theta_2 (S-L) + \theta_{10} = 0 \tag{A.34k}$$

$$\sum_{j=1}^{3} \alpha_j \eta_j^{(1)} \cosh(\lambda_j (S-L)) + A_{22}^{(1)} \alpha_4 = A_{22}^{(1)} \theta_6 + B_{22}^{(1)} \theta_3 \tag{A.34l}$$

$$\sum_{j=1}^{3} \alpha_j \eta_j^{(2)} \cosh(\lambda_j (S-L)) + A_{22}^{(2)} \alpha_5 = A_{22}^{(2)} \psi_5 \tag{A.34m}$$

$$\sum_{j=1}^{3} \alpha_j \eta_j^{(3)} \cosh(\lambda_j (S-L)) + A_{22}^{(3)} \alpha_4 = A_{22}^{(3)} \theta_5 + B_{22}^{(3)} \theta_1 \tag{A.34n}$$

$$\sum_{j=1}^{3} \alpha_j \xi_j^{(1)} \cosh(\lambda_j (S-L)) + B_{22}^{(1)} \alpha_4 = B_{22}^{(1)} \theta_6 + D_{22}^{(1)} \theta_3 \tag{A.34o}$$

$$\sum_{j=1}^{3} \alpha_j \xi_j^{(3)} \cosh(\lambda_j (S-L)) + B_{22}^{(3)} \alpha_4 = B_{22}^{(3)} \theta_5 + D_{22}^{(3)} \theta_1 \tag{A.34p}$$

$$A_{22}^{(1)} \alpha_4 + A_{22}^{(2)} \alpha_5 + A_{22}^{(3)} \alpha_6 = \frac{N + N_T}{2} \tag{A.34q}$$

Substituting (A.12), (A.15) in (A.5a) and (A.5b) we get,

$$\alpha_4 = \alpha_5 \text{ and } \alpha_5 = \alpha_6 \tag{A.35a,b}$$

Substituting (A.35a,b) in (A.34q),

$$\alpha_4 = \alpha_5 = \alpha_6 = \frac{N + N_T}{A_{22}} \tag{A.36}$$

Where, A_{22} is the extension stiffness of the laminate (See Appendix E).

From (A.34a), (A.34b) and (A.34d) we get,

$$\theta_2 = -\theta_1 S \tag{A.37}$$

$$\theta_4 = -\theta_3 S \tag{A.38}$$

$$\psi_5 = \int_{T_{ref}}^{T_f} \bar{\alpha}_y^{(2)} dT \tag{A.39}$$

Note that for the stitch crack model eq.(A.39) will not be applicable (refer Appendix D).

From (A.34b) and (A.34e), we get,

$$\sum_{j=1}^{3} \alpha_j P_j^{(1)} \sinh(\lambda_j (S - L)) = -\theta_3 L \tag{A.40}$$

From (A.34c) we get,

$$\theta_8 - \theta_7 = -(\theta_6 - \theta_5) S \tag{A.41a}$$

Subtracting (A.34i) from (A.34g)

$$\sum_{j=1}^{3} \alpha_j (\gamma_j^{(1)} - \gamma_j^{(3)}) \sinh(\lambda_j (S - L)) = (\theta_6 - \theta_5)(S - L) + (\theta_8 - \theta_7) \tag{A.41b}$$

Substituting (A.41a) in (A.41b),

$$\sum_{j=1}^{3} \alpha_j (\gamma_j^{(1)} - \gamma_j^{(3)}) \sinh(\lambda_j (S - L)) = -(\theta_6 - \theta_5) L \tag{A.42}$$

Rearranging (A.34l) we get,

$$\theta_6 = \sum_{j=1}^{3} \alpha_j \frac{\eta_j^{(1)}}{A_{22}^{(1)}} \cosh(\lambda_j (S-L)) - \frac{B_{22}^{(1)}}{A_{22}^{(1)}} \theta_3 + \frac{N+N_T}{A_{22}} \tag{A.43a}$$

Similarly, from (A.34n),

$$\theta_5 = \sum_{j=1}^{3} \alpha_j \frac{\eta_j^{(3)}}{A_{22}^{(3)}} \cosh(\lambda_j (S-L)) - \frac{B_{22}^{(3)}}{A_{22}^{(3)}} \theta_1 + \frac{N+N_T}{A_{22}} \tag{A.43b}$$

Substituting (A.43a) in (A.34o) we get,

$$\theta_3 = \sum_{j=1}^{3} \alpha_j P_j^{(1)} \lambda_j \cosh(\lambda_j (S-L)) \tag{A.44}$$

Similarly substituting (A.43b) in (A.34p) gives,

$$\theta_1 = \sum_{j=1}^{3} \alpha_j \lambda_j \cosh(\lambda_j (S-L)) \tag{A.45}$$

Substituting (A.44) and (A.45) in (A.43a,b) respectively,

$$\theta_6 = \sum_{j=1}^{3} \alpha_j \gamma_j^{(1)} \lambda_j \cosh(\lambda_j (S-L)) + \frac{N+N_T}{A_{22}} \tag{A.46}$$

$$\theta_5 = \sum_{j=1}^{3} \alpha_j \gamma_j^{(3)} \lambda_j \cosh(\lambda_j (S-L)) + \frac{N+N_T}{A_{22}} \tag{A.47}$$

Substituting (A.44) in (A.40) we get,

$$\sum_{j=1}^{3} \alpha_j P_j^{(1)} \left(\sinh(\lambda_j (S-L)) + L\lambda_j \cosh(\lambda_j (S-L)) \right) = 0 \tag{A.48}$$

Substituting (A.46) and (A.47) in (A.42) we get,

$$\sum_{j=1}^{3} \alpha_j (\gamma_j^{(1)} - \gamma_j^{(3)}) \left(\sinh(\lambda_j (S-L)) + L\lambda_j \cosh(\lambda_j (S-L)) \right) = 0 \tag{A.49}$$

Rearranging terms in (A.34m) we get,

$$\sum_{j=1}^{3} \alpha_j \eta_j^{(2)} \cosh(\lambda_j (S-L)) = A_{22}^{(2)} (\psi_5 - \alpha_5) \tag{A.50}$$

If Stitch Crack is not present then, $\psi_5 = \int_{T_{ref}}^{T_f} \bar{\alpha}_y^{(2)} dT$ else for a stitch crack model we get, $\psi_5 = \dfrac{N_T^{(2)} + \dfrac{K_{spring}^{(5)} (S-L)(N+N_T)}{A_{22}}}{A_{22}^{(2)} - K_{spring}^{(5)} L}$ (refer Appendix D).

From (A.34g) and (A.34i),

$$\theta_7 = \sum_{j=1}^{3} \alpha_j \gamma_j^{(3)} \sinh(\lambda_j (S-L)) + \frac{N+N_T}{A_{22}} (S-L) - \theta_5 (S-L) \tag{A.51}$$

$$\theta_8 = \sum_{j=1}^{3} \alpha_j \gamma_j^{(1)} \sinh(\lambda_j (S-L)) + \frac{N+N_T}{A_{22}} (S-L) - \theta_6 (S-L) \tag{A.52}$$

And from eq. A.34a, b, j and k, we get,

$$\theta_9 = -\frac{1}{2} \theta_3 (S^2 - L^2) \tag{A.53}$$

$$\theta_{10} = -\frac{1}{2} \theta_1 (S^2 - L^2) \tag{A.54}$$

Eq. (A.48) – (A.50) can be written in a matrix form as below,

$$[\mathbf{F}]\{\boldsymbol{\alpha}\} = \{\mathbf{R}\} \tag{A.55a}$$

Where,

$$\begin{aligned} F_{1j} &= P_j^{(1)} \left(\sinh(\lambda_j (S-L)) + L\lambda_j \cosh(\lambda_j (S-L)) \right) \\ F_{2j} &= (\gamma_j^{(1)} - \gamma_j^{(3)}) \left(\sinh(\lambda_j (S-L)) + L\lambda_j \cosh(\lambda_j (S-L)) \right) \\ F_{3j} &= \eta_j^{(2)} \cosh(\lambda_j (S-L)) \end{aligned} \tag{A.55b}$$

Are elements of the 3x3 matrix **F** (j=1 to 3).

While, $\{\boldsymbol{\alpha}\}=\begin{Bmatrix}\alpha_1\\ \alpha_2\\ \alpha_3\end{Bmatrix}$ and $\{\mathbf{R}\}=\begin{Bmatrix}0\\ 0\\ A_{22}^{(2)}(\psi_5-\alpha_5)\end{Bmatrix}$.

α_1, α_2 and α_3 can be solved from the simultaneous solution of (A.55a).

APPENDIX B

FIVE-LAYER MODEL ANALYSIS (CASE 3)

In this section, the governing equations for the five-layer model (FLM) are presented and solved for the case of laminate with the generalized ply orientation $[90/\theta_p/\phi_q/.../\varphi_r]_s$. Fig. A.1. shows the quarter model selected from the FLM (Fig. 3.5(a)) from symmetry of load and boundary conditions.

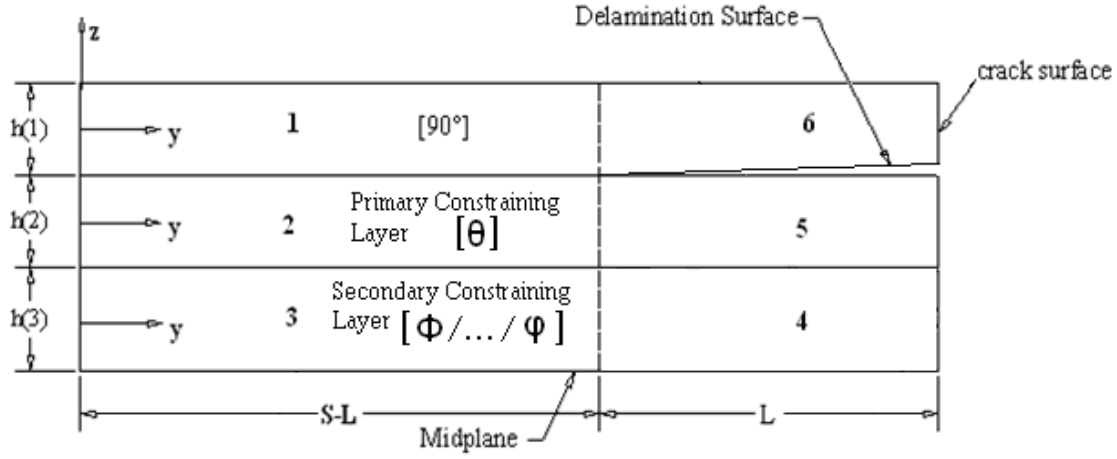

Fig. B.1. One quarter repeating interval of the FLM (Case 2)

The quarter symmetry model is divided into 6 sublaminate groups. Sublaminates 1, 2 and 3 are intact and extend from y=0 to y=S-L. Sublaminate group 4 and 5 are a

continuation of plies 1 and 3 respectively and are unbroken. Sublaminate 6 represents the delaminated portion, extending from y=S-L to y=S.

From first order shear deformation theory assumptions we have the displacement field as,

$$v^{(i)}(y,z) = V^{(i)}(y) + z\beta^{(i)}(y) \tag{B.1a}$$

$$w^{(i)}(y) = W^{(i)}(y) \tag{B.1b}$$

Where, V(y) is the mid-plane displacement in the y-direction, β(y) is the slope of the normal to the mid-plane of the sublaminate in the y-direction. Note that, the displacement in the z-direction, W(y) does not vary through the thickness.

The governing equations for each sublaminate are,

$$N_{,y} + T_t - T_b = 0 \tag{B.2a}$$

$$M_{,y} - Q + \frac{h}{2}(T_t + T_b) = 0 \tag{B.2b}$$

$$Q_{,y} + P_t - P_b = 0 \tag{B.2c}$$

Where, N, M and Q are the Axial Force, Bending Moment and Shear resultants, while P and T denote the inter-laminar peel and shear stresses with t and b denote the top and bottom surfaces. The constitutive relations are: (the 'm' subscripts denote the "mechanical")

$$N_M = A_{22}V_{,y} + B_{22}\beta_{,y} - \bar{Q}_{22}h\int_{T_{ref}}^{T_f} \bar{\alpha}_y dT \tag{B.3a}$$

$$M_M = B_{22}V_{,y} + D_{22}\beta_{,y} - \bar{Q}_{22}h\bar{Z}\int_{T_{ref}}^{T_f} \bar{\alpha}_y dT \tag{B.3b}$$

$$Q = A_{44}(\beta + W_{,y}) \tag{B.3c}$$

Where, A_{22}, B_{22}, D_{22} & A_{44} are components of the A, B and D stiffness matrices from classical lamination theory, h is the thickness of the lamina, $\bar{Z}$ is the centroidal distance of the lamina from laminate mid-plane, $\bar{\alpha}_y$ is the coefficient of thermal expansion in y-direction. Plugging in (B.3a – B.3c) into (B.2a – B.2c) we have the governing equations,

$$A_{22}V_{,yy} + B_{22}\beta_{,yy} + T_t - T_b = 0 \tag{B.4a}$$

$$\left(D_{22} - \frac{B_{22}^2}{A_{22}}\right)\beta_{,yy} - A_{44}(\beta + W_{,y}) + \left(\frac{h}{2} - \frac{B_{22}}{A_{22}}\right)T_t + \left(\frac{h}{2} + \frac{B_{22}}{A_{22}}\right)T_b = 0 \tag{B.4b}$$

$$A_{44}(\beta_{,y} + W_{,yy}) + P_t - P_b = 0 \tag{B.4c}$$

In the sections to follow, the governing equations listed above will be modified as required by the lamina (or sublaminate) boundary conditions.

Since, sublaminates 1, 2 and 3 are intact their solutions will be determined first. Since, the derivation for these sublaminates follow the solution procedure presented in section A.1 exactly, only the solutions for displacements and forces are repeated here.

A.1. Laminated Portion: Sublaminate 1, 2 and 3 ($0 \le y \le S\text{-}L$)

The derivation for this portion has already been given in detail in section A.1. Hence only the solutions for these sublaminates are given here.

$$\beta^{(i)} = \sum_{j=1}^{3} \alpha_j P_j^{(i)} \sinh(\lambda_j y) \tag{B.5}$$

$$V^{(i)} = \sum_{j=1}^{3} \alpha_j \gamma_j^{(i)} \sinh(\lambda_j y) + \alpha_{3+i} y \tag{B.6}$$

$$N_M^{(i)} = \sum_{j=1}^{3} \alpha_j \eta_j^{(i)} \cosh(\lambda_j y) + A_{22}^{(i)} \alpha_{3+i} - \bar{Q}_{22}^{(i)} h^{(i)} \int_{T_{ref}}^{T_f} \bar{\alpha}_y^{(i)} dT \tag{B.7}$$

$$M_M^{(i)} = \sum_{j=1}^{3} \alpha_j \xi_j^{(i)} \cosh(\lambda_j y) + B_{22}^{(i)} \alpha_{3+i} - \bar{Q}_{22}^{(i)} h^{(i)} \bar{Z}^{(i)} \int_{T_{ref}}^{T_f} \bar{\alpha}_y^{(i)} dT \tag{B.8}$$

The definition of the constants $\gamma_j^{(i)}$, $\eta_j^{(i)}$ and $\xi_j^{(i)}$ remain the same and have been listed in Appendix E.

A.2. Laminated Portion: Sublaminate 4 and 5 (S-L ≤ y ≤ S)

The sublaminates 4 and 5 are an intact ply group, unsymmetric about its mid-plane (Fig. B.1) and has to be solved as a coupled set of equations. Since, this solution procedure has already been examined in detail in Zhang *et al* [21] and further extended to include the effect of thermal load by Roy and Benjamin [36] only the solutions to the equations are presented here.

Assuming that $W^{(4)}=W^{(5)}\neq 0$ and applying the traction boundary conditions $T_t^{(5)} = 0$, $T_b^{(5)} = T_t^{(4)}$, $T_b^{(4)} = 0$, $P_t^{(5)} = 0$, $P_b^{(5)} = P_t^{(4)}$ and $P_b^{(4)} = 0$ [‡] to the sublaminate governing equations, we get the solutions for this sublaminate as (refer [21]),

$$\begin{Bmatrix} \beta^{(4)} \\ \beta^{(5)} \end{Bmatrix} = \theta_1 e^{\omega y} \begin{Bmatrix} q \\ 1 \end{Bmatrix} + \theta_2 e^{-\omega y} \begin{Bmatrix} q \\ 1 \end{Bmatrix} + \theta_3 y \begin{Bmatrix} 1 \\ 1 \end{Bmatrix} + \theta_4 \begin{Bmatrix} 1 \\ 1 \end{Bmatrix} \tag{B.9}$$

[‡] Refer Section 3.4 for details about the error with this assumption.

Where,

$$\omega = \sqrt{\frac{A_{44}^{(2)} A_{44}^{(3)} (b_{11} + b_{22} + 2b_{12})}{(A_{44}^{(2)} + A_{44}^{(3)})(b_{11} b_{22} - b_{12}^2)}}$$

$$q = -\frac{b_{22} + b_{12}}{b_{11} + b_{12}}$$

The mid-plane displacements will be,

$$V^{(4)} = -k_1(\theta_1 e^{\omega y} + \theta_2 e^{-\omega y}) + \theta_5 y + \theta_7 \tag{B.10}$$

$$V^{(5)} = k_3(\theta_1 e^{\omega y} + \theta_2 e^{-\omega y}) + \theta_6 y + \theta_8 \tag{B.11}$$

$$W^{(4)} = W^{(5)} = -\frac{A_{44}^{(2)} + qA_{44}^{(3)}}{\omega(A_{44}^{(2)} + A_{44}^{(3)})}(\theta_1 e^{\omega y} - \theta_2 e^{-\omega y}) - \frac{1}{2}\theta_3 y^2 - \theta_4 y + \theta_9 \tag{B.12}$$

The force and moment resultants for are,

$$N_M^{(4)} = -k_3 A_{22}^{(2)} \omega(\theta_1 e^{\omega y} - \theta_2 e^{-\omega y}) + B_{22}^{(3)} \theta_3 + A_{22}^{(3)} \theta_5 - \bar{Q}_{22}^{(3)} h^{(3)} \int_{T_{ref}}^{T_f} \bar{\alpha}_y^{(3)} dT \tag{B.13}$$

$$N_M^{(5)} = k_3 A_{22}^{(2)} \omega(\theta_1 e^{\omega y} - \theta_2 e^{-\omega y}) + A_{22}^{(2)} \theta_6 - \bar{Q}_{22}^{(2)} h^{(2)} \int_{T_{ref}}^{T_f} \bar{\alpha}_y^{(2)} dT \tag{B.14}$$

$$M_M^{(4)} = (qD_{22}^{(3)} - k_3 B_{22}^{(3)})\omega(\theta_1 e^{\omega y} - \theta_2 e^{-\omega y}) + D_{22}^{(3)} \theta_3 + B_{22}^{(3)} \theta_5 - \bar{Q}_{22}^{(3)} h^{(3)} \bar{Z} \int_{T_{ref}}^{T_f} \bar{\alpha}_y^{(3)} dT \tag{B.15}$$

$$M_M^{(5)} = k_2(\theta_1 e^{\omega y} - \theta_2 e^{-\omega y}) + D_{22}^{(2)} \theta_3 - \bar{Q}_{22}^{(2)} h^{(2)} \bar{Z} \int_{T_{ref}}^{T_f} \bar{\alpha}_y^{(2)} dT \tag{B.16}$$

A.3. Delaminated Portion: Sublaminate 6 (S-L ≤ y ≤ S)

The solution for rotations in the delaminated portion is solved using the elastic foundation solutions described in Section 3.4. Since, the cracked layer is decoupled from

the solution to the rest of the laminate we can discuss the solution for rotations and displacements separately.

The equilibrium equation for the cracked lamina is,

$$A_{22}^{(1)} V_{,yy}^{(6)} = 0 \tag{B.17}$$

Solving the above equation we get,

$$V^{(6)} = \psi_5 y + \psi_6 \tag{B.18}$$

From, the above solution we can derive the solution for mechanical load in the cracked sublaminate as,

$$N_M^{(6)} = A_{22}^{(1)} V_{,y}^{(6)} - \bar{Q}_{22}^{(1)} h^{(1)} \int_{T_{ref}}^{T_f} \bar{\alpha}_y^{(1)} dT = A_{22}^{(1)} \psi_5 - \bar{Q}_{22}^{(1)} h^{(1)} \int_{T_{ref}}^{T_f} \bar{\alpha}_y^{(1)} dT \tag{B.19}$$

Hence, we need to specify 17 boundary conditions to solve for the 17 constants ($\alpha_1, \alpha_2, ..., \alpha_6, \theta_1, \theta_2, ..., \theta_9, \psi_5, \psi_6$).

A.4. Solutions for constants: $\alpha_1, \alpha_2, ..., \alpha_6, \theta_1, \theta_2, ..., \theta_9, \psi_5, \psi_6$

The boundary conditions that need to be satisfied for this case are:

$$\beta^{(4)}(S) = 0 \tag{B.20a}$$

$$\beta^{(5)}(S) = 0 \tag{B.20b}$$

$$V^{(4)}(S) = V^{(5)}(S) \tag{B.20c}$$

$$N_M^{(6)}(S) = 0 \tag{B.20d}$$

$$N_M^{(4)}(S) + N_M^{(5)}(S) = \frac{N}{2} \tag{B.20e}$$

$$\beta^{(1)}(S-L) = \beta^{(6)}(S-L) \tag{B.20f}$$

$$\beta^{(3)}(S-L) = \beta^{(4)}(S-L) \tag{B.20g}$$

$$V^{(1)}(S-L) = V^{(6)}(S-L) \tag{B.20h}$$

$$V^{(2)}(S-L) = V^{(5)}(S-L) \tag{B.20i}$$

$$V^{(3)}(S-L) = V^{(4)}(S-L) \tag{B.20j}$$

$$W^{(4)}(S-L) = W^{(5)}(S-L) = 0 \tag{B.20k}$$

$$N_M^{(1)}(S-L) = N_M^{(6)}(S-L) \tag{B.20l}$$

$$N_M^{(2)}(S-L) = N_M^{(5)}(S-L) \tag{B.20m}$$

$$M_M^{(2)}(S-L) = M_M^{(5)}(S-L) \tag{B.20n}$$

$$N_M^{(1)}(0) + N_M^{(2)}(0) + N_M^{(3)}(0) = \frac{N}{2} \tag{B.20o}$$

The above 15 boundary conditions and the two continuity equations (A.5a, b) (17 boundary conditions in total) have to be satisfied. Following the solution procedure given in Zhang *et al* [21], we can solve using the following equations,

$$[\mathbf{F}]\{\boldsymbol{\alpha}\} = \{\mathbf{R}\} \tag{B.21a}$$

Where,

$$\begin{aligned} F_{1j} &= (P_j^{(2)} - 1)\sinh(\lambda_j(S-L)) + (1-q)\rho_j \frac{\tanh(\omega L)}{\omega}\cosh(\lambda_j(S-L)) \\ F_{2j} &= \eta_j^{(1)}\cosh(\lambda_j(S-L)) \\ F_{3j} &= (qP_j^{(2)} - 1)\sinh(\lambda_j(S-L)) - (1-q)\delta_j L\cosh(\lambda_j(S-L)) \end{aligned} \tag{B.21b}$$

Are elements of the 3x3 matrix **F** (j=1 to 3).

While, $\{\boldsymbol{\alpha}\}=\begin{Bmatrix}\alpha_1\\ \alpha_2\\ \alpha_3\end{Bmatrix}$ and $\{\mathbf{R}\}=\begin{Bmatrix}\dfrac{(1-q)\tanh(\omega L)}{\omega(k_4-k_3)}\phi_0\\ N_T^{(1)}-A_{22}^{(1)}\dfrac{N+N_T}{A_{22}}\\ \dfrac{(1-q)L}{(k_4-k_3)}\phi_0\end{Bmatrix}$.

Where, $\phi_0=\dfrac{N+N_T}{A_{22}}-\dfrac{N+2(N_T^{(2)}+N_T^{(3)})}{2(A_{22}^{(2)}+A_{22}^{(3)})}$

The solutions for the other constants are as follows,

$$\alpha_4=\alpha_5=\alpha_6=\frac{N+N_T}{A_{22}} \tag{B.22}$$

$$\theta_1=\frac{1}{2\omega e^{\omega S}\cosh(\omega L)}\left[\sum_{j=1}^{3}\alpha_j\rho_j\cosh(\lambda_j(S-L))+\frac{\phi_0}{k_3-k_4}\right] \tag{B.23}$$

$$\theta_2=-\theta_1 e^{2\omega s} \tag{B.24}$$

$$\theta_3=\sum_{j=1}^{3}\alpha_j\delta_j\cosh(\lambda_j(S-L))+\frac{\phi_0}{k_3-k_4} \tag{B.25}$$

$$\theta_4=-\theta_3 S \tag{B.26}$$

$$\theta_5=\frac{N+2(N_T^{(2)}+N_T^{(3)})}{2(A_{22}^{(2)}+A_{22}^{(3)})}-k_5\theta_3 \tag{B.27}$$

$$\theta_6=\frac{N+2(N_T^{(2)}+N_T^{(3)})}{2(A_{22}^{(2)}+A_{22}^{(3)})}+k_4\theta_3 \tag{B.28}$$

$$\theta_7=\sum_{j=1}^{3}\alpha_j\gamma_j^{(3)}\sinh(\lambda_j(S-L))+\frac{N+N_T}{A_{22}}(S-L)+2\theta_1k_3e^{\omega S}\sinh(\omega L)-\theta_5(S-L) \tag{B.29}$$

$$\theta_8=\sum_{j=1}^{3}\alpha_j\gamma_j^{(1)}\sinh(\lambda_j(S-L))+\frac{N+N_T}{A_{22}}(S-L)-2\theta_1k_1e^{\omega S}\sinh(\omega L)-\theta_6(S-L) \tag{B.30}$$

$$\theta_9=\frac{2(A_{44}^{(2)}+qA_{44}^{(3)})}{\omega(A_{44}^{(2)}+A_{44}^{(3)})}\theta_1e^{\omega S}\cosh(\omega L)-\frac{1}{2}\theta_3(S^2-L^2) \tag{B.31}$$

APPENDIX C

DERIVATION OF THE ELASTIC FOUNDATION MODEL

The moment and shear equilibrium equations for the cracked sublaminate are,

$$D_{22}^{(3)}\beta_{,yy}^{(4)} - A_{44}^{(3)}(\beta^{(4)} + W_{,y}^{(4)}) = 0 \tag{C.1}$$

$$A_{44}^{(3)}(\beta_{,y}^{(4)} + W_{,yy}^{(4)}) - \frac{2E_3}{h^{(3)}}W^{(4)} = 0 \tag{C.2}$$

Equilibrium equations (C.1) & (C.2) can be written as follows,

$$(D_{22}^{(3)}D^2 - A_{44}^{(3)})\beta^{(4)} = A_{44}^{(3)}DW^{(4)} \tag{C.1a}$$

$$-A_{44}^{(3)}D\beta^{(4)} = (A_{44}^{(3)}D^2 - \frac{2E_3}{h^{(3)}})W^{(4)} \tag{C.2a}$$

Where, $D \equiv \frac{d}{dy}, D^2 \equiv \frac{d^2}{dy^2}$

Simultaneously solving (C.1a) & (C.2a) for $\beta^{(4)}$ we get the governing differential equation to the system,

$$\left[(D_{22}^{(3)}D^2 - A_{44}^{(3)})(D_{22}^{(3)}D^2 - A_{44}^{(3)}) + (A_{44}^{(3)}D)^2\right]\beta^{(4)} = 0$$

$$\Rightarrow \left[D_{22}^{(3)} A_{44}^{(3)} D^4 - \frac{2D_{22}^{(3)} E_3}{h^{(3)}} D^2 + \frac{2E_3 A_{44}^{(3)}}{h^{(3)}} \right] \beta^{(4)} = 0$$

$$\Rightarrow D_{22}^{(3)} A_{44}^{(3)} \frac{d^4 \beta^{(4)}}{dy^4} - \frac{2D_{22}^{(3)} E_3}{h^{(3)}} \frac{d^2 \beta^{(4)}}{dy^2} + \frac{2E_3 A_{44}^{(3)}}{h^{(3)}} \beta^{(4)} = 0 \tag{C.3}$$

The characteristic equation to the above equation is (assuming solution is of the form $\beta^{(4)} = e^{\omega y}$),

$$D_{22}^{(3)} A_{44}^{(3)} \omega^4 - \frac{2D_{22}^{(3)} E_3}{h^{(3)}} \omega^2 + \frac{2E_3 A_{44}^{(3)}}{h^{(3)}} = 0$$

We can reduce the 4th order auxiliary equation to its equivalent 2nd order form by the transformation,

$$\omega^* = \omega^2 \tag{C.4}$$

The equation now becomes,

$$D_{22}^{(3)} A_{44}^{(3)} \omega^{*2} - \frac{2D_{22}^{(3)} E_3}{h^{(3)}} \omega^* + \frac{2E_3 A_{44}^{(3)}}{h^{(3)}} = 0$$

Let, $a = D_{22}^{(3)} A_{44}^{(3)}, b = \frac{2D_{22}^{(3)} E_3}{h^{(3)}}, c = \frac{2E_3 A_{44}^{(3)}}{h^{(3)}}$.

The roots to the reduced equation will be,

$$\omega_{1,2}^* = \frac{b \pm \sqrt{b^2 - 4ac}}{2a}$$

Plugging in values for a, b & c.

$$\omega_{1,2}^{*}=\frac{\frac{2D_{22}^{(3)}E_3}{h^{(3)}}\pm\sqrt{\left(\frac{2D_{22}^{(3)}E_3}{h^{(3)}}\right)^2-4\left(D_{22}^{(3)}A_{44}^{(3)}\right)\left(\frac{2E_3A_{44}^{(3)}}{h^{(3)}}\right)}}{2D_{22}^{(3)}A_{44}^{(3)}}$$

$$\Rightarrow\omega_{1,2}^{*}=\frac{E_3}{h^{(3)}A_{44}^{(3)}}\left(1\pm\sqrt{1-\frac{2h^{(3)}A_{44}^{(3)2}}{D_{22}^{(3)}E_3}}\right)$$

Case I. Assume that the parameter, $\frac{2h^{(3)}A_{44}^{(3)2}}{D_{22}^{(3)}E_3}>1$, for the given material system.

Then, $\omega_{1,2}^{*}$ become complex numbers.

If we set, $\Delta_1^2=\frac{E_3}{h^{(3)}A_{44}^{(3)}}\sqrt{1^2+\left(\sqrt{\frac{2h^{(3)}A_{44}^{(3)2}}{D_{22}^{(3)}E_3}-1}\right)^2}=\sqrt{\frac{2E_3}{h^{(3)}D_{22}^{(3)}}}$

also, set $2\Delta_2=\tan^{-1}\sqrt{\frac{2h^{(3)}A_{44}^{(3)2}}{D_{22}^{(3)}E_3}-1}$.

We will have, $\omega_1^{*}=\Delta_1^2e^{i2\Delta_2};\omega_2^{*}=\Delta_1^2e^{-i2\Delta_2}$.

Using (C.4), we get the roots to the original 4th order equation as,

$\Delta_1e^{i\Delta_2},-\Delta_1e^{i\Delta_2},\Delta_1e^{-i\Delta_2},-\Delta_1e^{-i\Delta_2}$.

Thus, the solution to (C.3) is,

$$\beta^{(4)}=\psi_1^{*}e^{\Delta_1e^{i\Delta_2}y}+\psi_2^{*}e^{-\Delta_1e^{i\Delta_2}y}+\psi_3^{*}e^{\Delta_1e^{-i\Delta_2}y}+\psi_4^{*}e^{-\Delta_1e^{-i\Delta_2}y} \tag{C.5}$$

Next we set,

$$C_1=\Delta_1\cos\Delta_2;C_2=\Delta_1\sin\Delta_2 \tag{C.6}$$

Using (C.6) we can rewrite (C.5) as follows,

$$\beta^{(4)} = \psi_1^* e^{(C_1+iC_2)y} + \psi_2^* e^{(-C_1-iC_2)y} + \psi_3^* e^{(C_1-iC_2)y} + \psi_4^* e^{(-C_1+iC_2)y}$$

Or, we can write,

$$\beta^{(4)} = e^{C_1 y}(\psi_1 \cos C_2 y + \psi_2 \sin C_2 y) + e^{-C_1 y}(\psi_3 \cos C_2 y + \psi_4 \sin C_2 y) \tag{C.7}$$

$W^{(4)}$ can be solved from (C.1) and (C.7).

Boundary conditions for $\beta^{(4)}$.

$$\begin{aligned}
&(\mathrm{i})\beta^{(3)}(\mathrm{S}-\mathrm{L}) = \beta^{(4)}(\mathrm{S}-\mathrm{L}) \\
&(\mathrm{ii})\mathrm{M}_{\mathrm{M}}^{(3)}(\mathrm{S}-\mathrm{L}) = \mathrm{M}_{\mathrm{M}}^{(4)}(\mathrm{S}-\mathrm{L}) \\
&(\mathrm{iii})\mathrm{M}_{\mathrm{M}}^{(4)}(\mathrm{S}) = 0 \\
&(\mathrm{iv})\mathrm{Q}^{(4)}(\mathrm{S}) = 0
\end{aligned}$$

The equation for moment follows from the constitutive relation listed below

$$M_M^{(4)} = D_{22}^{(3)} \beta_{,y}^{(4)} - M_t^{(3)} \tag{C.8}$$

For Shear: we have from relation (C.1),

$$Q^{(4)} = A_{44}^{(3)}(\beta^{(4)} + W_{,y}^{(4)}) = D_{22}^{(3)} \beta_{,yy}^{(4)} \tag{C.9}$$

Plugging in (C.7) into the above equations,

$$\begin{aligned}
M_M^{(4)} = D_{22}^{(3)}\Delta_1 \Big[& e^{C_1 y}\left(\psi_1 \cos(C_2 y + \Delta_2) + \psi_2 \sin(C_2 y + \Delta_2)\right) \\
& - e^{-C_1 y}\left(\psi_3 \cos(C_2 y - \Delta_2) + \psi_4 \sin(C_2 y - \Delta_2)\right)\Big] - M_t^{(3)}
\end{aligned} \tag{C.10}$$

$$\begin{aligned}
Q^{(4)} = D_{22}^{(3)}\Delta_1^2 \Big[& e^{C_1 y}\left(\psi_1 \cos(C_2 y + 2\Delta_2) + \psi_2 \sin(C_2 y + 2\Delta_2)\right) \\
& + e^{-C_1 y}\left(\psi_3 \cos(C_2 y - 2\Delta_2) + \psi_4 \sin(C_2 y - 2\Delta_2)\right)\Big]
\end{aligned} \tag{C.11}$$

Applying Boundary conditions, we get 4 equations from which we can solve the 4 unknowns $\psi_1, \psi_2, \psi_3, \psi_4$.

Case II. If the parameter $\frac{2h^{(3)}A_{44}^{(3)2}}{D_{22}^{(3)}E_3} < 1$, Then, $\omega_{1,2}^*$ are real positive numbers.

Using (C.4) we have the solutions to the 4th order equation as: $\omega_1, -\omega_1, \omega_2, -\omega_2$. Where, $\omega_i = \sqrt{\omega_i^*}$.

Hence, the solution to (C.3) is:

$$\beta^{(4)} = \psi_1 e^{\omega_1 y} + \psi_2 e^{-\omega_1 y} + \psi_3 e^{\omega_2 y} + \psi_4 e^{-\omega_2 y} \tag{C.12}$$

Using (C.8), (C.9) & (C.12) we can show the Moment and Shear relations to be,

$$M_M^{(4)} = D_{22}^{(3)}\left[\omega_1\left(\psi_1 e^{\omega_1 y} - \psi_2 e^{-\omega_1 y}\right) + \omega_2\left(\psi_3 e^{\omega_2 y} - \psi_4 e^{-\omega_2 y}\right)\right] - M_t^{(3)} \tag{C.13}$$

$$Q^{(4)} = D_{22}^{(3)}\left[\omega_1^2\left(\psi_1 e^{\omega_1 y} + \psi_2 e^{-\omega_1 y}\right) + \omega_2^2\left(\psi_3 e^{\omega_2 y} + \psi_4 e^{-\omega_2 y}\right)\right] \tag{C.14}$$

Applying Boundary conditions (i) - (iv), we can solve for constants $\psi_1, \psi_2, \psi_3, \psi_4$.

APPENDIX D

DERIVATION OF THE STITCH CRACK MODEL

The inclusion of the linear spring at the end of the FLM cracked layer is assumed to only affect the solution of the mid-plane displacement of the cracked layer. Since, the off-axis plies are usually located within the laminate and almost never in the outer or on the mid-plies the derivation given here, models the stitch crack as an extension to the FLM-Case 2. However, since the cracked layer solutions for all FLM cases are the same we can easily modify the solution given below to any generic case of the FLM.

The equilibrium equation for the cracked lamina is,

$$A_{22}^{(5)} V_{,yy}^{(5)} = 0 \tag{D.1}$$

Solving the above equation we get,

$$V^{(5)} = \psi_5 y + \psi_6 \tag{D.2}$$

From, the above solution we can derive the solution for mechanical load in the cracked sublaminate as,

$$N_M^{(5)} = A_{22}^{(2)} V_{,y}^{(5)} - N_T^{(2)} = A_{22}^{(2)} \psi_5 - N_T^{(2)} \tag{D.3}$$

where, we have set,

$$N_T^{(2)} = \bar{Q}_{22}^{(2)} h^{(2)} \int_{T_{ref}}^{T_{final}} \bar{\alpha}_y dT \tag{D.4}$$

Since there is a pseudo-force introduced by the inclusion of the linear spring at the end of the model, the boundary conditions for the cracked lamina will now become,

$$V^{(2)}(S-L) = V^{(5)}(S-L) \tag{D.5a}$$

$$N_M^{(5)}(S) = K_{spring}^{(5)} V^{(5)}(S) \tag{D.5b}$$

Where, $K_{spring}^{(5)}$, the stiffness of the spring defined is,

$$K_{spring}^{(5)} = \varepsilon A_{22}^{(2)} \tag{D.6}$$

We see that when the parameter ε=0, we revert to the original set of boundary conditions for the FLM cracked layer (see Appendix A).

Using the modified solution for $V^{(2)}$ (see section 3.2), and plugging in the solutions (D.2) and (D.3) into (D.5a) and (D.5b) we get,

$$\psi_5(S-L) + \psi_6 = \left(\frac{N + N_T}{A_{22}} \right)(S-L) \tag{D.7a}$$

$$A_{22}^{(2)} \psi_5 - N_T^{(2)} = K_{spring}^{(5)} (\psi_5 S + \psi_6) \tag{D.7b}$$

Solving (D.7a) and (D.7b) simultaneously we get,

$$\psi_5 = \frac{N_T^{(2)} + \dfrac{K_{spring}^{(5)}(S-L)(N+N_T)}{A_{22}}}{A_{22}^{(2)} - K_{spring}^{(5)} L} \tag{D.8a}$$

$$\psi_6 = \frac{N+N_T}{A_{22}}(S-L) - \psi_1(S-L) \tag{D.8b}$$

APPENDIX E

ALL CONSTANTS OF THE FIVE-LAYER MODEL

$$A_{22} = 2(A_{22}^{(1)} + A_{22}^{(2)} + A_{22}^{(3)}) \tag{E.1}$$

$$N_T^{(i)} = \bar{Q}_{22}^{(i)} h^{(i)} \int_{T_{ref}}^{T_f} \bar{\alpha}_y^{(i)} dT \text{ for i=1,2 or 3} \tag{E.2}$$

$$N_T = 2(N_T^{(1)} + N_T^{(2)} + N_T^{(3)}) \tag{E.3}$$

$$a_{11} = D_{22}^{(1)} + \frac{h^{(1)}(4B_{22}^{(1)} + h^{(1)}A_{22}^{(1)})(A_{22}^{(2)} + A_{22}^{(3)}) - 4B_{22}^{(1)2}}{2A_{22}} \tag{E.4}$$

$$a_{12} = a_{21} = \frac{h^{(2)}(B_{22}^{(1)} + \frac{1}{2}h^{(1)}A_{22}^{(1)})(A_{22}^{(2)} + 2A_{22}^{(3)})}{A_{22}} \tag{E.5}$$

$$a_{13} = a_{31} = \frac{(\frac{1}{2}h^{(1)}A_{22}^{(1)} + B_{22}^{(1)})(h^{(3)}A_{22}^{(3)} - 2B_{22}^{(3)})}{A_{22}} \tag{E.6}$$

$$a_{22} = D_{22}^{(2)} + \frac{h^{(2)2}(4A_{22}^{(1)}A_{22}^{(3)} + A_{22}^{(1)}A_{22}^{(2)} + A_{22}^{(2)}A_{22}^{(3)})}{2A_{22}} \tag{E.7}$$

$$a_{23} = a_{32} = \frac{h^{(2)}(h^{(3)}A_{22}^{(3)} - 2B_{22}^{(3)})(2A_{22}^{(1)} + A_{22}^{(2)})}{2A_{22}} \tag{E.8}$$

$$a_{33} = D_{22}^{(3)} - \frac{B_{22}^{(3)2}}{A_{22}^{(3)}} + \frac{(h^{(3)}A_{22}^{(3)} - 2B_{22}^{(3)})^2(A_{22}^{(1)} + A_{22}^{(2)})}{2A_{22}A_{22}^{(3)}} \tag{E.9}$$

$$b_{11} = D_{22}^{(3)} - \frac{B_{22}^{(3)2}}{A_{22}^{(3)}} + \frac{A_{22}^{(2)}(h^{(3)}A_{22}^{(3)} - 2B_{22}^{(3)})^2}{4A_{22}^{(3)}(A_{22}^{(2)} + A_{22}^{(3)})} \tag{E.10}$$

$$b_{22} = D_{22}^{(2)} + \frac{h^{(2)2}A_{22}^{(2)}A_{22}^{(3)}}{4A_{22}^{(3)}(A_{22}^{(2)} + A_{22}^{(3)})} \tag{E.11}$$

$$b_{12} = b_{21} = \frac{h^{(2)}A_{22}^{(2)}(h^{(3)}A_{22}^{(3)} - 2B_{22}^{(3)})}{4(A_{22}^{(2)} + A_{22}^{(3)})} \tag{E.12}$$

$$k_1 = \frac{(h^{(2)} + qh^{(3)})A_{22}^{(2)} + 2qB_{22}^{(3)}}{2(A_{22}^{(2)} + A_{22}^{(3)})} \tag{E.13}$$

$$k_2 = \omega D_{22}^{(2)} \tag{E.14}$$

$$k_3 = \frac{(h^{(2)} + qh^{(3)})A_{22}^{(2)} - 2qB_{22}^{(3)}}{2(A_{22}^{(2)} + A_{22}^{(3)})} \tag{E.15}$$

$$k_4 = \frac{(h^{(2)} + h^{(3)})A_{22}^{(2)} - 2B_{22}^{(3)}}{2(A_{22}^{(2)} + A_{22}^{(3)})} \tag{E.16}$$

$$k_5 = \frac{(h^{(2)} + h^{(3)})A_{22}^{(2)} + 2B_{22}^{(3)}}{2(A_{22}^{(2)} + A_{22}^{(3)})} \tag{E.17}$$

$$\gamma_j^{(1)} = \frac{P_j^{(1)}(h^{(1)}(A_{22}^{(2)} + A_{22}^{(3)}) - 2B_{22}^{(1)}) + P_j^{(2)}h^{(2)}(A_{22}^{(2)} + 2A_{22}^{(3)}) + h^{(3)}A_{22}^{(3)} - 2B_{22}^{(3)}}{A_{22}} \tag{E.18}$$

$$\gamma_j^{(2)} = -\frac{P_j^{(1)}(h^{(1)}A_{22}^{(1)} + 2B_{22}^{(1)}) + P_j^{(2)}h^{(2)}(A_{22}^{(1)} - A_{22}^{(3)}) + 2B_{22}^{(3)} - h^{(3)}A_{22}^{(3)}}{A_{22}} \tag{E.19}$$

$$\gamma_j^{(3)} = -\frac{P_j^{(1)}(h^{(1)}A_{22}^{(1)} + 2B_{22}^{(1)}) + P_j^{(2)}h^{(2)}(2A_{22}^{(1)} + A_{22}^{(2)}) + 2B_{22}^{(3)} + h^{(3)}(A_{22}^{(1)} + A_{22}^{(2)})}{A_{22}} \tag{E.20}$$

$$\eta_j^{(1)} = (B_{22}^{(1)}P_j^{(1)} + A_{22}^{(1)}\gamma_j^{(1)})\lambda_j \tag{E.21}$$

$$\eta_j^{(2)} = A_{22}^{(2)}\gamma_j^{(2)}\lambda_j \tag{E.22}$$

$$\eta_j^{(3)} = (B_{22}^{(3)} + A_{22}^{(3)}\gamma_j^{(3)})\lambda_j \tag{E.23}$$

$$\xi_j^{(1)} = (D_{22}^{(1)}P_j^{(1)} + B_{22}^{(1)}\gamma_j^{(1)})\lambda_j \tag{E.24}$$

$$\xi_j^{(2)} = D_{22}^{(2)}P_j^{(2)}\lambda_j \tag{E.25}$$

$$\xi_j^{(3)} = (D_{22}^{(3)} + B_{22}^{(3)}\gamma_j^{(3)})\lambda_j \tag{E.26}$$

VITA

Abilash Rajendran Nair

Candidate for the Degree of

Master of Science

Thesis: MODELING AND VERIFICATION OF CRYOGENIC PERMEABILITY OF GRAPHITE EPOXY LAMINATES WITH DELAMINATIONS AND STITCH CRACKS

Major Field: Mechanical Engineering

Biographical:

Education: Received Bachelor of Technology degree in Aerospace Engineering from Indian Institute of Technology, Kharagpur, India in June 2003. Completed requirements for Master of Science degree with a major in Mechanical and Aerospace Engineering at Oklahoma State University in July 2006.

Experience: Graduate Research Assistant in Mechanical and Aerospace Engineering Department, Oklahoma State University, Stillwater, Oklahoma, January, 2004 – July, 2006.

Professional Memberships: Phi Kappa Phi.

Name: Abilash R. Nair Date of Degree: July, 2006

Institution: Oklahoma State University Location: Stillwater, Oklahoma

Title of Study: MODELING AND VERIFICATION OF CRYOGENIC PERMEABILITY OF GRAPHITE EPOXY LAMINATES WITH DELAMINATIONS AND STITCH CRACKS

Pages in Study: 131 Candidate for the Degree of Master of Science

Major Field: Mechanical Engineering

Scope and Methodology of Study: Composites are extensively used for various aerospace applications and one of the important uses is as cryogenic fuel tank materials for reusable launch vehicles. Composites offer high strength to weight ratio and therefore are preferred to many other materials. However under structural mechanical loads and/or thermal loads, transverse micro-cracks are developed in the polymer matrix. These cracks along with interlaminar delaminations produced at the crack tips, lead to passage of cryogenic fuel permeation through the laminates. In this thesis, a mathematical model based on first order shear deformation theory has been developed to find the delaminated crack opening for each ply through the thickness of laminate and the associated permeability of the damaged composite. In addition a stitch crack model has been included in this model to address experimental observations. The model is also employed to predict evolution of damage within the cracked plies.

Findings and Conclusions: In this thesis, a five-layer model has been proposed to predict delaminated crack opening displacement in graphite epoxy laminates. The DCOD predicted by this mathematical model, with and without stitch cracks, shows good agreement with two dimensional finite element analysis. The DCOD values predicted for IM7/5250-4 laminate of lay-up $[0/45/-45/90]_s$ were used to predict permeability using Darcy's law for fluid flow through porous media. The analysis results were benchmarked using test data from Air Force Research Laboratory. A parametric study for permeability conducted with varying stitch crack lengths shows that the permeability of the composite is affected by the extent of damage in individual plies. Further, the proposed damage model was verified using 2-D finite element analysis. These observations and model verifications have been made for IM7/5250-4 graphite epoxy laminate system and conclusions may not be transferable to other types of laminates.

Advisor's approval: Samit Roy .